Development of an Assessment Tool for Prioritizing Influencing Factors of Sustainability in Higher Education

Siripong Jungthawan and Ronnachai Tiyarattanachai

Logistics and Supply Chain Management Program, Department of Civil Engineering, Faculty of Engineering, King Mongkut's Institute of Technology Ladkrabang (KMITL), Bangkok, Thailand, 59610005@kmitl.ac. and ronnachai.ti@kmitl.ac.th

Abstract.

The United Nations set 17 Sustainable Development Goals (SDGs) in August 2015 as a blueprint to achieve sustainable future for all nations at all levels. Higher education institutions are expected to significantly contribute to the goal, as they must produce the human resources and research necessary for achieving sustainability. In October 2019, Times Higher Education (THE) launched the THE University Impact Rankings, which encouraged universities to focus efforts that pose positive impacts on SDGs in the areas related to the university's operation. Since SDGs and their targets may have different priorities in different countries, we examined the perspectives of stakeholders in 16 Thai universities ranked in the THE World University Rankings to prioritize the SDG areas on which the universities should focus. We expect that this study will be used by Thai university executives to optimize resources spent on achieving better sustainability performance.

Keywords. Higher Education, Higher Education Institution (HEI), Sustainable Development Goals (SDGs), Sustainability in Higher Education (SHE), University Impact Ranking.

1. INTRODUCTION

United Nations (UN) announced Sustainable Development Goals (SDGs) in August 2015; it was a blueprint to achieve a better and more sustainable future for all including, but not be limited to governments, businesses, civil society, the general public, and also Higher Education Institution (HEI) [1].

With only 10 years left to achieve the SDGs, world leaders at the Sustainable Development Goals Summit (SDGs Summit) in September 2019 called for a decade of action and delivery for sustainable development and pledged to mobilize financing, enhance national implementation and strengthen institutions to achieve the goals by the 2030 target, leaving no one behind [2, 3].

Thailand is one of the 193 UN member states, which joined the UN in 1946, and has contributed constructively in peacekeeping, human rights, and sustainable development. Prayut Chan-o-cha, the Prime Minister of Thailand and the Chair of ASEAN, made a statement at the 52 ASEAN foreign ministers' meeting that leave no one behind and looks to the future as well as the adoption of the ASEAN leaders' vision statement on partnership for sustainability in all members [4].

Moreover, he attended the 74 United Nations General Assembly (UNGA 74) Session, New York. He joined the SDGs Summit, which was the first gathering at the summit level of leaders from countries, that in 2015 adopted the "SDGs Agenda 2030", aiming to assess and expedite implementation of SDGs by 2020. Prayut stated that ASEAN must accelerate the implementation of SDGs by enhancing the partnership network, tackling the problems through education, science and technology, and protecting the environment, especially through the responsible use of natural resources such as soil, water, air, and mineral [5]. As a result, Thai government agencies in all levels have been trying to drive the SDGs through their policies and executions. Private sectors are also expected to contribute to the effort. For the education sector, Thai Higher Education Institution (THEI) takes many important roles in the SDGs.

HEIs are the important units that develop human resources and research necessary for achieving self-sustainability and their communities. Moreover, Times Higher Education (THE) announced the THE University Impact Rankings (THEUIR) in October 2019. One of the objectives of the rankings is to encourage universities to focus efforts that pose positive impacts on SDGs in the areas related to the university's roles and the systems that will be linked to the 17 SDGs [6] .

Cause SDGs and their targets have different priorities and context in different countries, there is a need for a study to examine the perspectives of stakeholders in THEI. This is especially important considering the fact that Thai universities may have relatively more limited resources to boost SDGs compared to other universities in more developed countries.

This study focuses on the 16 pioneer Thai universities ranked in the 2019 THE World University Rankings. This study aims to design and develop an assessment tool. We will understand the linkage between the factor of awareness SDG and the SDG policy. They are the factors of sustainability in HEI. Furthermore, it will help and support the Thai university executives to optimize resources spent for achieving better sustainability performance.

2. LITERATURE REVIEW

2.1. Sustainable Development Goals

HEIs are expected to significantly contribute to the SDGs, otherwise known as the Global Goals, build on the Millennium Development Goals (MDGs) especially quality education. The 8 goals that the world committed to achieve by 2015. The UN member countries signed the declaration in September 2000 to combat poverty, hunger, disease, illiteracy, environmental degradation, and discrimination against women. SDGs are illustrated as Figure 1 consist of 17 goals that are "the global goals" to be achieved by 2030.

Figure 2.1. 17 Sustainable Development Goals (SDGs) [7]

2.2. University Ranking System

HEIs have been ranked by many organizations: some are listed in Table 1. While most of the ranking systems focus on academic performance, only 8 URSs from 34 URS (only 23.53%) focus on Sustainability in Higher Education (SHE).

Out of these university ranking institutions, THE is deemed as one of the most well-known institution. There were a total of 1,396 universities ranked, some 11,554 scholars from 135 countries took part of THE World University Rankings (THEWUR) in 2019 [8]. In 2019, there were 16 pioneer Thai universities ranked in the THEWUR. They apply to all the SDGs criteria [9].

2.3. Times Higher Education University Impact Rankings

THE launched the THE University Impact Rankings (THEUIR) in October 2018, which rank the key performance index and contribution of universities towards the SDGs [9]. The 2018 version (the first version) focused on 11 SDGs deemed more relevant to university operations. The level of relevance of SDGs to universities is presented as Figure 2. Based on THE study of the 17 SDGs, there are only 11 SDGs that were at least 30% relevant to HEI's operation. THEUIR except the SDGs had the level of relevance less than 30% as Goal 1: No Poverty, Goal 2: Zero Hunger, Goal 6: Clean Water and Sanitation, Goal 7: Affordable and Clean Energy, Goal 14: Life Below Water, and Goal 15 Life on Land.

In October 2019, THE launched the new version of THEUIR, the 2.0B 2019-0903 version, which then covered all 17 SDGs. THEUIR encourage the universities to submit data for at least four SDGs, that must include SDG 17 – partnerships for the goals. The score calculation formula consists of the mandatory SDG 17 and the scores from the best 3 SDG scores as Equation 1 [9].

$$\text{SDG } 17+\text{SGD A}+\text{SDG B}+\text{SDG C}=100\% \quad (2.\ 1)$$

And the weight of scores are in Equation 2 [9].

$$(22\%*\text{SDG } 17)+26\%*(\text{SDG A}+\text{SDG B}+\text{SDG C})=100\% \quad (2.\ 2)$$

This method was designed to allow universities to participate as widely as possible. The methodology was made flexible considering that different universities in different region may have different priorities and statuses on the SDGs.

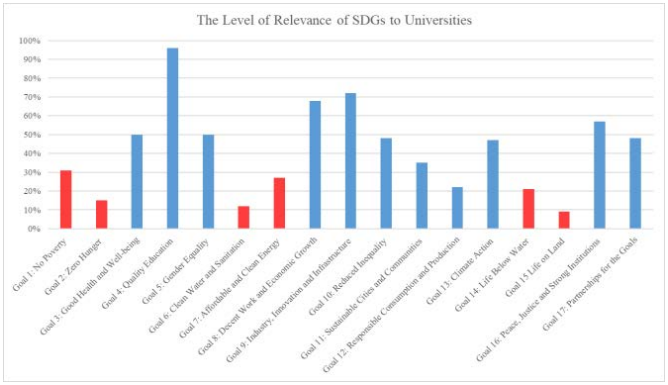

Figure 2.2. The Level of Relevance of SDGs to Universities

2.4. Thai Higher Education Institution (THEI)

Thai education system was mapped and presented in Figure 4. It shows how a young child went to kindergarten for studying and passed to an elementary school (“Prathom” in Thai). After that, they can choose between two paths; a general path toward higher education and a vocational path. For the general path, the students would go to junior high school followed by high school (“Mathayom 1-6” in Thai).

If they choose a junior high school (“Mathayom 1-3”), they will study at a technical college or a senior high school (“Mathayom 4-6”). Council of University Presidents of Thailand (CUPT) officially developed and launched the new entrance system called Thai University Central Admission System (TCAS) in 2018.

TCAS solve the problem of students taking too many university entrance exams, as well as too much emphasis on tutoring schools. Thai students must pass TCAS examination to entrance in a public university or they can apply to an open university that does not require one. Graduates at bachelor level work in a startup, small or medium enterprises, large corporates, or governmental instrumentalities.

3. RESEARCH METHODOLOGY

3.1. Research Framework

We followed the steps in Figure 4 as described below.

Figure 3.1. Research framework

Step 1: we set the sample size to be at least 400 persons, calculated by Yamane's formula [39]. The sample size consists of 2 groups of samples 1) 340 students and 2) 60 lecturers.

Step 2: we searched the literature for keywords - SDGs; HEIs; THEI; SHE; University Impact Ranking - to find the gaps in research on SDGs for THEI. A questionnaire as an assessment tool was developed for SDGs and THEUIR criteria that we discuss in part B.

Step 3: we will analyze the questionnaire responses. We aim to find community needs and demands as guides for SDG policy implementation.

Step 4: we will set up a focus group containing members of our academic management team and other THEI staff to discuss, prioritize, and summarize SDG policies for THEI. This research will help them to form SDG policies and implement them.

3.2. Developing the questionnaire as an assessment tool

We designed a questionnaire consisting of 149 questions, as the quantitative and qualitative tools. The 3 sections of the questionnaire in Figure 5 are described below. The questionnaire was designed based on general information; the independent variables, identified as the community wants, that we call "X factors"; and dependent variables, suggested for policy implementation that we call "Y factors".

Section I: General information

This section consists of 10 questions. It aims to collect demographic information of the respondents including name surname, university, address, department, faculty, position, experience, gender, age, and income.

Section II: Awareness towards SDGs

This section consists of 70 questions. It aims to collect information regarding the level of awareness of the respondents towards SDGs (X Factors).

Section III: Perceptions on policy related to SHE

This section consists of 69 questions. It aims to collection information regarding perception and priorities of the respondents towards different policies related to SHE (Y Factors).

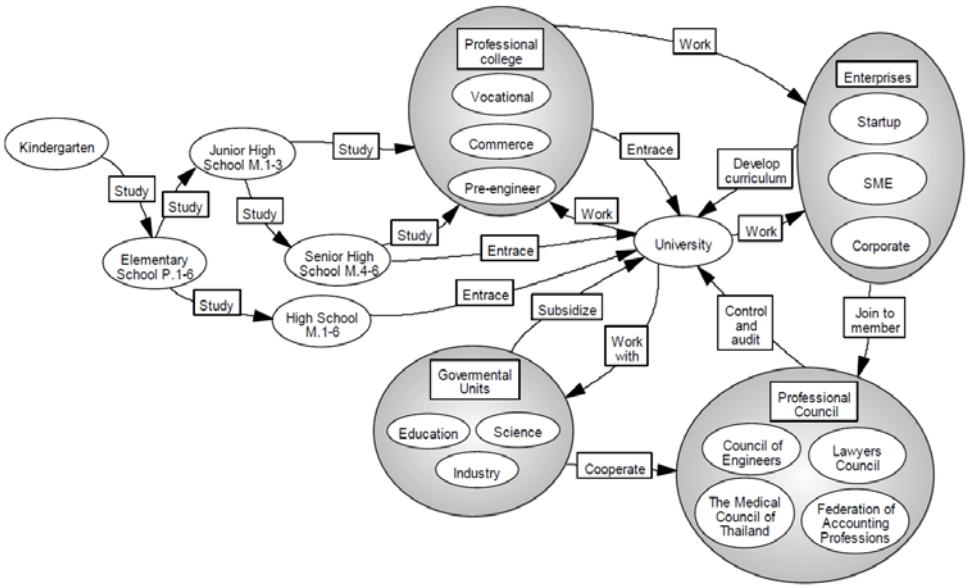

Figure 3.2. THEI systems: [38]

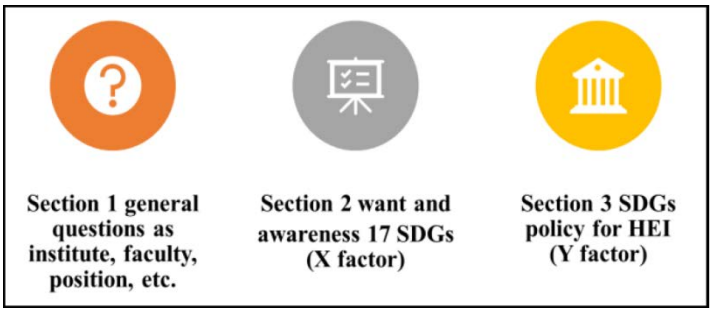

Figure 3.3. Sections of the SDGs questionnaire

We designed the linkage of relationships between awareness towards SDGs called SDG X, and perceptions on policy related to SHE called SDG Y based on the Structural Equation Modeling (SEM) method. The factors will be analyzed with SEM to identify the underlying factors and relationships from the responses. It can see the relationships between SDGx 1 and SDGx 1.1, SDGx 1.2, and SDGx 1.3. These arrows point from the latent variables to the manifest variables. It can see the relationships between SDGy 1 and SDGy 1.1, SDGy 1.2, and SDGy 1.3. SEM uses the convention that the measurements of the manifest variables. SDGx 1 was caused by the latent variables, such as SDGx 1.1, SDGx 1.2, and SDG 1.3.

Table 1 University Ranking Organization [10]-[18]

URS	Developer	Website	Green Metrics/ SDGs Metrics
A National Report Card on Environmental Performance and Sustainability in Higher Education [19]	National Wildlife's Federation's State of the Campus Environment (SCE)	n/a	
Adaptable Model for Assessing Sustainability in Higher Education (AMAS) [20]	Pontificia Universidad Católica de Chile	n/a	
Alternative University Appraisal (AUA) [21]	Hokkaido University and United Nations University	global.hokudai.ac.jp	/
Auditing Instrument for Sustainability in Higher Education (AISHE) [22]	Dutch Foundation for Sustainable Higher Education	niko.roorda.nu	/
Business School Impact System (BSIS) [23]	EFMD Global Network	efmdglobal.org/assessments/bsis	
Campus Sustainability Assessment Framework (CSAF) [24]–[26]	Linsay Cole, University of Victoria, Canada	n/a	
German Centre for Higher Education Development (CHE)	Centrum für Hochschulentwicklung (CHE), German	che.de	
College Scorecard	Department of Education, U.S.	collegescorecard.ed.gov	
College Sustainability Report Card (CSRC) [27]	Sustainable Endowments Institute	greenreportcard.org	/
CSA Framework [28]	Western Michigan University	n/a	

Table 1 Continued

URS	Developer	Website	Green Metrics/ SDGs Metrics
Webometrics	Cybermetrics Lab, the Consejo Superior de Investigaciones Científicas (CSIC), Spain	webometrics.info	
DPSEEA-Sustainability Index Model (D-SiM) [29]	Waheed, Khan, and Veitch (2011)	n/a	
Global Reporting Initiative's Sustainability Report	Global Reporting Initiative (GRI)	globalreporting.org	/
Good Company's Sustainable Pathways Toolkit (SPT) [30]	University of Oregon	n/a	
Graphical Assessment of Sustainability in Universities (GASU) [31]	Rodrigo Lozano, Cardiff University	n/a	
Graz Model of Integrative Development (GMID)	University of Graz, Austria	regional-centre-of-expertise.uni-graz.at/en/research/resources-downloads/graz-model-for-integrative-development	
IREG Observatory on Academic Ranking and Excellence	International Rankings Expert Group Observatory (IREG)	ireg-observatory.org	
Penn State Indicators Report (PENN) [32]	Pennsylvania State University	n/a	

Table 1 Continued

URS	Developer	Website	Green Metrics/ SDGs Metrics
People and Planet's University League (P&K)	People & Planet Student Activities Limited	peopleandplanet.org	
QS World University Rankings (QSWUR)	QS Quacquarelli Symonds (QS)	qs.com	
Scimago Institutions Rankings (SIR)	Scimago Lab, SRG S.L.	scimagoir.com	
Academic Ranking of World Universities (ARWU)	Shanghai Ranking Consultancy	shanghairanking.com	
Sustainability Assessment of Food and Agriculture Systems (SAFA) [33]	Food and Agriculture Organization (FAO)	fao.org/nr/sustainability/sustainability-assessments-safa	/
Sustainability Assessment Questionnaire (SAQ) for Colleges and Universities [34]	Association of University Leaders for a Sustainable Future (ULSF)	ulsf.org/sustainability-assessment-questionnaire	
Sustainability Self-assessment Concept for Higher Education Institute	German Commission for UNESCO (DUK)	n/a	
Sustainability Tool for Auditing for University Curricula in Higher Education	Rodrigo Lozano, University of Gävle, Sweden	n/a	
Sustainability Tracking, Assessment and Rating System (STARS) [26], [35]	Association of the Advancement of Sustainability in Higher Education (AASHE)	stars.aashe.org	/

Table 1 Continued

URS	Developer	Website	Green Metrics/ SDGs Metrics
Assessment of Higher Education Learning Outcomes (AHELO)	The Organisation for Economic Co-operation and Development (OECD)	oecd.org/site/ahelo	
Three-dimensional University Ranking (TUR)	University of Maribor	n/a	
Times Higher Education University Impact Rankings (THEUIR)	Time Higher Education (THE)	timeshighereducation.com	/
US News and World Report (USNWR)	U.S. News & World Report	usnews.com/rankings	
UI Green Metric University Rankings	University of Indonesia, Indonesia	greenmetric.ui.ac.id	/
U-Multirank's approach to university rankings	U-Multirank	umultirank.org	
Unit-based Sustainability Assessment Tool (USAT) [36], [37]	United Nations Environment Programme (UNEP) and Rhodes University, South Africa	auc.org.uk/theplatform/usat_unit-based_sustainability_assessment_tool	

3.3. Validity and Reliability of the Questionnaire

The questionnaire was checked for the both validity and reliability using

Cronbach's Alpha

The questionnaire was checked for reliability by function Analyze > Scale > Reliability Analysis in IBM SPSS Statistics 20. Cronbach's Alpha must be greater than 0.6 [40, 41].

Domain Experts

We invite five domain experts (see Table 2) to validate the questionnaire by using an Index of Item-Objective Congruence (IOC) method. IOC developed by Rovinelli and Hambleton

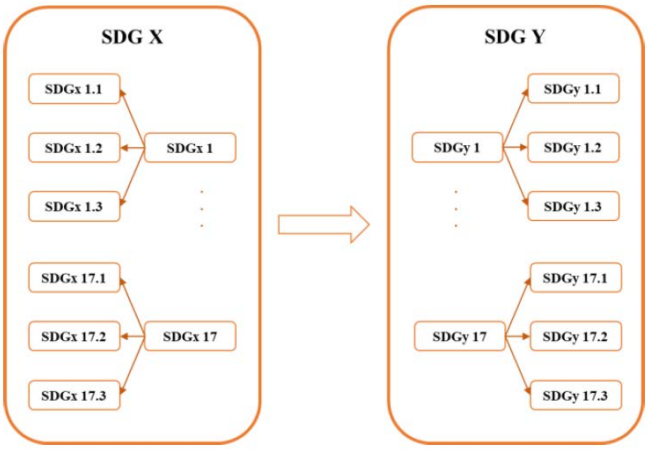

Figure 3.4. Structure and Relation of the SDG X and SDG Y factors

(1977) [42] is a procedure used in test development for evaluating content validity when we design the factors stage. IOC should be greater than 0.6 [43].

Table 2 Domain Experts

Name	Position, Organization
Dr. Kankanit Kamolkittiwong	Head of Logistics Management Department, Faculty of Business Administration, Rangsit University, Thailand
Dr. Chodchanok Attaphong	Assistant Professor, Department of Civil Engineering, KMITL
Adhipat Warangkanand	Consultant, UNFPA Thailand and UNICEF Thailand
Dr. Weerawit Lertthaitrakul	Associate Dean, School of Logistics and Supply chain, Sripatum University, Thailand
Dr. Pornsri Laurujisawat	Lecturer, Faculty Administration and Management, KMITL

4. RESULTS AND DISCUSSION

Briefly, the reliability of the assessment tool was measured using Cronbach's alpha. Cronbach's alpha is 0.992, which means the items of the questionnaire are constructed and connected to the inter-relatedness. The corrected item-total correlation (discrimination) are 0.311 – 0.890 for a trial sample of 50 respondents (see Tables 3 and 4), and the IOC 0.600 - 1.000 [43], that mean the high of validity and reliability of the questionnaire.

Table 3 SDG X Factors from The Trial

SDGs (Cronbach's Alpha = 0.992)	Corrected Item-Total Correlation (Discrimination)			
	SDGx	*SDGx.1*	*SDGx.2*	*SDGx.3*
SDG 1: No poverty	0.458	0.392	0.342	0.418
SDG 2: Zero hunger	0.462	0.491	0.517	0.391
SDG 3: Good health and well-being	0.586	0.523	0.581	0.311
SDG 4: Quality education	0.534	0.564	0.722	0.646
SDG 5: Gender equality	0.702	0.623	0.750	0.739
SDG 6: Clean water and sanitation	0.789	0.783	0.850	0.767
SDG 7: Affordable and clean energy	0.761	0.890	0.875	0.816
SDG 8: Decent work and economic growth	0.760	0.842	0.825	0.758
SDG 9: Industry, innovation, and infrastructure	0.716	0.840	0.827	0.784
SDG 10: Reduced inequalities	0.751	0.861	0.772	0.733
SDG 11: Sustainable cities and communities	0.784	0.735	0.785	0.826
SDG 12: Responsible consumption and production	0.817	0.789	0.782	0.774
SDG 13: Climate action	0.786	0.726	0.820	0.871
SDG 14: Life below water	0.788	0.782	0.791	0.819
SDG 15: Life on land	0.777	0.763	0.692	0.767
SDG 16: Peace, justice and strong institutions	0.783	0.797	0.613	0.649
SDG 17: Partnerships for the Goals	0.768	0.716	0.733	0.720

Source: IBM SPSS Statistics 20

After that, we will diffuse the SDGs questionnaire, throughout the 16 pioneer THEIs. Next, the statistical results will be prioritized by the focus group. Finally, we will form SDG policy guidelines and implementation suggestions for THEI to implement and improve their THE rankings also.

The X factors and the Y factors link systems together, that can balance between demand (community wants) and supply (SDGs policy). Moreover, the results help us to push and drive THEIs in the same direction, and align them to the 17 SDGs, at the same time. We expect that this study will be used by Thai university executives to optimize resources spent for achieving better sustainability performance.

Table 3 SDG Y Factors from The Trial

SDGs (Cronbach's Alpha = 0.992)	Corrected Item-Total Correlation (Discrimination)			
	SDGy	*SDGy.1*	*SDGy.2*	*SDGy.3*
SDG 1: No poverty	0.676	0.811	0.673	0.590
SDG 2: Zero hunger	0.768	0.719	0.730	0.713
SDG 3: Good health and well-being	0.792	0.720	0.684	0.499
SDG 4: Quality education	0.722	0.711	0.600	0.617
SDG 5: Gender equality	0.695	0.651	0.700	0.720
SDG 6: Clean water and sanitation	0.824	0.725	0.557	0.679
SDG 7: Affordable and clean energy	0.713	0.628	0.770	0.711
SDG 8: Decent work and economic growth	0.738	0.505	0.599	0.728
SDG 9: Industry, innovation, and infrastructure	0.753	0.659	0.619	0.676
SDG 10: Reduced inequalities	0.743	0.803	0.585	0.687
SDG 11: Sustainable cities and communities	0.723	0.662	0.604	0.564
SDG 12: Responsible consumption and production	0.775	0.739	0.697	0.631
SDG 13: Climate action	0.757	0.604	0.577	0.655
SDG 14: Life below water	0.749	0.617	0.636	0.727
SDG 15: Life on land	0.755	0.698	0.595	0.679
SDG 16: Peace, justice and strong institutions	0.732	0.690	0.683	0.485
SDG 17: Partnerships for the Goals	0.705	0.622	0.698	0.549

Source: IBM SPSS Statistics 20 by the author

5. ACKNOWLEDGMENT

We thank our colleagues in the Ph.D. program in Logistics and Supply Chain Management, Faculty of Engineering, KMITL for support with valuable knowledge and information sharing. We also thank the Faculty of Engineering, KMITL, for funding this research.

6. BIOGRAPHIES

Siripong Jungthawan is a Ph.D. student majoring in Logistics and Supply Chain Management, Department of Civil Engineering, Faculty of Engineering, KMITL, and a senior professional engineer in industrial engineering. His interests are in SDGs, digital transformation, lean management, logistics and supply chain management, and systems approaches. He wrote the best selling book LEAN series in Thailand.

Ronnachai Tiyarattanachai is an associate professor in Department of Civil Engineering, Faculty of Engineering, KMITL. He received his Ph.D. in Environmental Sciences (Environmental Policy Concentration) from the New Jersey Institute of Technology. Prior to joining KMITL, he worked as an engineer in the Remedial Design group of the Louis Berger Group, Morristown, New Jersey.

7. REFERENCES

[1] United Nations, "Transforming Our World: The 2030 Agenda for Sustainable Development," 2016.

[2] United Nations Development Programme (UNDP), "What does it Mean to Leave No One Behind? A UNDP discussion paper and framework for implementation," 2018.

[3] UN Sustainable Development Group (UNSDG), "Leaving No One Behind: A UNSDG Operational Guide for UN Country Teams," 2019.

[4] Minister of Foreign Affairs, "Statement by the Prime Minister of the Kingdom of Thailand at the Opening Ceremony of the 52nd ASEAN Foreign Ministers' Meeting and Related Meetings," 2019.

[5] Minister of Foreign Affairs, "Thailand's voluntary national review on the implementation of the 2030 agenda for sustainable development, June 2018," 2018.

[6] Times Higher Education (THE), "User Guide THE University Impact Rankings," 2019.

[7] United Nations, "Sustainable Development Goals: Guidelines for the Use of the SDG Logo Including the Colour Wheel, and 17 Icons," 2019.

[8] Times Higher Education, "THE World University Rankings," United Kingdom, 2020.

[9] Times Higher Education (THE), "Data Colleciton Portal: THE University Impact Rankings Version 1.5.1," United Kingdom, 2018.

[10] M. Davis, "Can College Rankings Be Believed?," She Ji, vol. 2, no. 3, pp. 215–230, 2016.

[11] M. Torres-samuel, C. L. Vásquez, M. L. Cardozo, N. Bucci, A. Viloria, and D. Cabrera, "Clustering of Top 50 Latin American Universities in SIR, QS, ARWU, and Webometrics Rankings," in Procedia Computer Science, 2019, vol. 160, pp. 467–472.

[12] K. S. Reddy, E. Xie, and Q. Tang, "Higher education, high-impact research, and world university rankings: A case of India and comparison with China," Pacific Sci. Rev. B Humanit. Soc. Sci., vol. 2, no. 1, pp. 1–21, 2016.

[13] G. Abramo and C. A. D'Angelo, "Evaluating university research: Same performance indicator, different rankings," J. Informetr., vol. 9, no. 3, pp. 514–525, 2015.

[14 H. Jöns and M. Hoyler, “Global geographies of higher education: The perspective of world university rankings,” Geoforum, vol. 46, pp. 45–59, 2013.
[15] B. Millot, “International rankings: Universities vs. higher education systems,” Int. J. Educ. Dev., vol. 40, pp. 156–165, 2015.
[16] A. Pavel, “Global university rankings - a comparative analysis,” in Economics and Finance, 2015, vol. 26, pp. 54–63.
[17] A. Lauder, R. Fitri, N. Suwartha, and G. Tjahjono, “Critical review of a global campus sustainability ranking : GreenMetric,” J. Clean. Prod., vol. 108, pp. 852–863, 2015.
[18] Global University Network for Innovation (GUNI), Implementing the 2030 Agenda at Higher Education Institutions: Challenges and Responses. Barcelona: Global University Network for Innovation (GUNI), 2019.
[19] National Wildlife Federation, “Campus environment 2008: : A National Report Card on Sustainability in Higher Education,” Philadelphia, 2008.
[20] F. J. Urquiza, “Adaptable Model to Assess Sustainability in Higher Education: Aplication to Five Chilean Institutions,” PONTIFICIA UNIVERSIDAD CATÓLICA DE CHILE ESCUELA DE, 2013.
[21] Dzulkifli Abdul Razak, Zainal Abidin Sanusi, Govindran Jegatesen, and Hamoon Khelghat-Doost, “Alternative University Appraisal (AUA): Reconstructing Universities’ Ranking and Rating Toward a Sustainable Future,” Sustain. Assess. Tools High. Educ. Institutions, pp. 139–154, 2013.
[22] P. Pipjelink, “AISHE - Auditing Instrument for Sustainability in Higher Education,” Econ. Transdiscipl. Cogn., vol. 14, no. 1, pp. 461–467, 2011.
[23] EFMD Global Network, “The Key Tool for Measuring your Business School’ s Impact on the World Around It,” Geneva, 2014.
[24] Z. F. Fadzil, H. S. Hashim, A. I. Che-Ani, and S. Aziz, “Developing a Campus Sustainability Assessment Framework for the National University of Malaysia,” in World Academy of Science, Engineering and Technology, 2012, vol. 6, no. 6, pp. 751–755.
[25] O. Saadatian, E. Salleh, O. M. Tahir, L. C. Haw, and K. Sopian, “A survey on Campus Sustainability Assessment Framework (CSAF) in Malaysia,” J. Des. + Built, vol. 4, no. 1, pp. 9–22, 2011.
[26] L. Cole, “Assessing Sustainability on Canadian University Campuses: Development of a Campus Sustainability Assessment Framework,” 2003.
[27] Sustainable Endowments Institute, “College Sustainability Report Card: A Review of Campus & Endowment Policies at Leading Institutiions,” Cambridge, 2012.
[28] A. Nixon, “Improving the Campus Sustainability Assessment Process,” Western Michigan University, 2002.
[29] B. Waheed, F. I. Khan, and B. Veitch, “Developing a Quantitative Tool for Sustainability Assessment of HEIs,” Int. J. Sustain. High. Educ., vol. 12, no. 4, pp. 355–368, 2011.
[30] G. Company, “Sustainability Assessment of the University of Oregon,” 2002.
[31] R. Lozano, “A Tool for a Graphical Assessment of Sustainability in Universities (GASU),” J. Clean. Prod., vol. 14, pp. 963–972, 2006.
[32] Pennsylvania State University, “Penn State Indicators Report 2000: Steps Toward A Sustainable University,” 2000.
[33] Food and Agricuture Organization of the United Nations, “Sustainability Assessment of Food and Agriculture Systesm (SAFA Tool) User Manual version 2.2.40,” Rome, 2014.

[34] Association of University Leaders for a Sustainable Future, “Sustainability Assessment Questionnaire (SAQ) for Colleges and Universities,” 2009.
[35] D. M. Salvioni, S. Franzoni, and R. Cassano, “Sustainability in the Higher Education System: An Opportunity to Improve Quality and Image,” Sustainability, vol. 9, no. 6, pp. 1–27, 2017.
[36] Togo, Muchaiteye and H. Lotz-Sisitka, Unit-Based Sustainability Assesment Tool: A Resource Book to Complement the UNEP Mainstreaming Environment and Sustainability in African Universities Partnership. 2009.
[37] M. Togo, “Sustainability Assessment Using a Unit-based Sustainability Assessment Tool: The Case of Three Teaching Departments at Rhodes University, South Africa,” South. African J. Environ. Educ., vol. 25, 2008.
[38] S. Jungthawan, V. Suharitdamrong, and R. Tiyarattanachai, “Applying Systems Approach the Case Study of Tertiary Education Institutions in Thailand,” in 2019 IEEE 6th International Conference on Industrial Engineering and Applications, ICIEA 2019, 2019, no. 6, pp. 682–688.
[39] T. Yamane, Statistics: an Introductory Analysis. Harper & Row, 1973.
[40] L. J. Cronbach, “Coefficient Alpha and the Internal Structure of Tests,” Psychometrika, vol. 16, no. 3, pp. 297–334, 1951.
[41] M. Tavakol and R. Dennick, “Making Sense of Cronbach’s Alpha,” Int. J. Med. Educ., vol. 2, pp. 53–55, 2011.
[42] R. J. Rovinelli and R. K. Hambleton, “On the Use of Content Specialists in the Assessment of Criterion-referenced Test Item Validity,” Lab. Psychom. Eval. Res. Rep., vol. 24, 1976.
[43] R. C. Turner and L. Carlson, “Indexes of Item-Objective Congruence for Multidimensional Items,” Int. J. Test., vol. 3, no. 2, pp. 163–171, 2003.

Development of locally designed smart bike-sharing system on Thai campus: Lessons learnt of a pilot-scale study

Chitsanu Pakdeewanich[1] , Ronnachai Tiyarattanachai[2] and Isara Anantavrasilp[3]

Faculty of Engineering, King Mongkut's Institute of Technology Ladkrabang, Ladkrabang, Bangkok, 10520, Thailand

E-mail: 60610003@kmitl.ac.th, ronnachai.ti@kmitl.ac.th and isara.an@kmitl.ac.th

Abstract.

Campus-wide bike-sharing program is one of the solutions for achieving sustainability in higher education. It also contributes to the UN's Sustainable Development Goals (SDGs). Smart bike-sharing systems have been implemented in some Thai cities and Thai universities since 2012. The systems were provided by foreign companies and developers. A locally designed smart bike-sharing system have been developed and pilot-scale tested at a Thai university. Many problems were found throughout the test-period, while design changes and application modifications were conducted to address the issues. The changes were done to make the system appropriate for the context of Thai university and users' demands. This paper discusses the development process and lessons learnt from this locally designed system. The results can be used by developers and software designers of bike-sharing industry to provide better design and implementation for Thailand market.

Keywords. bike-sharing program, sustainability, sustainability in higher education.

1. INTRODUCTION

Bike-sharing systems have been around for about 50 years. The White Bikes in Amsterdam, the Netherlands was the first system with the first system implemented in 1965 [1]. The purpose of public bicycle is to ride short distances or first or last mile trips. Also, these programs were developed for people who have to connect to other public transportations, for example, subways and buses. Bike-sharing programs reduce personal car usage and traffic jams in peak hours. Shared bikes, also, allow environmentally friendly transport, which is a part of UN's Sustainable Development Goals (SDGs). part of UN's Sustainable Development Goals (SDGs).

Bike-sharing programs have been implemented in more than 700 cities around the world [2]. It showed that people were interested in low-priced and eco-friendly transportation. Many startup companies were established in the 2000s, for example, Ofo

(China), Mobike (Singapore) and Lime (US). Bike-sharing services and accessibility have been continuously improved to support the lifestyle of the younger generation. A second generation of bike-sharing systems added stations and coin deposits for riders, but there were problems with theft and accessibility. Third generation systems allowed easy log in by smartphone or smart cards. Also, Global Positioning System (GPS) was used for identifying bicycles in an area. Some systems were developed to be 'station-free' systems, where users could ride anywhere in a designated area

In 2012, Thailand had a bike-sharing system in Bangkok, 'PUN PUN', which was implemented by the Bangkok Metropolitan Administration (BMA). This program is deemed one of the first step in sustainable transportation. Meanwhile, Thai universities were influenced by UN's Sustainable Development Goals (SDGs). Several Thai universities provided shared bikes on campus including Asian Institute of Technology (AIT), Chulalongkorn University (CU), Khon Kaen University (KKU), King Mongkut's Institute of Technology Ladkrabang (KMITL), King Mongkut's University of Technology North Bangkok (KMUTNB), Kasetsart University (KU), Naresuan University (NU), Phranakhon Rajabhat University (PRU), Prince of Songkla University (PSU), Rajamangala University of Technology Thanyaburi (RMUTT), Thammasat University (TU), University of Phayao (UP) and Huachiew Chalermprakiet University (HCU).

Some studies found that bike-sharing systems were mostly used by younger generation [3]. Many universities supported this sustainable transportation mode and provided shared bicycle for students, staff and visitors. Some universities cooperated with private companies to provide such program. For example, KU has signed Memorandum of Understanding (MOU) with Mobike to launch bike-sharing program on campus. Some of them were coordinated with local government to develop program. For example, CU and BMA have developed station-based bike-sharing program together on campus.

In the United States, there are awards granted for bikesharing system on campus so-called "Bicycle Friendly University (BFU) Award". Examples of BFU awards are presented in Table 1 [4].

Table 1 Examples of BFU Awards

University	BFU since	Awards
Colorado State University	2011	Platinum
Stanford University	2011	Platinum
The University of Arkansas	2016	Gold
University of California, Los Angeles	2011	Gold
The Ohio State University	2011	Silver
University of Illinois at Urbana-Champaign	2011	Silver
University of Massachusetts Lowell	2015	Silver
California State University Northridge	2019	Bronze
Kent State University	2016	Bronze
University of Buffalo	2012	Bronze

Based on BFU Awards list, most universities used a campus bike plan for increasing campus rider numbers. In Thailand, bike-sharing system on campus contributed to the SDGs. Many Thai universities started bike-sharing program in the 2000s. Most of them provided bike-sharing systems by signing contracts with private companies. Some of them created systems themselves: one example of self-system development is KMITL Bike.

KMITL Bike, a dockless bike-sharing program, was first launched as a senior project of International College, KMITL. Three software engineering students were interested in a universal locking system for public bicycles, started in 2017: its purpose was to develop locking system for public bicycles. They aimed to develop the system to provide shared bicycles through mobile application on KMITL Bangkok campus. To overcome different kinds of problems throughout the development and service periods, several changes were made. This study summarizes the development of KMITL Bike in each phase along with the lessons learnt and solutions. The findings can be adopted by bicycle manufacturers and software developers to optimize their design for the broader markets using KMITL Bike as a case study.

2. LITERATURE REVIEW

Campus bike-sharing programs were discussed in many aspects. Some universities developed their own systems. For example, Yi and Nie designed an efficient mobile system based on Android system aiming to improve travel for students at institutions of higher education in China. They claimed that most ofthe younger generations used their phone 4.5 hours per day in China, so their system engaged students with information on bike-sharing and entertainment together [5]. Rachman et al. discussed the distribution system of campus bike sharing for increasing bike service availability in Telkom University, Bandung, Indonesia. They offered a new bike-sharing system based on Internet of Thing (IoT). They used Message Queue Telemetry Transport (MQTT) as a communication method between bicycle and bike station. Riders was noticed about available station via LCD screen on a bicycle [6]. Mete et al. analyzed the possible stations of bikesharing on the Gaziantep University campus, Turkey by using mathematical models. Their purposes were to cover demand on campus and also minimize walking distances. It was used as input for university administrators considering the bikesharing stations, but it did not interact with other public transportations and consider the cost of the system [7]. Kellstedt et al. launched and examined the free-floating bikesharing program on campus; most of riders were students who lived on campus. Cost was a main barrier to cycling. Also, publicity needed to be improved [8]. Kaplan developed a bikesharing program at Kent State University, USA. There were 60% of students who can connect to a shared bike. He surveyed the students for demand and studied the possibility of a third generation bike-sharing program, including financial issues. Finally, he provided options of the third generation bike-sharing program at Kent State University. Also, he compared fixed and variable cost based on several private companies [9].

Some researchers focused on a feasibility of a campus bike-sharing program. Ashley studied bike-sharing programs as alternative transportation in Bridgewater State University, Massachusetts, USA. They started with brainstorming with essential members

of campus and explored the bike-sharing program. Students, staff and others on campus were surveyed for interest and usage of bike-sharing program. Most participants were interested in this program and half of them stated that they would ride the bicycle more than ten times a year [10]. Barrier to cycling were also examined. Manaugh et al. analyzed factors influencing the use or not of campus bikesharing programs. The bicycle lanes were strongly related to a frequency of cycling. Meanwhile, a lack of safety was the most important barriers to increase cycling [11]. Nahal and Mitra compared cycling throughout the year and cycling only in autumn or spring. They studied the barriers to cycling in winter on campus. Less than 30% of respondents commuted in winter. An appropriate plan for bicycle infrastructure may encourage the current cyclists to ride in winter [12].

Many researchers studied factors influencing campus demand. Chevalier et al. studied bicycle acceptance in five universities in Shanghai. They surveyed, over 1,100 respondents about built environment and bike sharing. Limiting speed on cycling and suitable infrastructure were the major issues on campuses. As awareness of environmental impact increased, bike-sharing usage increased on campus [13]. Olio et al. examined the most important variables and the most efficient policies for promoting sustainable transportation on campus. They suggested that management policies could contribute to change in transportation patterns such as usage of private cars and parking on campus. Travel times by bus and shared bike were acceptable, which means that they were efficient alternatives [14]. Other factors were also studied, for example, socio-demographic factor, travel behavior, weather and temporal variables [15-18]. Research of factors affecting campus usage continued as is still on-going

Many researchers focused on variables and built environment based on systems, which provided by private companies. Some of them studied feasibility to launch bikesharing program on their campuses. A few studies showed that they developed bike-sharing programs by themselves. In Thailand, there were limited researches on the development of campus bike-sharing program. This research focused on development of a locally designed smart bike-sharing system for the KMTIL campus. The pilot scale development is discussed here. A campus scale is discussed in other work [19].

3. DEVELOPMENT OF KMITL BIKE AND LESSONS LEARNT

3.1. KMITL Bike with InfiniLock

KMITL Bike was founded in 2016, as a senior project. Three students of the Software Engineering Program, International College were interested in a locking system for public transportation. Their first reviewed several locking systems implemented in Thailand and other countries, including MU White Bike, CU Bike, MuniBike, weBike, BitLock and Noke [20]. Table 2 compares local and international bike-sharing systems.

Mobile applications were widely used for log in. KMITL Bike used a secure cloud-based lock sharing system called ‘InfiniLock’. Also, the application had nine user activities including Login, Register, Logout, Borrow Bike, Return Bike, Find Bike and View History. Figure 1 shows the use case diagram of the KMITL Bike application.

Table 2 Local and International Bike Sharing Systems

Name	Authentication Tools	BikeLocating	Powering Method
MU White Bike Bangkok	Physical Key and Student ID card	None	None
CU Bike Bangkok	Membership RFID card	None	Rechargeable Battery
MuniBike California	SMS, phone call,mobile application	GPS	Dynamo battery charger
weBike Maryland	SMS with combination lock	None	None
BitLock California	Mobile application	None	Non-rechargeable battery
Noke Utah	Mobile application	Phone's GPS	Rechargeable battery

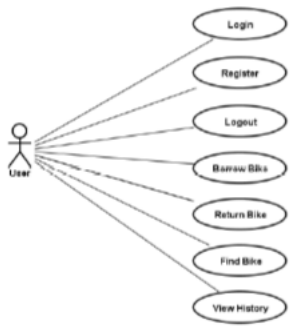

Figure 1 Use case diagram of KMITL Bike application

To lock and unlock the shared bike, they considered that using traditional lock with key or code is not practical. Therefore, automatic wheel lock was developed from scratch. It is equipped with a Bluetooth-based automated locking system. Only authorized users could unlock and ride the bike. Figure 2 shows the first wheel lock design.

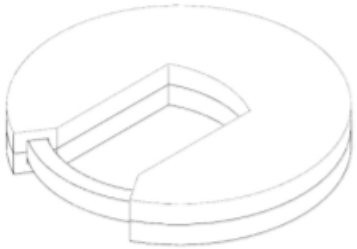

Figure 2 First wheel lock design

The design of wheel lock was reconsidered to adjust some issues. For example, the lock could not detect, if it was locked or not. This was solved by attaching sensor on a bike. Table 3 lists lessons learnt in each of ours three improvements of this design.

Table 3 Design Improvement of Wheel Lock

Design	Description(s)
First design: Cable Locking System	1. The lock could not detect, if it was locked or not 2. It was too fragile to external forces while riding and transporting
Second design: Automated Lock	1. The lock could not detect, if it was locked or not 2. It was too fragile to external forces while riding and transporting
Third design Semi-Automated Lock	1. A new design using teeth-based mechanism was modelled. 2. The battery was used to pull the teeth of the lock package in unlocking process.

Concurrent with the hardware development, they also created an application, ‘KMITL Bike’: its main functions were logging in, borrowing bike, returning bike and finding bike. Figure 3 shows two developments of the KMITL Bike user interface.

Figure 3 First interface of KMITL Bike application

Two types of bicycle were used for initials test, a small bicycle fleet were established. It consists of three city bikes and five commuting bikes. Both kinds of bikes illustrated in Figure 4.

The user must have KMITL email account in order to log in to the system. Then, to borrow a bike, the user must scan barcode on the bike, he wishes to borrow. Then scan barcode on the bike, the application will send unlock command to the lock via Bluetooth connection.

Figure 4 City bike (upper image) and commuting bike (lower image)

Due to the delay in hardware development, the first test adopted passcode to unlock the bike. The second test used barcode to unlock the bike. After tests on the first and the second bike-sharing programs, engineering faculty students and others became interested

in the program. Daily users were clearly increased during both tests as presented on Figure 5.

This project ended in June 2017 as it was still part of the senior project course. They have identified several problems and lessons learnt in the first program. For instance, developing maintainable and scalable programs required more experience and examples and was a challenge for inexperience students. Also, designing the application for public use was challenging as each platform had a different guidelines (i.e., Android application follows Google's Material Design guideline and iOS application follows Apple's iOS Human Interface Guidelines). In addition, hardware controlling parts on both kinds of devices are different.

In the hardware development, 3D printing technology was used. The lock prototypes were developed using 3D printer. However, it took at least eight hours to print each sample. To make the matter worse, the plastic locks are not strong enough for intended purposes. The team then turned to aluminum. Nevertheless, the CNC milling cost is rather high and must be done in a workshop. As a result, development cost and time were high, rendering design iterations difficult. Cost per lock was also much more expensive than plastic counterpart.

Another problem that the team encountered is to find and order all necessary components. This is because the bike has limited space and some parts are expected to have higher durability than usual. Some were ordered and shipped from China, so it took several weeks to arrive.

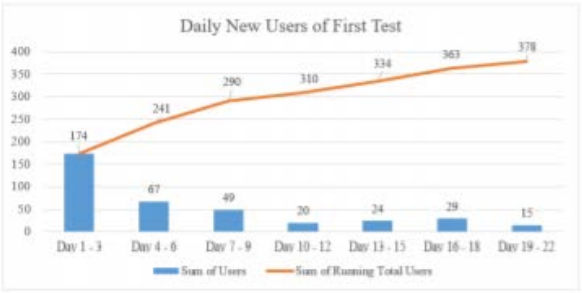

(a) Daily Users – First Test

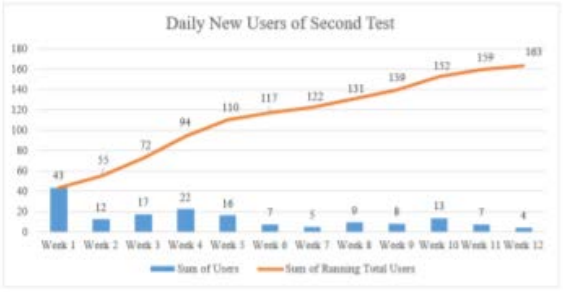

(b) Daily Users – Second Test

Figure 5 Number of Users during (a) First Test and (b) Second Test

3.2. An Extension System of KMITL Bike

Later in August 2017, KMITL Bike was continued by a next senior generation - three students from the department of software engineering. The objectives of their project were to eliminate the problems and to provide more convenient ways for system administrators and the bike maintenance team. They developed an administration application and real-time monitoring system to prevent users from improper actions, such as overloading and not reading instructions.

After investigating other bike-sharing systems (shown in Figure 3), in many major aspects as well as discussing within the team which are the most important features, they decided to add geo-fencing, near real-time tracking and contact administrator features into the system.

Table 4 International Bike Sharing Systems

Name	Authentication Tools	Bike Locating	Penalty
SG Bike	Scan QR code	Geostation device	Fine via user e-wallet
Ofo	Combination lock	GPS	Phone call
Mobike	Scan QR code	GPS	Receive warning
oBike	Scan QR code	GPS	Deduct user's credits

They also found that KMITL Bike created by the previous team was not well design and implemented using outdated technology and libraries. This led to difficulty in creating an extension system, so, they decided to re-construct the application (both Android and iOS application), to support system extension and further development.

In addition to KMITL Bike revamp, the team had developed another app, Bike Admin, which is aimed to assist bike-sharing provider. The features of Bike Admin included showing user status, user history, bike status, bike location and contact user. Figure 6 shows the use case diagram of the new system.

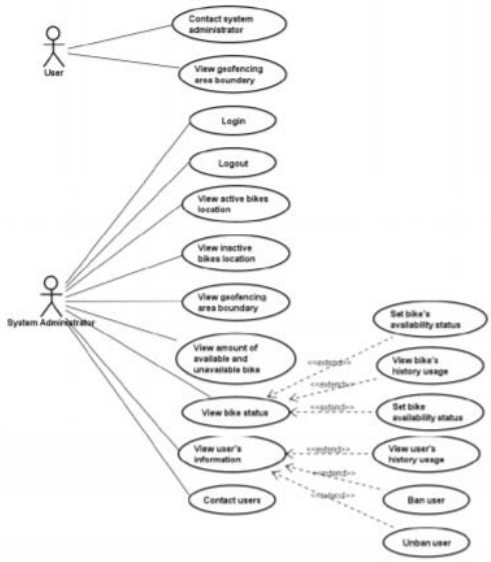

Figure 6 Use Case Diagram of KMITL Bike and Bike Admin Apps

Hardware was also improved. The components in the InfiniLock were replaced several times during the test. In a short period, replacement parts were created by 3D printing, using PLA plastic filament. Figure 7 compares the original and modified mechanism

International College. There was a KMITL team to support users who had problems in using bicycles. This program was developed and discussed in details by Pakdeewanich et al. [19].

4. CONCLUSION AND DISCUSSION

We described development of a locally designed smart campus bike-sharing system, KMITL Bike, as a case study. The use data over the period of 2-year were discussed. The use rates were clearly increased during the pilot study period. The results confirmed that students and staff were interested in sustainable transportation. The admin application and physical assets, especially InfiniLock, were significantly improved.

However, there were a few challenges in the development of a locally designed program, mainly the cost of physical assets and prototypes of the locking system. The design of prototypes of the locking system was analyzed and simulated by programming. This is to be studied further in the future.

In terms of sustainable transport on campus, funding support for physical assets and a number of bicycles should be further studied to provide better use

5. ACKNOWLEDGMENT

We thank our colleagues in the International College, King Mongkut's Institute of Technology Ladkrabang, for support and information sharing. We also thank the Faculty of Engineering, KMITL, for funding this research.

6. REFERENCES

[1] P. DeMaio, "Bike-sharing: History, impacts, models of provision, and future," Journal of public transportation, vol. 12, no. 4, p. 3, 2009.

[2] Earth Policy Institute, "Bike share fact sheet," Earth Policy Institute, 2015. [Online].Available:http://www.earthpolicy.org/images/uploads/press_room/Bicycle_Share.pdf.

[3] E. Eren and V. E. Uz, "A Review on Bike-Sharing: The Factors Affecting Bike-Sharing Demand," Sustainable Cities and Society, p. 101882, 2019.

[4] The League of American Bicyclists, "2019 BFU Awards," The League of American Bicyclists,2019.[Online].Available:https://bikeleague.org/sites/default/files/BFU_Award_ List_2019_only.pdf. [Access Feb 13, 2020].

[5] H.-B. Yi and Z. Nie, "Mobility Innovation through an Efficient Mobile System for Bike Sharing on Campus," in 2017 International Conference on Network and Information Systems for Computers (ICNISC), 2017: IEEE, pp. 153-157.

[6] F. A. Rachman, A. G. Putrada, and M. Abdurohman, "Distributed Campus Bike Sharing System Based-on Internet of Things (IoT)," in 2018 6th International Conference on Information and Communication Technology (ICoICT), 2018: IEEE, pp. 333-336.

[7] S. Mete, Z. A. Cil, and E. Özceylan, "Location and coverage analysis of bike-sharing stations in university campus," Business Systems Research Journal, vol. 9, no. 2, pp. 80-95, 2018.

[8] D. Kellstedt, J. O. Spengler, K. Bradley, and J. E. Maddock, "Evaluation of free-floating bike-share on a university campus using a multi-method approach," Preventive medicine reports, vol. 16, p. 100981, 2019.

[9] D. H. Kaplan, "Developing a bike-sharing program at Kent State University and Kent, Ohio," Ohio Transportation Consortium, 2012.

[10] J. Ashley, "Bike sharing as alternative transportation at Bridgewater State University," Undergraduate Review, vol. 8, no. 1, pp. 16-25, 2012.

[11] K. Manaugh, G. Boisjoly, and A. El-Geneidy, "Overcoming barriers to cycling: understanding frequency of cycling in a University setting and the factors preventing commuters from cycling on a regular basis," Transportation, vol. 44, no. 4, pp. 871-884, 2017.

[12] T. Nahal and R. Mitra, "Facilitators and barriers to winter cycling: case study of a downtown university in Toronto, Canada," Journal of Transport & Health, vol. 10, pp. 262-271, 2018.

[13] A. Chevalier, M. Charlemagne, and L. Xu, "Bicycle acceptance on campus: Influence of the built environment and shared bikes,"Transportation research part D: transport and environment, vol. 76, pp. 211-235, 2019.

[14] L. dell'Olio, M. Bordagaray, R. Barreda, and A. Ibeas, "A methodology to promote sustainable mobility in college campuses,"Transportation Research Procedia, vol. 3, pp. 838-847, 2014.

[15] N. Barbour, Y. Zhang, and F. Mannering, "A statistical analysis of bike sharing usage and its potential as an auto-trip substitute," Journal of Transport & Health, vol. 12, pp. 253-262, 2019.

[16] J. Mattson and R. Godavarthy, "Bike share in Fargo, North Dakota: Keys to success and factors affecting ridership," Sustainable cities and society, vol. 34, pp. 174-182, 2017.

[17] D. M. Scott and C. Ciuro, "What factors influence bike share ridership? An investigation of Hamilton, Ontario's bike share hubs,"Travel behaviour and society, vol. 16, pp. 50-58, 2019.

[18] B. Kutela and H. Teng, "The influence of campus characteristics, temporal factors, and weather events on campuses-related daily bikeshare trips," Journal of Transport Geography, vol. 78, pp. 160-169, 2019.

[19] C. Pakdeewanich, R. Tiyarattanachai, I. Anantavrasilp, "Domestically designed campus smart bike sharing system: Lessons learned and design optimization for Thailand," in 2020 IEEE 7th International Conference on Industrial Engineering and Applications (ICIEA), 2020: IEEE, pp. 721-725.

[20] C. ChanChua, P. Imamnuaysup, S. Chanate, "Universal Locking System: InfiniLock," Thesis, International College, King Mongkut's Institute of Technology Ladkrabang, Bangkok, Thailand, 2016.

Low Wind Speed Wind Turbine Blade Design for Thailand

Natchanon Suppaadirek[1], Noppakoon Saengsuwan[2], Sirichai Tammaruckwattana[3]

[1,2,3] Faculty of Engineering, King Mongkut's Institute of Technology Ladkrabang, Bangkok, Thailand.

Corresponding author; E-mail address: 62601186@kmitl.ac.th[1], 62601255@kmitl.ac.th[2], sirichai.ta@kmitl.ac.th[3]

Abstract.

Renewable energy is a reason why this study has been chosen. In this paper focused on an analysis of the characteristics of the wind when the wind turbine blade is encountered using a commercial fluid dynamics solver such as Fluent by selecting the impact angle of 5, -5, 10, 15, 20, -10, -15 and -20 degrees. Aerodynamic characteristics such as lift coefficient, drag coefficient, lift to drag ratio has been evaluated in this study. Fluent simulation results will be compared with the result of the milling airfoil tested in wind tunnel. Our goal is to a construction of wind turbine in low wind speed country like Thailand

Keywords. Airfoil, Wind turbine blade, lift coefficient, Wind tunnel experiment

1. INTRODUCTION

Nowadays, the increase in energy requirement have been observed due to increasing in technology and industrialization. Energy requirement and development level of the countries have shown parallelism. However, except for renewable energy methods, the other methods in the generation of energy causes to increase greenhouse gas and also, increase global warming. Wind energy is one of the renewable energy sources and wind turbines are used to generate electrical energy by using the kinetic energy of wind.

One of the most important part of wind turbines is their aerodynamic effectiveness, the base of which is the design of the airfoils forming the wind turbine blade shape.

As a major component of wind turbine generator system, blade has been paid more and more attention to, and its design and manufacture have become a kind of hot technology problem [1~3] in wind power industry. The shape, airfoil, materials, number of blades, structure and processing technology of the blade have been deeply studied both at home and abroad [4~7]. Aerodynamic shape which affects the strengths and weaknesses of the whole unit performance is an important factor. On the basis of the previous study [8], by improved the current optimal design method.

In this paper proposes the wind turbine blade shape design and the use of Ansys Fluent. The simulation results obtained from Fluent are compared to the data from real wind tunnel. Airfoil data presented here, were obtained from airfoil tools.

2. AIRFOIL PROFILE DESIGN

An airfoil is the cross-sectional shape of a wind turbine blade, its body moving through a fluid produces an aerodynamic force. The wind come contact with lead edge part of airfoil

Airfoil configuration has been mention in [5]. The component of aerodynamic force perpendicular to the direction of motion is called lift and the component parallel to the direction of motion is called drag, also the angle between the direction of the apparent or relative wind and the chord line of the blade is called Angle of attack.

In this paper NACA 4412 airfoil is considered as base airfoils. NACA 4412 wing profile is a generic geometry frequently used as an industrial and academic test case to validate simulation and experimental methods and it has low drag and increased lift forces at relatively low wind speeds which is suitable for our research that focus on low wind speed turbine.

NACA MPXX, the first digit expresses the maximum camber divided by 100, the second digit gives the position of the maximum camber divided by 10, and the last two digits gives the thickness divided by 100. Thus 4412 has a maximum camber of 4% of chord located at 40% chord back from the leading edge and it thickness is 12% [7].

NACA 4412 Dimension taken from the NACA four digits generator in airfoiltool. After obtained the coordinate data XY from airfoil NACA 4412, the next step is to convert it to Text file using Microsoft Excel in XY coordinate.

The XY coordinate data of NACA4412 are used to draw an airfoil in Fluent ANSYS.

3. AIRFOIL SIMULATION

In this study using the method of Fluent, where the process sequence from Modeling to produce images contours of wind velocity can be described as follows:

- Run ANSYS Workbench in the Fluid Flow (Fluent) category. The first thing to do is to insert XY coordinate data from text file into Geometry block (Design modeler geometry) and draw airfoil from the coordinate point.
- Draw boundary to make a free-stream conditions.
- After finished the geometry, go to meshing.
- After meshing finished, the model parts are generated as Inlet, Outlet, walls and as airfoil surfaces.
- Thereafter the model is run into Fluent version 17.2 by providing airflow velocity rates, external air pressure, material type, experimental temperature, air viscosity, and air density

- After the data are complete, then Fluent can do running by entering the amount of data iteration.
- Create a picture of velocity contour.
- Input angle of attack, lift and drag coefficient equation in parameter box.
- Then the Fluent will calculate lift and drag coefficient base on angle of attack and velocity.

After finishing the simulation process, the program can change into variety velocity image depended on angle of attack that been put into before the calculate sequence, also can calculate lot of aerodynamic data conditional on parameter input.

From our research and another reference that been use in this paper, we can group them into three methods. First method shown wind or pressure behaver upon airfoil which [1] use CATIA to create model and STAR-CCM to simulate. Ananth S Sharma [3] using ICEM-CFD software to mesh model and transfer it into Fluent. Second method is Q-blade technique which [5],[8] focus on obtain the aerodynamics data rather than contour image. Third method use BEM equation to calculated aerodynamics data base on NACA 4412 [7]. Three method detail has shown in Figure. 1.

Method	Paper Reference	Program design	Program Simulation	Lift	Drag	Cl	Cd	Cl/Cd	Cp	Wind Tunnel
Simulation with velocity or pressure contour and collected data	Our	Design modeler	Fluent	✓	✓	✓	✓	✓	✗	✓
	[1]	CATIA	STAR-CCM	✓	✓	✓	✓	✓	✗	✓
	[3]	ICEM CFD	Fluent	✗	✗	✗	✗	✗	✗	✗
Simulation with airfoil image and collected data	[5]	Q-blade	Q-blade	✓	✓	✓	✓	✓	✗	✗
	[8]	Q-blade	Q-blade	✓	✓	✓	✓	✓	✓	✗
Calculated from equation	[7]	BEM	——	✓	✓	✓	✓	✓	✓	✗

Figure 1 Comparison of Simulation Method

In this paper, we use ANSYS fluent to simulate airfoil to collect velocity contour and aerodynamic data such as lift and drag. If we use STAR-CCM+ and ANSYS Fluent to simulate the same thing in same condition, the results reached grid independent solutions with the same mesh size, and the accuracy of the predicted results was similar but with

calculated airflow, ANSYS Fluent performed slightly better, and its userdefined functions were more user-friendly and suitable for low spec pc or laptop[9] ,so that why this paper using Fluent instead of STAR-CCM. Fluent can install the BEM equation to the parameter function and some of the equations are already exist in program. It simpler to use simulation program to generate data rather than calculate the data by hand and simulation is more visualize

In aerodynamic have aerodynamic force called lift and drag, so we also observed and collected lift and drag data to study their behavior compare to vary of velocity and angle of attack. Coefficient Cl and drag coefficient Cd of airfoil are calculated with Fluent with (1) and (2).

$$c_l = \frac{2L}{pv^2A} \tag{1}$$

$$c_d = \frac{2D}{pv^2A} \tag{2}$$

Where, ρ:air density L : Lift D : Drag A : area v :velocity

Base on Fig. 2 as angle of attack increases, the value of lift coefficient also increases to a certain point and then started to decease. Also, the value of lift coefficient also increases when velocity increases when tested in the same angle of attack condition.

We can assume that lift will continue to rise with angle of attack until it reaches maximum value and then started to fall.

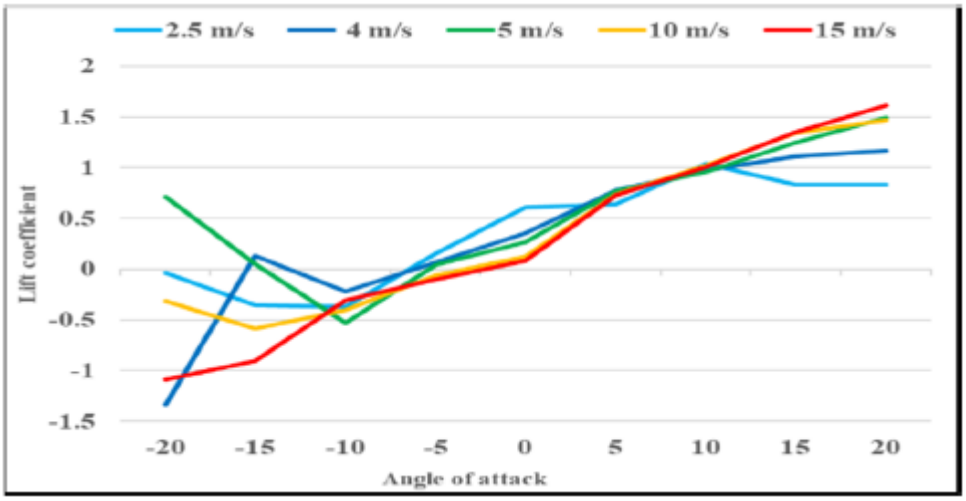

Figure 2 Lift coefficient

Another aerodynamics behavior that also contributes in producing good wind turbine is drag coefficient. The result of drag coefficient is presented in Fig. 3. It was show that, the drag coefficient is increased as angle of attack or velocity with an exception when drag reach its maximum value and start to fall down. In actual of wind turbine blade development, a resistant drag force which opposes the motion of the blade must also be minimum, so the main point is to minimize the drag force in order to make the lift more dominance.

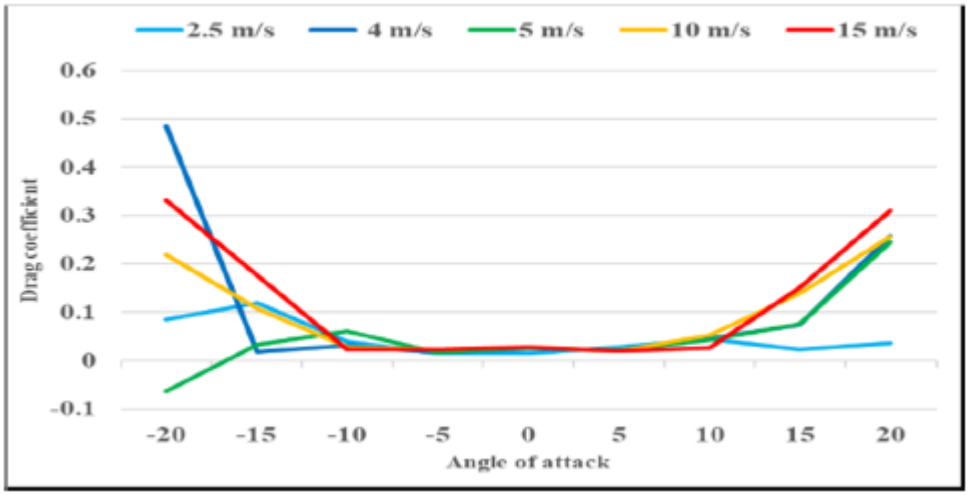

Figure 3 Drag coefficient

This result also relatively conflict with requirement of maximizing the lift coefficient to compensate the drag coefficient produced because lift coefficient and drag coefficient increases in the same way

In this case, we have to calculate lift to drag ratio to determine how much the dominance of lift coefficient compare to drag coefficient in each angle of attack .We can calculate lift to drag ratio with (3). The results will specify which angle of attack had to be choose as an appropriate point. High lift to drag ratio means that drag is less effective on that airfoil. Fig. 4 show the results of lift to drag ratio with the vary of velocity and angle of attack in graph.

$$Lift\ to\ drag\ ratio = \frac{Coefficient\ of\ Lift}{Coefficient\ of\ Drag} = \frac{C_L}{C_D} \tag{3}$$

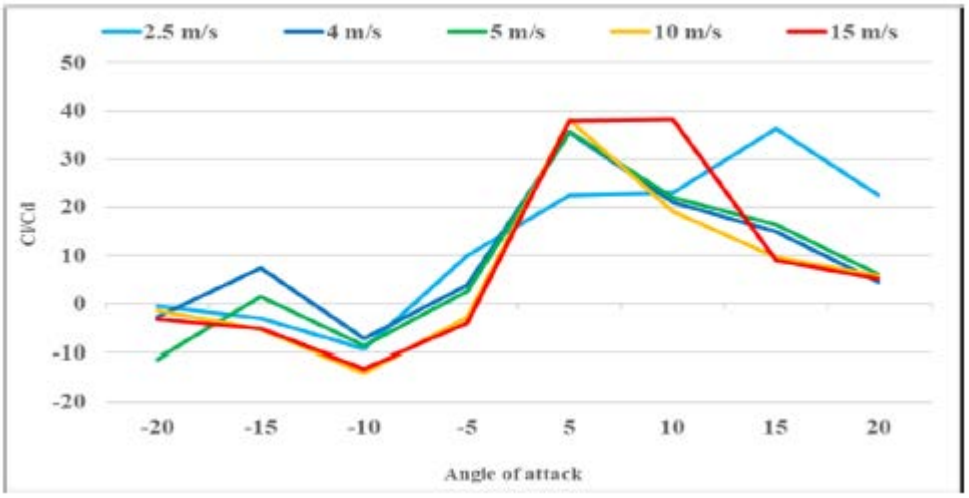

Figure 4 Graph of Lift to Drag Ratio

As you can see in Fig. 4 the maximum lift to drag ratio in each wind speed are not the same. For 15m/s the maximum lift to drag ratio is at 10°, for 5m/s is 5° and similar to 4m/s. We also can be observed that lift to drag ratio start to decease when it reached maximum value such as 15 m/s decrease at angle of attack of 10, 4 m/s at 5.

The example of the simulation results the aspect of velocity of NACA 4412 airfoil under different angles of attack is shown in the following Fig. 5 (a, b, c, d). The velocity coefficient varied largely under different attack angle It can be seen that in positive angles of attack, the velocity on the leading-edge surface was high and another side that didn't make contact with wind was low. In negative angles of attack, the wind behaves the same but with an opposite direction

4. EXPERIMENTAL SYSTEM

The 3D printing model of an airfoil will be used to test in wind tunnel. Fig. 5 and 6 show the simulation results of variety angle of attack and the experimental results of variety angle of attack. for the low wind speed wind turbine blade design are implemented by using Ansys designmodeler/Fluent. The simulation models consider the wind velocity, the wind turbine
blade shape. The all schemes were simulated for the same change of wind velocity. The simulation results verify the fundamental performance of the wind turbine blade shape

5. CONCLUSION

This paper work was proceeded to study the aerodynamics behavior of the chosen airfoil from Fluent simulation. From this research can be concluded as below.

1 Wind speed and angle of attack have influenced with Lift and Drag coefficient. Higher velocity and higher angle of attack increased Lift and Drag coefficient but the value will start to decease when reach their maximum value.
2 Maximum lift to drag ratio is different in each wind speed and show sign of decease when it reaches maximum value
3 It unsuitable to use angle of attack at negative degree when you want high lift to drag ratio.
4 The design for wind blade made from NACA 4412 used in low wind speed zone such as Thailand should be use at angle of attack between 5 to 15

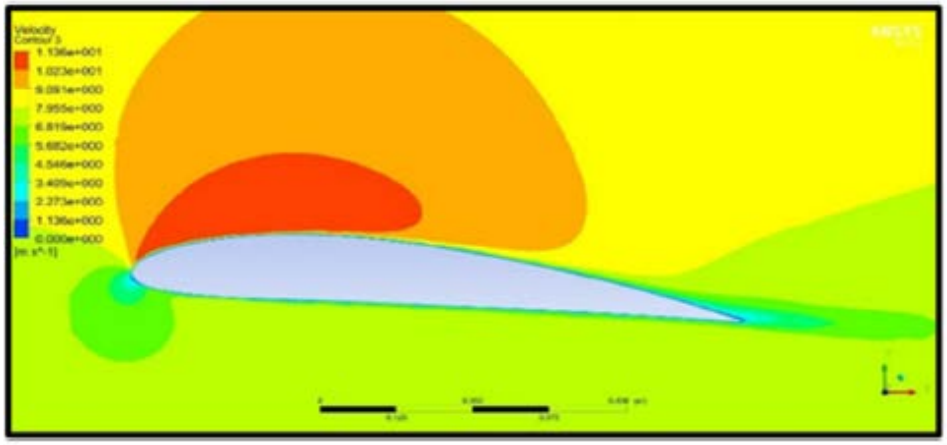

(a) Angle of Attack 5°

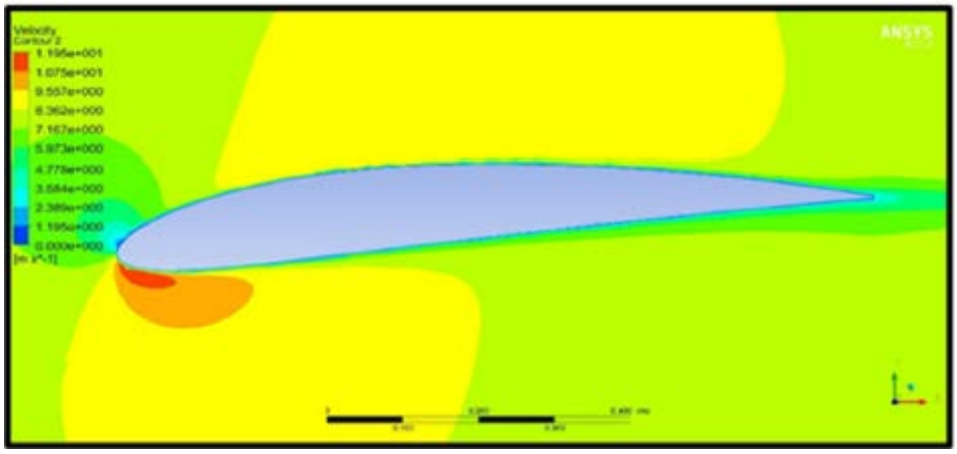

(b) Angle of Attack -5°

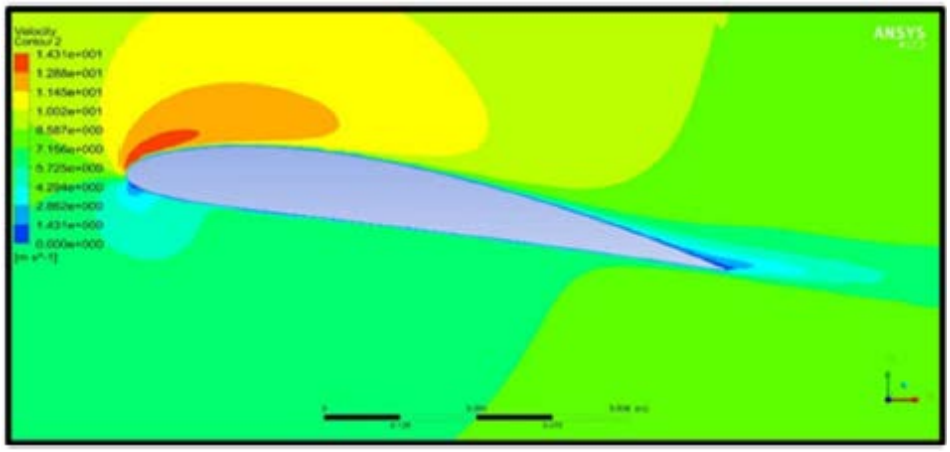

(c) Angle of Attack 10°

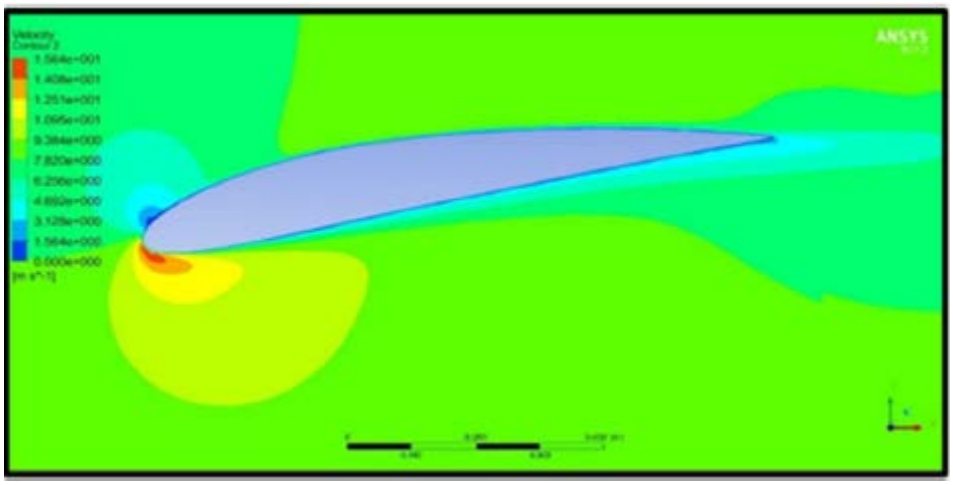

(d) Angle of Attack -10°

Figure 5 Simulation results for variety angle of attack

(a) Angle of Attack 5°

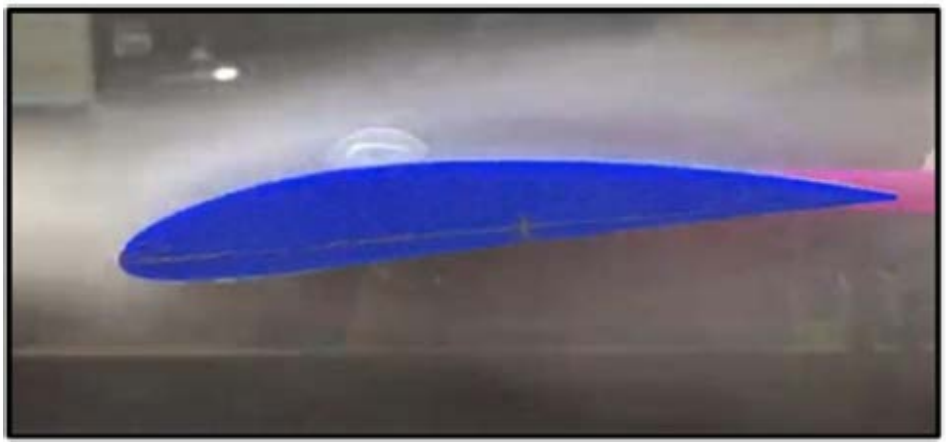

(b) Angle of Attack -5°

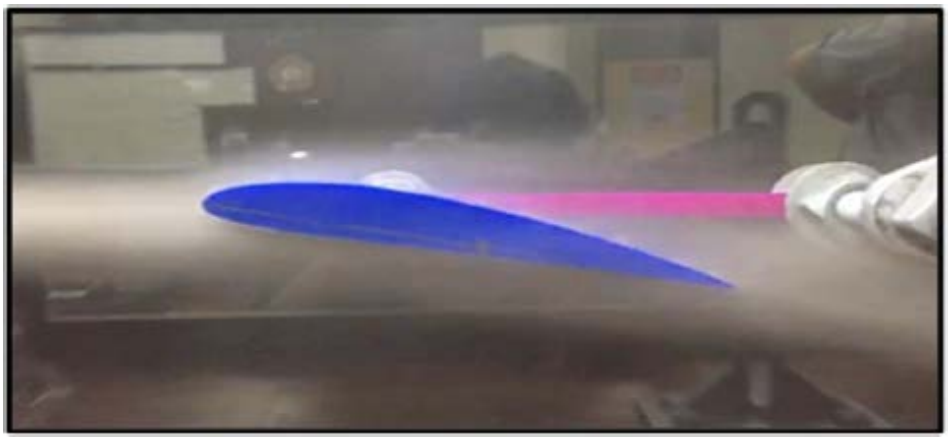

(c) Angle of Attack 10°

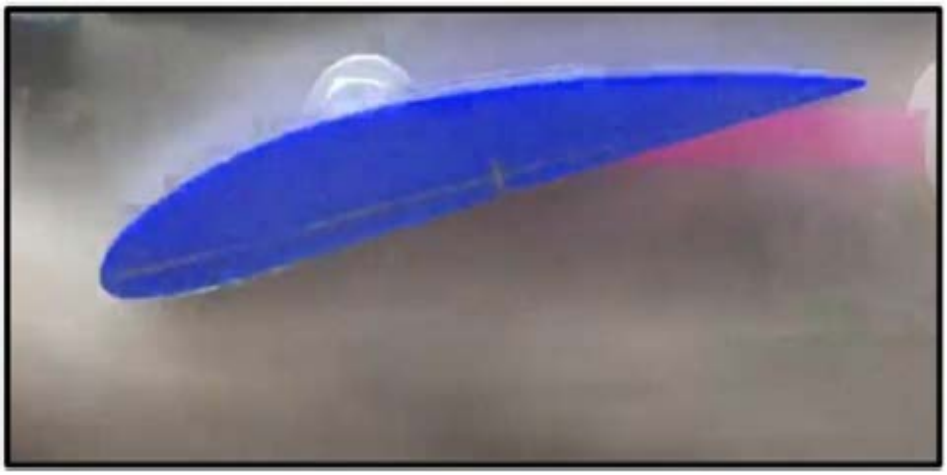

(d) Angle of Attack -10°

Figure 6 Experimental results for variety angle of attack

6. REFERENCES

[1] M.H.M. Noh, A.H.A. Hamid, H. Rashid, W. Wisnoe and M.S. Nasir, "Wind Tunnel Experiment for Low Wind Speed Wind Turbine Blade," Mechanics and Materials, Vols. 110-116 ,pp 1589-1593, 2012.

[2] P.J. Schubel and R.J. Crossley, "Wind Turbine Blade Design," Energies, Vol. 5, pp. 3425-3449, 2012.

[3] A.S. Sharma, Sudhakar S., Swathijayakumar and B.S.A. Kumar, "Investigation of Pressure Contours and Velocity Vectors of NACA 0015 in Comparison with Optimized NACA 0015 Using Gurney Flap," International Journal of Mechanical And Production Engineering, Vol. 3, Issue 9, 2015.

[4] M.F. Hidayat and Y. Nofendri, "Aerodynamic Study Airfoil NACA 0013 with ANSYS Fluent," Article, 2019.

[5] M.R. Birajdar and S.A. Kale, "Effect of Leading Edge Radius and Blending Distance from Leading Edge on the Aerodynamic Performance of Small Wind Turbine Blade Airfoils," International Journal of Energy and Power Engineering, Vol. 4(5-1), pp. 54-58, 2015.

[6] X. Baoqing and T. De, "Simulation and Test of the Blade Models Output Characteristics of Wind Turbine," Energy Procedia 17, pp. 1201-1208, 2012.

[7] S.A. Kale and R.M. Varma, "Aerodynamic Design of a Horizontal Axis Micro Wind Turbine Blade Using NACA 4412 Profile," International Journal of Renewable Energy Research, Vol.4, No.1, pp. 69-72, 2014.

[8] P.D Adb. Aziz, A.K.R. Mohamad, F.Z. Hamidon, N. Mohamad, N. Salleh and N.M. Yunus, “A Simulation Study on Airfoils Using VAWT Design for Low Wind Speed Application,” International Conference on Engineering Technology and Technopreneuship, Vol.4, pp. 105-109, 2014

[9] Y. Zou1, X.Zhao1 and Q. Chen, “Comparison of STAR-CCM+ and ANSYS Fluent for Simulating Indoor Airflows”, Building Simulation, Vol.11(1), pp 165-174, 2018

[10] E. Koc, O. Gunel and T. Yavuz, “Comparison of Qblade and CFD results for small-scale horizontal axis wind turbine analysis,” IEEE International Conference on Renewable Energy Research and Applications, 2016

Stress Analysis of Three-Span Prestressed Concrete Bridge According to Modified Span Length Subjected to Thai Truck Load

Atavit Sujaritpong[1], Wareeyot Thiradulkul[2]

[1,2] Department of Civil Engineering, Faculty of Engineering, King Mongkut's Institute of Technology Ladkrabang, Bangkok, Thailand.

[1] Corresponding author; E-mail address: asujaritpong@yahoo.com

Abstract.

In the limited construction area, it is an alternative method that has the least impact on the existing bridge structures. The construction of the columns to support the bridge at an alternate position caused the modification in span lengths was chosen to study in this research. This method must be also achieved with the least impact of traffic. The three-span prestressed concrete bridge was simulated and analyzed by the finite element method. The models were subjected to the vehicles according to the standard loadings of Thai truck loads. The moving loads were applied to the bridge models which have the existing spans and varied spans caused by the construction of replaced columns. The variations in bridge lengths were ranged from 5% to 25% with an interval of 5% and caused the shortening of the first span and lengthening of the middle span. The bridge lengths were varied from 26.25 to 43.75 meters respectively. The stress analyses were carried out to determine the stresses induced in concrete, tendons, and rebars and then compared to their allowable strength. The conclusions were made for the span lengths which could affect the serviceability of the bridge.

Keywords.-

1. INTRODUCTION

Transportation is continuously developing to support economic growth and increasing population. The design and modification of the existing structures to be constructed in limited areas are sometimes unavoidable. These infrastructures, including elevated structures and underground structures, and then have the role important for the near future.

In the limited construction area, this study is an alternative method to construct the infrastructure with the least impact on the existing structures. The three-span prestressed

concrete bridge was chosen and simulated in this study. The sky train route has been planned and affects the structural modification to the existing bridge caused the modification to replace the position of existing columns of the bridge in the route area. To replace the substitute supports, the variation of the bridge length will be shortened and lengthened in the adjacent spans. The method of design will be a benefit for the construction cost as well as the least effect of traffic.

However, the modification in span lengths play an important role in the stresses distorted in the existent bridge and affect the serviceability of the bridge as well. The structural analyses must be carried out to compare the stresses after the structural modification to their allowable stresses for the materials used to ensure its serviceability. The modified span length after the modified structure must not affect the capacity to carry truck loads or vehicles according to the design specifications. The methods and results of this study can be used as a guideline for the remodel of the bridge structure for the existing bridge structures in the limited construction areas.

2. BACKGROUND

2.1. Standard Loadings for Thai Truck

According to the standard loadings of the Department of Highway's regulations [1], the design specification is not specified for the axle loads and distance between wheels. Therefore, the truck load applied in this study is referred to from relevant research [5]-[7]. The compiled data is based on the trucks' manufacturers that are used in Thailand to determine the distance between the axles of different types of trucks. The vehicle that may cause damage to the highway is chosen in this study. The axle loads and positions of the front and rear wheels are shown in figure 1.

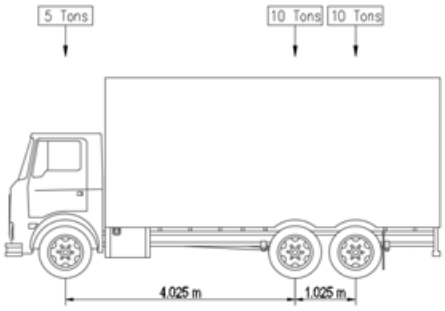

Figure 1 Thai Truck Loading.

2.2. The Bridge Span Length

Recently, the design and construction of major bridges in Thailand have been developed rapidly. In order to compare and select the most suitable form for the bridge design, we shall consider various forms of the bridges and their span lengths. These forms of bridges are shown in Table 1. Since the three-span prestressed concrete bridge has been chosen in

this study, the Cast-in-Place Posttensioned Box-Girder Conventional with the span length of 35 meters will be introduced in the analyses.

Table 1 Bridges and span lengths

Bridge Type	Span Length(m)
Precast Pretensioned I-Beam Conventional	0 - 45
Cast-in-Place Posttensioned Box-Girder Conventional	30 - 90
Precast Balance Cantilever Segmental Constant Depth	30 - 90
Precast Balance Cantilever Segmental Variable Depth	60 - 180
Cast-in-Place Cantilever Segmental	60 - 300
Cable-Stay with Balanced Cantilever Segmental	240 - 450

3. METHODS

3.1. Allowable Stress (Serviceability Limit State)

Prestressed concrete must be ensured so that the stress does not exceed the safe strength. The allowable stress limit for concrete according to the United States Standard (AASHTO) [4] must not exceed these values.

$$\text{Compressive Stress: } f_c = 0.45 f_c'$$

$$\text{Tensile Stress: } f_c = +1.60(f_c')^{1/2}$$

where f_c is the compressive stress in prestressed concrete.

f_c' is the compressive strength of concrete for use in design.

f_1 is the tensile stress in prestressed concrete.

The allowable stress limit for prestressing tendons at service limit state after losses according to the United States Standard (AASHTO) [4] must not exceed these values.

$$\text{Tensile Stress: } f_{pe} = 0.80 f_{py}$$

where f_{pe} is the effective stress in the prestressing tendon after losses.

f_{py} is the yield strength of prestressing tendon.

The nominal shear resistance for post-tensioned segmental box girder bridges according to the United States Standard (AASHTO) [4] The nominal shear resistance is given by the lesser of the two values and must not exceed these values.

$$V_n = V_c + V_s \tag{3.1}$$

In which $V_c = 0.166K(f_c' b_v d_v)^{1/2}$

$$V_s = \frac{A_v f_y d_v}{s}$$

$$V_n = f_c' b_v d_v \tag{3.2}$$

where A_v is the area of a transverse reinforcement within distance

b_v is the width of web adjusted for the presence of ducts.

d_v is the effective shear depth.

f_y is the minimum yield strength of compression reinforcement.

K is the stress variable used in calculating torsional cracking moment.

s is the spacing of reinforcing bar.

V_n is the nominal shear resistance of the section considered.

V_c is the nominal shear resistance provided by the concrete.

V_s is the nominal shear resistance provided by the shear reinforcement.

3.2. Materials and Method

The three-span prestressed concrete bridge with the span lengths of 35.00+35.00+35.00 meters was chosen for the existing structure. The depth of the box girder is 2.40 meters. The top flange of the box girder is 8.50 meters wide. The variations in bridge lengths due to the modification of replaced columns were ranged from 5% to 25% with an interval of 5% and caused the shortening of the first span and lengthening of the middle span. The shortening and lengthening of span lengths were varied from 26.25 to 43.75 meters respectively. Six models of existing and modified span of bridge were analysed and the stress results were then compared. For quantitative comparisons, the maximum stress induced in materials was determined. Bridge standard moving loads according to AASHTO LRFD Bridge Specifications for Highway Bridges for each span length were separately applied to the bridge. The analytical existing models for plan view and elevation view are shown in figure 2. The cross-section and dimensions of the box girder are shown in figure 3. The modified span lengths for each model are also shown in Table 2

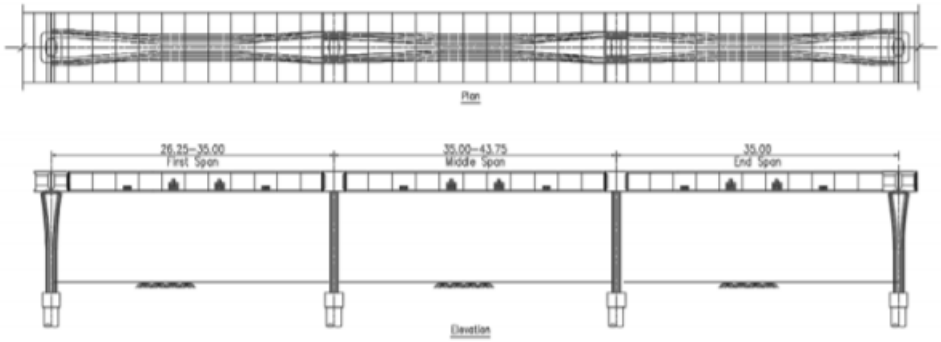

Figure 2 Existing span length of prestressed concrete bridge.

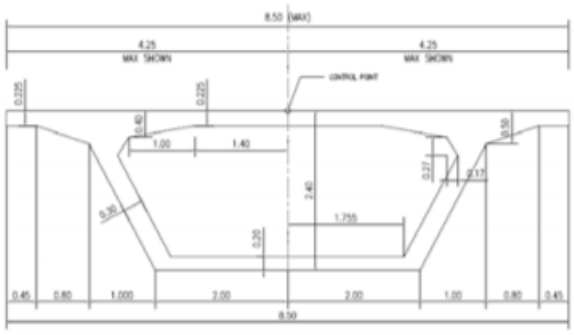

Figure 3 Cross section of prestressed concrete bridge.

Table 2 Modified span length bridge models

Case Study	Span Length(m)		
	First Span	Middle Span	End Span
Existing	35.00	35.00	35.00
Modified 5%	36.50	33.25	35.00
Modified 10%	38.50	31.50	35.00
Modified 15%	40.25	29.75	35.00
Modified 20%	42.00	28.00	35.00
Modified 25%	43.75	26.25	35.00

4. RESULT

From stress analyses, the stresses occurred in prestressed concrete bridge models were analyzed. Thai truck moving loads were applied to each modified span length model. The existing three-span prestressed concrete bridge with the span length of 35.00+35.00+35.00 meters was analyzed to obtain the stresses induced in each material and then compared to the other models by graphical depictions. The modified span lengths were ranged from 26.25 to 43.75 meters and the stress results were carried out. Figure 4 reveals the variations in stress analyses at the top fiber of the box girder cross-section compared to the allowable compressive and tensile strength according to the design standards. In order to compare the stresses occurred in concrete, tendons, and rebars, the allowable stresses regulated by the American Association of State Highway and Transportation Officials (AASHTO) by the Load and Resistance Factor Design (LRFD) method have been referred. The stress results for the bottom fiber of the cross-section are compared in figure 5. The results from stress analyses in concrete box girders indicate that the stresses induced in the existing bridge do not exceed the allowable design strength both in compression and tension. The results of the modified span bridges can be summarized as followings.

From the analytical results in figure 4, it was found that tensile stress of 37.21 kg/cm2 in concrete at top fiber exceeded the allowable Stress for modified 20% span length model (42.00+28.00+35.00), and the value of tensile stress obtained for modified 15% span length model (40.25+29.75+35.00) was 17.85 kg/cm2 and within the limit of allowable stress respectively.

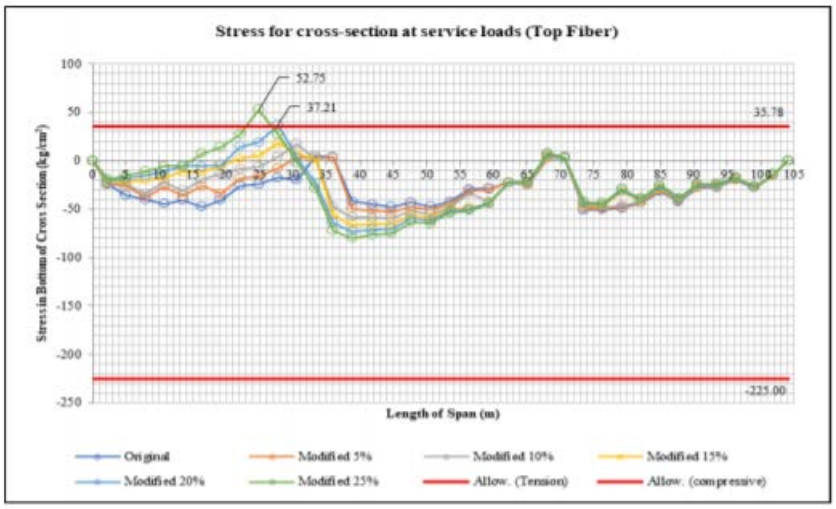

Figure 4 Stress for cross section at top fiber.

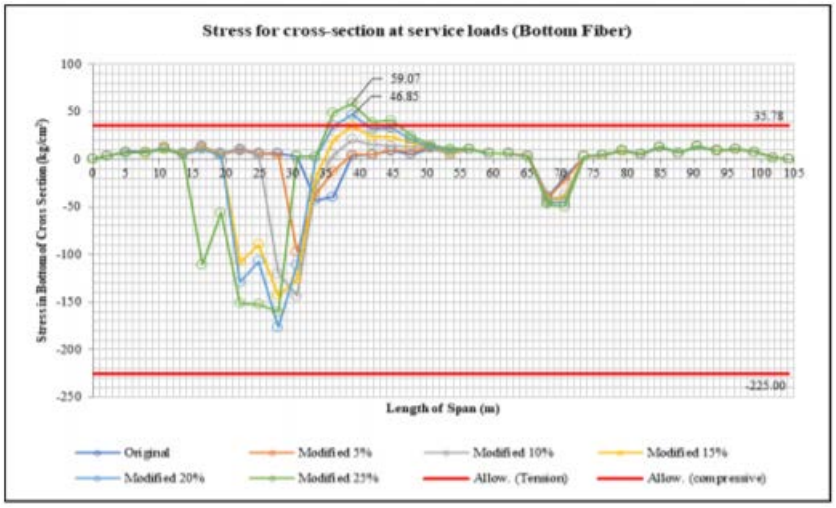

Figure 5 Stress for cross section at bottom fiber.

For the tensile stress in concrete at bottom fiber in figure 5, it was found that tensile stress of 46.85 kg/cm2 obtained from modified 20% span length model (42.00+28.00+35.00) was more than the allowable and the value of tensile stress obtained for modified 15% span length model (40.25+29.75+35.00) was 34.48 kg/cm2 and within the limit of allowable stress respectively.

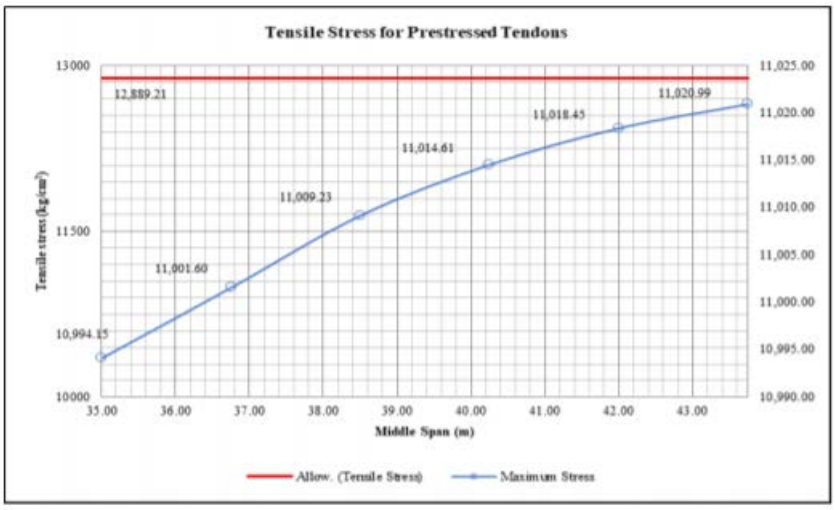

Figure 6 Tensile stress in prestressed tendons.

The maximum tensile stresses in prestressed tendons after losses were also obtained and compared for each model, it was found that the tensile stress in the tendons of

10,020.99 kg/cm2 obtained from modified 25% span length model (43.75+26.25+35.00) was still within allowable limit according to the design specification as shown in figure 6.

Maximum shearing strength at the web of box girder sections were also analyzed and depicted in figure 7. The shearing stresses in concrete and rebar obtained from modified 20% span length model (42.00+28.00+35.00) was calculated to be 518,922.39 kg/cm2 which was more than the allowable stress. However, the value of shear stress obtained for modified 15% span length model (40.25+29.75+35.00) was 482,450.01 kg/cm2 and within the limit of allowable stress respectively.

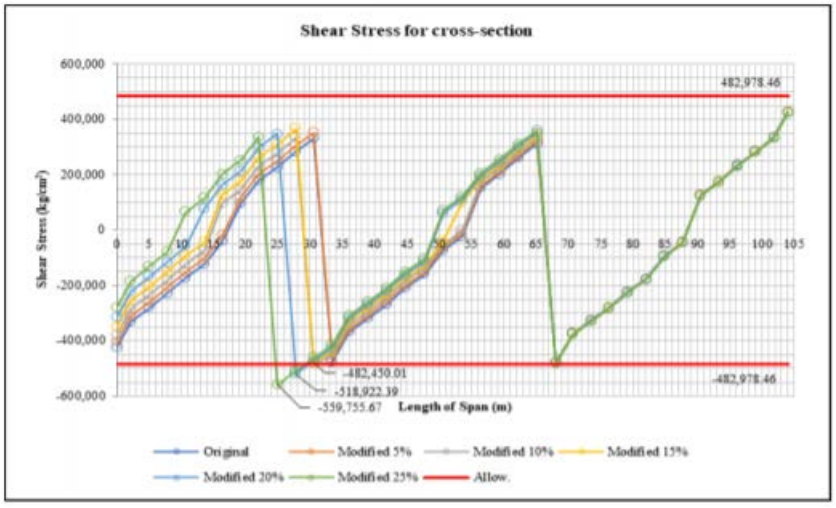

Figure 7 Shear Stress.

5. DISCUSSION

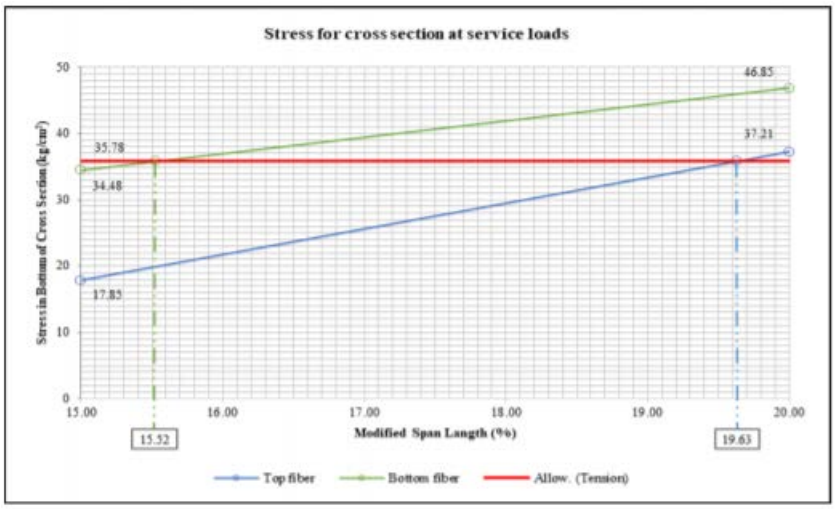

Figure 8 Comparison of tensile stress in concrete box girder.

In this topic, the stresses obtained for each modified span length were plotted and compared to determine the optimum modified span length which this modified span length can still sustain the serviceability of the remodeled bridge. The tensile stresses analyzed in concrete box sections and the shearing stresses obtained from the web of concrete box sections are considered and plotted for each modified span length. From the results in figure 8 compared to the allowable tensile stress of concrete, the modified span length which will not cause the exceeded allowable stress in top fiber in concrete is 41.87+28.13+35.00 meters or 19.63% of the original length. The optimum modified span length obtained from the bottom fiber is 40.43+29.57+35.00 meters or 15.52% of the existing span length, respectively. In this study, the tensile stress induced in bottom fiber is considered to preserve the serviceability of this bridge.

The shear strength obtained from the analyses were also plotted and compared to determine the optimum modified span length which can sustain the serviceability of the bridge. The optimum modified span length that will not cause the exceed of allowable stress is 40.27+29.73+35.00 meters or 15.07% of the existing length as shown in figure 9.

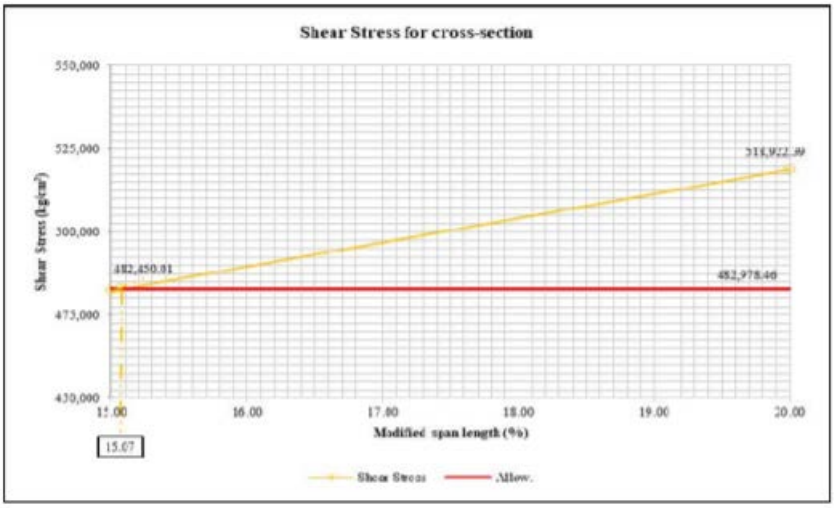

Figure 9 Comparison of shear strength in concrete box girder.

6. CONCLUSION

This objective of this research is to study the behaviour of the stresses induced in a prestressed concrete bridge while the existing bridge length has been modified. The modified span lengths decrease in the first span and the increase in the middle span ranged between 5% to 25%, with the interval change in the length of 5%. These cause the modified span range from 26.25 to 43.75 meters. The finite element models of the bridge were analysed by the moving load of the Thai truck according to standard loading of manufactures with the Midas Civil 2019 program. The stress analyses in concrete box section, tendon, and rebars were carried out and compared. to their allowable stresses [9] according to the design standards of the Highway Association and The American Association of State Highway and Transportation Officials (AASHTO) by the Load and Resistance Factor Design (LRFD) method. It can be concluded that the length of the optimum modified span of the bridge in this case study that will not cause the induced stresses to exceed the design values is 40.27+29.73+35.00 meters or 15.07% of the original length. The shear stress induced in box girder play a major role to preserve the serviceability of this bridge.

7. REFERENCES

[1] S. W. Tabsh and M. Tabatabai, “Live Load Distribution in Girder Bridges Subject to Oversized Trucks,” Journal of Bridge Engineering, vol 6, 2001.

[2] S. Vivithkeyoonwong and S. Rimdusit, “A Comparison fo Bending Moments and End Shears of Simple Span Birdge Girders Due to The Ten-Wheel Truck with the AASHTO Standard Truck”, Proc 43 Kasetsart University Annual Conf., 2005.

[3] S. Suparp and P. Joyklad, “A Comparison of Maximum Respones of Three-Span Continuous Bridges Due to Thai Trucks with AASHTO Highway Live Loadings,” KMUTT Research and Development Journal, vol 34, 2011.

[4] AASHTO, AASHTO LRFD Bridge Specifications for Highway Bridges, 2007

[5] S. Suparp and P. Joyklad, “A Comparison of Internal Forces of Simple Supported Bridges Due to Thai Truck Loads with AASHTO Highway Load,” Research and Development Journal of the Engineering Institute of Thailand, vol 22, pp 25-35, 2011.

[6] S. Suparp and P. Joyklad, “Maximum Response Ratios of Three-Span Continuous Bridge Girders Due to Thai Trucks and HL-93 Live Loadings,” KMUTT Research and Development Journal, vol 35, pp 501-518.

[7] T. Pinkaew and M. Chanintharila, “Bridge Design,” Engineering Expert International.

[8] P. Sawangwong, “Analysis and Design for Construction Stages of Balancing Cantilever Bridge in Accordant to AASHTO LRFD HL-93,” Proc 11 Annual Concrete Conf (Nakhon Ratchsima).

[9] Department of Highways, Declaration of Director of Motorways, Director of The National Highways, and Director of Concession Highways Forbidding any vehicles with weight, net weight carrying, over weight on each axle, or any damaged on the highways, motorways, and concession highways, The Government Gazette, Special session, No 122,150, pp 19-25, 2005.

Numerical Modelling for Energy Absorption of Reinforced Concrete Barriers Covered with Natural Rubber

Lwin Lwin Aung1, Amphon Jarasjarungkiat2, Suvisit Banyam

[1,2]*Department of Civil Engineering, Faculty of Engineering, King Mongkut's institute of Technology Ladkrabang, Bangkok, Thailand.*

[1]*Corresponding author; E-mail address: lwinlwinaung2281995@gmail.com*

Abstract.

Due to the oversupplying, applications of natural rubber are widely introduced in Thailand. In this research, a deployment of natural rubber with typical road safety concrete barrier is investigated numerically. There are many various kinds of barriers to be used not only to prevent vehicles from collision with an opposite vehicle but also to protect from roadside hazards. Therefore, nonlinear finite element modelling was employed to investigate the more efficiencies of barrier covered with rubber sheets by means of finite element analysis. The three-dimensional model is involved with three different homogeneous materials under static analysis while applying an area load representing a car colliding to the barrier. The results have shown that barrier with rubbers can absorb impact force from the vehicles.

Keywords. -

1. INTRODUCTION

Nowadays, amount of producing rubber is increased in Thailand and also many concrete barriers are applied for safety on the road to reduce the danger of accidents. To attain safe roadways, there are three facts by [9] such as safer people —to limit the driver not to drive after drinking alcohol, to use seatbelts while driving, safer vehicles —to apply optimum safety devices for vehicles and safer roads — to build and maintain roads, to improve safety barriers. Many researchers mainly focus on the strength of concrete, however, in this paper, the authors focus on using rubber latex not only to improve the strength of barriers but also not to damage cars. Analysis of barrier by means of experimental test is expensive, therefore, simulation with theoretical finite element with various software is quite easy to apply to test the model. Among them, LS-DYNA, ANSYS, ABAQUS and Virtual CRASH 4.0 (2019) were used to analyze the strength of concrete barriers by [8],

[6], [3], [1] and [2]. In this paper, numerical simulation is carried out concrete damage plasticity (CDP) barrier with or without rubber to compare how much energy they stored

2. FINITE ELEMENT MODELLING OF BARRIER

The non-linear finite element under Standard was employed to CDP concrete reinforced barrier covering with or without rubber.

2.1. Modelling of concrete barrier

In the finite element software, the following equations are used to find the uniaxial compressive and tensile behavior to create concrete damage plasticity model to examine the sensitivity of the damage while predicting formation of cracks in concrete [5].

Uniaxial Compressive Behavior

$$\sigma_c=(1-d_c)E_0(\varepsilon_c-\varepsilon_c^{pl}) \tag{2.1}$$

$$\varepsilon_c^{in}=\varepsilon_c-\sigma_c/E_0 \tag{2.2}$$

$$\varepsilon_c^{pl}=\varepsilon_c^{in}-d_c/(1-d_c).\sigma_c/E_0 \tag{2.3}$$

Uniaxial Tensile Behavior

$$\sigma_t=(1-d_t)E_0(\varepsilon_t-\varepsilon_t^{pl}) \tag{2.4}$$

$$\varepsilon_t^{ck}=\varepsilon_t-\sigma_t/E_0 \tag{2.5}$$

$$\varepsilon_t^{pl}=\varepsilon_t^{ck}-d_t/(1-d_t).\sigma_t/E_0 \tag{2.6}$$

where σ_c and ε_c were nominal compressive stress and strain, d_c and d_t were two scalar damage variables, E_0 was the initial (undamaged) elastic stiffness of the material, $\varepsilon^{pl}{}_c$ and $\varepsilon^{pl}{}_t$ were plastic hardening strain in compression and tension, $\varepsilon^{in}{}_c$ was inelastic hardening strain, σ_t and ε_t were nominal tensile stress and strain and $\varepsilon^{ck}{}_t$ was hardening cracking strain respectively. Although the uniaxial compressive and tensile behaviour could be explored by experimental tests, in this study, simplified concrete damage plasticity with 20 grades by [4] was used and data was shown in Table 1. The concrete barrier with 2.4E-009 kg/mm3 was 600 mm wide at the base, 300 mm wide at the top and 1 m high. The 25 mm diameters reinforced steels and 9 mm stirrups at 75 mm apart from each other were embedded in the concrete as shown in Figure 1(a). Moreover, the density of steel 7.8E-009 kg/mm^3, the elastic modulus 21000 MPa and 0.3 poison ratio was applied.

2.2. Properties of rubber sheet

There are different forms for strain energy potential to evaluate hyper-elastic material behavior such a s Arruda-Boyce, Marlow, Mooney-Rivlin, Neo-Hookean, Ogden, Polynomial, Reduced polynomial, Van der Waals and Yeoh form. Among them, Mooney-Rivlin, Neo-Hookean and Ogden are famous for materials like rubber. However, in this paper, Mooney-Rivlin form was employed.

Table 1 Material Properties for Concrete with SCDP Model in Class B20

Material's Parameters	B20	Plasticity Parameters	
Concrete Elasticity		Eccentricity	0.1
E (GPa)	21.2	Fb0/fc0	1.16
	0.2	K	0.67
Concrete Compressive Behaviour		Concrete Compression Damage	
10.2	0	0	0
12.8	7.73585E-005	0	7.73585E-005
15	0.000173585	0	0.000173585
16.8	0.000288679	0	0.000288679
18.2	0.000422642	0	0.000422642
19.2	0.000575472	0	0.000575472
19.8	0.00074717	0	0.00074717
20	0.000937736	0	0.000937736
19.8	0.00114717	0.01	0.00114717
19.2	0.001375472	0.04	0.001375472
18.2	0.001622642	0.09	0.001622642
16.8	0.001888679	0.16	0.001888679
15	0.002173585	0.25	0.002173585
12.8	0.002477358	0.36	0.002477358
10.2	0.0028	0.49	0.0028
7.2	0.003141509	0.64	0.003141509
3.8	0.003501887	0.81	0.003501887
Concrete Tensile Behaviour		Concrete Tension Damage	
Yield Stress (MPa)	Cracking Strain	Damage Parameter T	Cracking Strain
2	0	0	0
0.02	0.000943396	0.99	0.000943396

The form of the Mooney-Rivlin strain energy potential

$$U = C_{10}(\bar{I}_1 - 3) + C_{01}(\bar{I}_2 - 3) + 1/D_1.(J^{el} - 1)^2 \quad (2.7)$$

$$\bar{I}_1 = J^{(-1/3)}(\lambda_1^2 + \lambda_2^2 + \lambda_3^2) \text{ and } \bar{I}_2 = J^{(-1/3)}(\lambda_1^{(-2)} + \lambda_2^{(-2)} + \lambda_3^{(-2)}) \quad (2.8)$$

Hence, U was strain energy per unit of reference volume, C_{10}, C_{01} and D_1 were temperature-dependent material parameters, $\bar{I}_1$ and $\bar{I}_2$ were the first and second deviatoric strain invariants, J^{el} was the elastic volume ratio, J was total volume ratio and λ was the principal stretches. However, C_{10} and C_{01} were applied as 0.142 and 0.011 from the material parameters of [7].

The 1500 mm × 500 mm × 15 mm rubber sheets were attached to concrete barrier. The rubber latex was separated three parts to cover the front, back and top of concrete barrier instead of using only one sheet of rubber to avoid maximum distortional errors. In finite element analysis, tie function was applied to attach rubber sheets as slave with concrete as master surfaces. For contact property, frictionless and hard contact were submitted as Figure 1(b).

3. INVESTIGATION OF BARRIER STRENGTH BASED ON USING FINITE ELEMENT ANALYSIS

In this section, the non-linear finite element under static analysis was carried out. Moreover, the light passenger car, 2,300lbs (1,043kg) with NCHRP – TL3 (100 kph) by [2] speed within crushing time 2 seconds was assumed to analyze by using Newton's second law of motion:

$$\text{Force} = \text{mass} \times (\text{velocity}/\text{time}) \tag{3.1}$$

Therefore, the total load (14,500 N) was applied to the 375mm x 250mm area on the front surface of barrier with or without rubber sheets. The simulation was carried out to investigate the capabilities and strength of reinforced barrier containing with various elastic modulus and properties between concrete and natural rubber

Then, finite element mesh was provided to each model. There are many different control mesh assignments and also mesh element shapes like hexahedral, hexahedral-dominated, tetrahedral and wedge. The mesh element shape is based on element type to assign the mesh while choosing element family and geometric order and shape of specific element controls. In this field, hexahedral element shape with sweep technique and reduced integration was used for concrete and structure technique with hybrid formulation was selected for rubber. The linear 3D stress was defined for barrier and rubber; however, the linear truss was selected for steels as Figure 2.

4. RESULTS AND CONCLUSION

The results were shown that the barrier covering with rubber latex could absorb impact force from crushing test than the one without covering with rubber. Moreover, the principal stress without attaching is higher than with rubber as Figure 3. The graph from Figure 3 was shown that the values of positive maximum principal stress in the concrete and negative maximum principal stress in the rubber. The costs of concrete barrier covering with natural rubber is around 102USD/ Meter by [2]. The cost is less than the

cost of accident cost. Moreover, using natural rubber can reduce the damage of vehicles and injuries for road users. Then, the consuming rates for rubber can be increased and the people who produce rubber can get profits than the previous days.

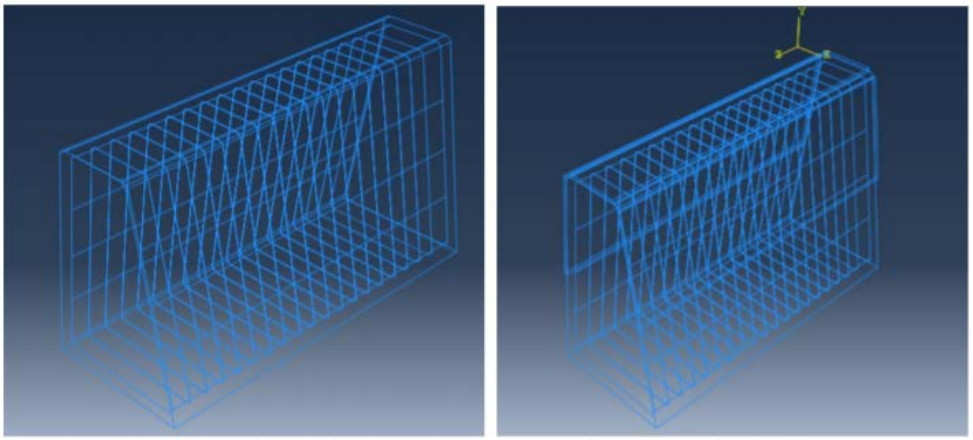

(a) Concrete barrier without rubber (b) Concrete barrier with rubber

Figure 1 Barrier Models with Finite-Element

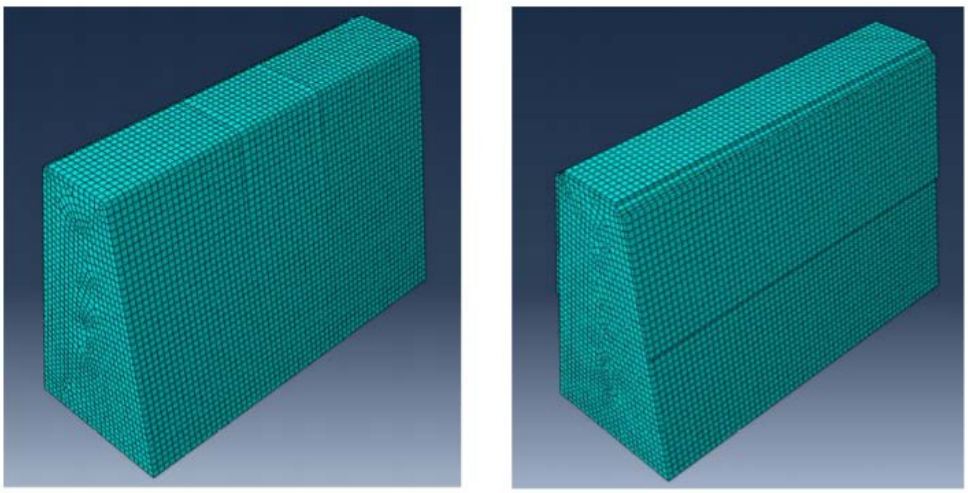

(a) Concrete barrier without rubber (b) Concrete barrier with rubber

Figure 2 Barrier models with finite-element meshing

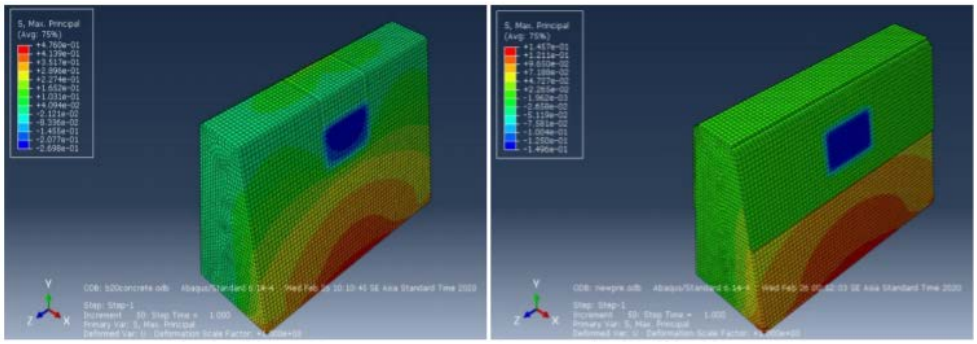

(a) Concrete barrier without rubber (b) Concrete barrier with rubber

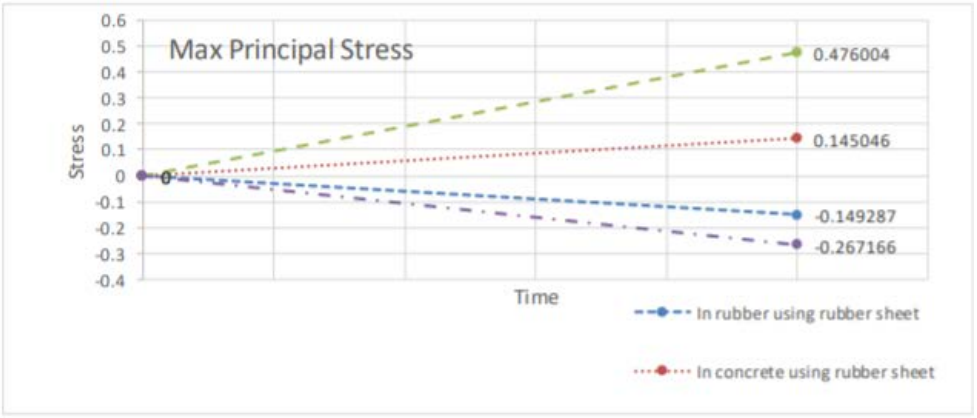

Figure 3 Maximum principal stress of concrete barrier

5. REFERENCES

[1] G. Bonin, G. Cantisani, and G. Loprencipe, "Computational 3D models of vehicle's crash on road safety systems," in *8th International Symposium on Heavy Vehicle Weights and Dimensions*, pp. 1-15, 14-18 March.

[2] W. Cheewapattananuwong, and P. Chaloeywares, "The Innovation of Natural Rubber applied with Concrete Road Barriers in Thailand."

[3] P. Dziewulski and S. Stanisławek, "The impact of forming processes on road barrier strength," in *AIP Conference Proceddings*, vol. 2078, American Institute of Physics Inc.

[4] M. Hafezolghorani, F. Hejazi, and R. Vaghei et al, "Simplified damage plasticity model for concrete," in S*tructural Engineering International: Journal of the International Association for Bridge and Structural Engineering (IABSE)*, vol. 27, pp. 68-78, Int. Assoc. for Bridge and Structural Eng. Eth-Honggerberg.

[5] M. Hanif, Z. Ibrahim, and K. Ghaedi et al, "Finite element simulation of damage in reinforced beams," vol. 9(1), pp. 50-57.

[6] S. Hedjazi, H. Khederzadeh, and K. Sennah, “Numerical modeling for structural behavior of bridge deck barriers made of fiber reinforced concrete,” in proceedings, Annual ConferenceCanadian Society for Civil Engineering, vol. 3, pp. 2327-2337, Canadian Society for Civil Engineering.

[7] H. Khajehsaeid, J. Arghavani, and R. Naghdabadi, “A hyper-elastic constitutive model for rubberlike materials,” European Journal of Mechanics, A/Solids, vol. 38, pp. 144-151.

[8] M. Muhammad, and H. Mohammed, “Concrete road barriers subjected to impact loads: An overview,” Latin American Journal of Solids and Structures, vol. 12(10), pp. 1824-1858.

[9] Z. Ren, and M. Vesenjak, “Computational and experimental crash analysis of the road safety barrier,” Engineering Failure Analysis, 12(6 SPEC. ISS.), pp. 963-973.

Proposed Methods to Prevent Continuous Collapse of Utility Concrete Poles

Petchsasitorn Arthit[1], Sujaritpong Atavit[2]

[1,2] Department of Civil Engineering, Faculty of Engineering, King Mongkut's Institute of Technology Ladkrabang, Bangkok, Thailand.

Corresponding author; E-mail address: art_arthit@hotmail.com[1], asujaritpong@yahoo.com[2]

Abstract.

From the accidental reporting statistics of utility concrete poles in Thailand, they were often found that lots of continuous collapses of more than one pole occurred from cars, storms or cable lines hooked by falling trees or trucks. This type of failure is induced by the tensile forces through the electric cables to the adjacent poles and cause the consequent collapse. Due to the brittle behavior of concrete, the cracked positions were mostly found near the base of poles due to maximum bending moment. Because the tensile force induced in electric cables occurs from weight above the downed position of collapsed pole. Therefore, the proposed method to prevent this collapse was introduced by reducing the mass of pole above the snapped point, leading to the reduction in tensile force to the adjacent poles, then decreasing the number of collapsed poles respectively. The analytical finite element (FEM) models were employed to determine the optimum position on each type of poles in order that the weight induced above those parts would not be able to transfer adequate forces to topple adjacent poles. Carbon fiber reinforced polymer (CFRP) and steel plates were then introduced to strengthen the existing poles and the poles in future manufacturing process consecutively. The experiments were conducted and compared to the analytical results. It is indicated that the utility poles were strengthened and the tensile forces induced by the weight above the toppled positions could be reduced significantly.

Keywords. -

1. INTRODUCTION

Utility poles used in Thailand have been manufactured by prestressed concrete material which can resist high compressive and bending loads. In conventional design, the utility poles are designed to sustain from the wind speed at or below 96 km/hr. However, lots of continuous collapses were reported from the accidents concerning utility poles e.g. car accidents or strong wind. These result from the poor ductility behavior of concrete as well

as the conventional design does not concern the effect of evolved failure induced from the tensile force in cable lines when any poles have been toppled. The higher length from the cracking point the more pulling force is created through the cables to the adjacent poles. The propose of this study is to reduce the tensile force induced in the cable lines by strengthen the utility poles and control the cracking points when they are subjected to the force transferred from the toppled poles. The optimum cracking positions of poles will be determined primarily in order to reduce weight induced beyond when poles are subjected to the pulling force from toppled pole adjacent to them. Thus, tensile forces generated from this weight in cables can be decreased to the next poles respectively. In this study, 2 transmission systems of utility poles are chosen which are 12/24 KV and 69/115 KV. Three height models are studied for 12/24 KV system and two height models of 69/115 KV system are selected according to Metropolitan Electricity of Authority (MEA) standards. The graphical proposed study is shown in figure 1

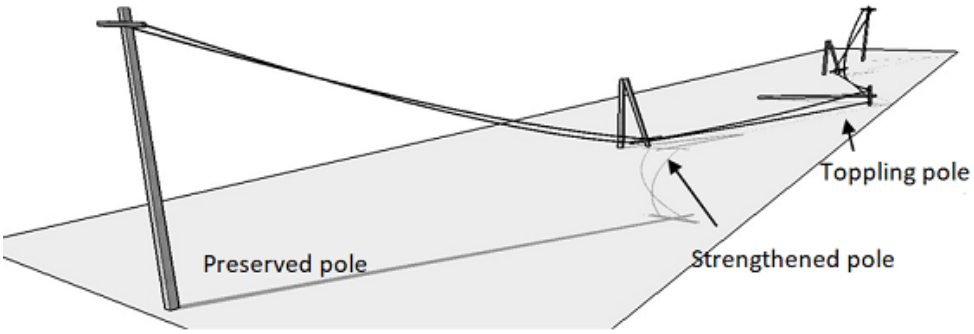

Figure 1 The idea of proposed study.

In order to strengthen the poles to control the cracking positions for each type of utility pole systems, Steel plates are introduced to reinforce the poles in modern design criteria and plate type of Carbon fiber reinforced polymer (CFRP) will be fabricated for the existing poles. The strength and properties of Materials used in this study are indicated in Table 1 for concrete, prestressed wire, stirrup and steel plate grade SS400 while the properties of CFRP are indicated in Table 2.

Table 1 Strength and Properties of Materials

Strength	Materials			
	Concrete	Prestressed wire	Stirrup	Steel plates
Yield (MPa)	-	1570	235	235 (t≤16mm) 245 (t>16mm)
Tensile (MPa)	-	1226	295	400-510
Compressive (MPa)	44	-	-	-

Young's modulus (MPa)	31,413	169,655	50,014	50,014

Table 1 Continued

Strength	Materials			
	Concrete	Prestressed wire	Stirrup	Steel plates
Density (kg/m3)	2,400	7,850	7,850	7,850
Poisson's ratio	0.18	0.30	0.30	0.30

Table 2 Properties of CFRP

Design Thickness (cm)	Ultimate Elongation	Tensile strength (MPa)	Tensile E-Modulus (MPa)
1.2	1.8%	3,100	170,000 MPa

2. FEM MODELS AND ANALYTICAL RESULTS

2.1. FEM models to determine the optimum cracking positions.

In this step of analyses, 5 FEM models of height as stated in Metropolitan Electricity of Authority (MEA) standards were analyzed to obtain the optimum cracking positions when subjected to the pulling force from adjacent downed pole. The models were composed of 12.00 m.GW, 12.00 m. 5 Tm., and 12.35 m. 6.5 T-m for 12/24 KV system and 22.00 m. 18 T-m. and 22.00 m. 25 T-m. for 69/115 KV system. The tensile forces induced from cables line were calculated from the span of 40 m for 12/24 KV system and 80 m for 69/115 KV system respectively. The details of the reinforcements of poles in corresponding with MEA standards are stated in table 3.

Table 3 Details of reinforcements

Model	Prestressed wire	Stirrup	Extra rebars
12.00 m.GW	32 Ø 4mm.	Ø 3 mm. @ 30 cm.	-
12.00 m. 5 T-m	1.8%		4 Ø 25 mm L=5 m. 4 Ø 12 mm L=5 m.
12.35 m. 6.5 T-m	20 Ø 7mm.		-
22.00 m. 18 T-m	36 Ø 7mm		-
22.00 m. 25 T-m	36 Ø 7mm		4 Ø 19 mm L=5 m.

The boundary condition of the bases was assumed to be fixed support. The prestressed forces in prestressed wires were preloaded as well as the pulling forces induced from the cable lines calculated from the weight assumed to act beyond the cracking points of downed pole. The accumulations of heights beyond the assumed cracking position intervals every 1 meter from the base of poles were used to calculate the weights for the utility poles in 12/24 KV system while intervals every 2 meters were used in 69/115 KV system. For an example, the summations of weights of 3, 4, 5, 6, 7, 8, 9, 10 and 10.25 m. from the top of pole were represented the cracking positions at 9, 8, 7, 6, 5, 4, 3, 2, and 1.75 meter from the base of pole for 12.00 m. pole, respectively. When it is required to installed 1.75 m of the pole base underneath the ground, that means the pole is modeled to crack at the base of ground initially and then higher to the upper parts. The weight assumed to generate the tensile force in cable lines for 12.00 m. GW model are shown in Table 4.

Table 4 weights assumed to create tensile force in cable lines for 12.00 GW model

Height from pole base (cracking point) (m)	Weight (kg)	Height from pole base (cracking point)	Weight (kg)
1.75	1,017	5.00	650
2.00	986	6.00	548
3.00	869	7.00	452
400	756	8.00	349
		9.00	251

The effect of surged load from cable lines were also concerned in the analyses by adding the impact factor of 1.3 to the calculations. In each analysis model, when the distances x, y, and z in coordinated system are known, the forces in x, y and z axes which will consequently acted to the cable line position adjacent pole can be calculated as depicted in figure. 2

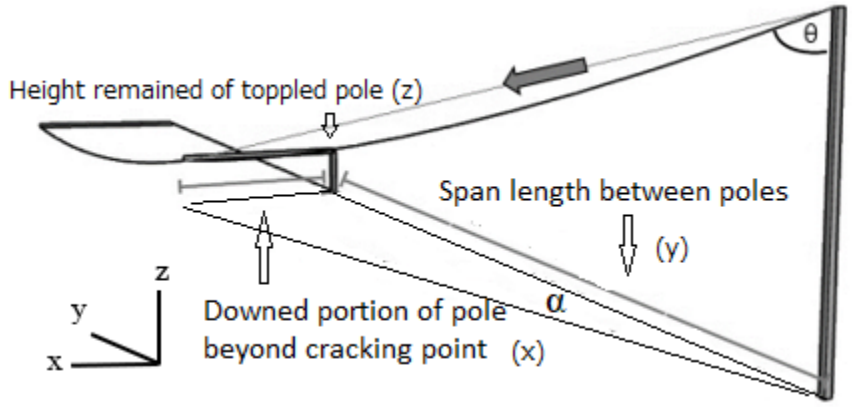

Figure 2 Pulling forces used for the FEM models.

In each analytical model, the stress occurred in each height of pole would be compared to the limit strength of concrete in order to determine the safety factor. When the value of safety factor is greater than 1, it means the pole can sustain the weight of downed portion of adjacent pole induced through pulling load in cable lines. The value of 1 was used to obtain the optimum height of each pole to be strengthened. The heights of pole versus safety factor values were plotted in figure 3 and figure 4 to determine the optimum cracking positions in each utility pole systems where safety factor is equal to 1

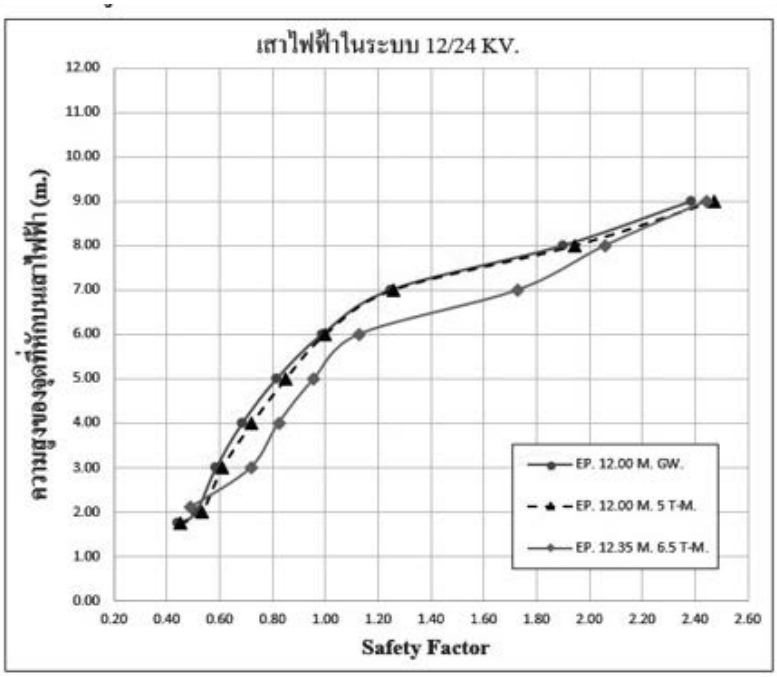

Figure 3 The height of poles versus safety factors in 12/24 KV.

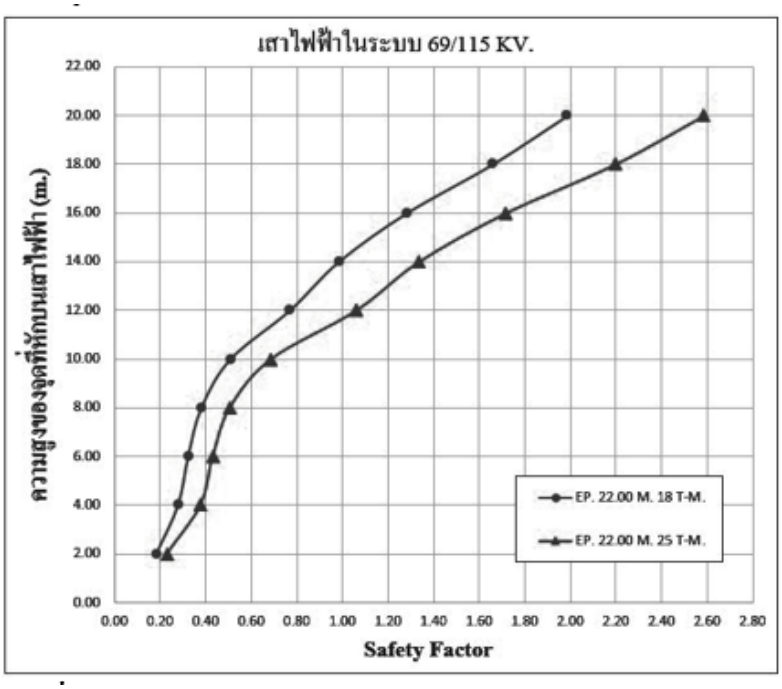

Figure 4 The height of poles versus safety factors in 69/115 KV system.

From the results obtained in figure 3 and figure 4, the optimum cracking positions for each model are concluded in table 5.

Table 5 Recommended positions to be Strengthened for utility poles.

Optimum cracking height from pole base to be strengthened (m)				
	12/24 KV		69/115 KV	
12.00 m.GW	12.00 m. 5 T-m	12.35 m. 6.5 T-m	22.00 m. 18 T-m	2.00 m. 25 T-m
6.05	6.00	5.30	14.10	11.70

2.2. FEM models to strengthen the utility poles by CFRP

In this step, utility poles wrapped with plate type of CFRP were modelled according to the analytical results obtained from the previous step. The specific heights of CFRP were applied to each type of the pole systems and push over analyses were carried out. The

stress analyses were calculated to compare with the strength of materials as well as to define the safety of factor values. The failure was determined by obtaining the safety of factor of concrete material along the height of pole in compressive area. The cracking of pole was judged to present when the safety factors were less than 1. On the other hand, the poles were considered to sustain the applied load when all safety values in the confined area were greater than 1. The amount numbers of wrapping to each pole were determined by the thickness values in multiply of the thickness used which is 1.2 mm. In this report, only one model of the pole in 12/24 KV system and 69/115 KV system would be expressed and discussed. For 12/24 KV system, 12.00 m GW model was selected to discuss herein in figure 5. The safety factor values calculated along the length of pole for 12.00 m. GW models when the width of 1.2 mm, 2.4 mm, 3.6 mm and 4.8 mm of CFRP were applied.

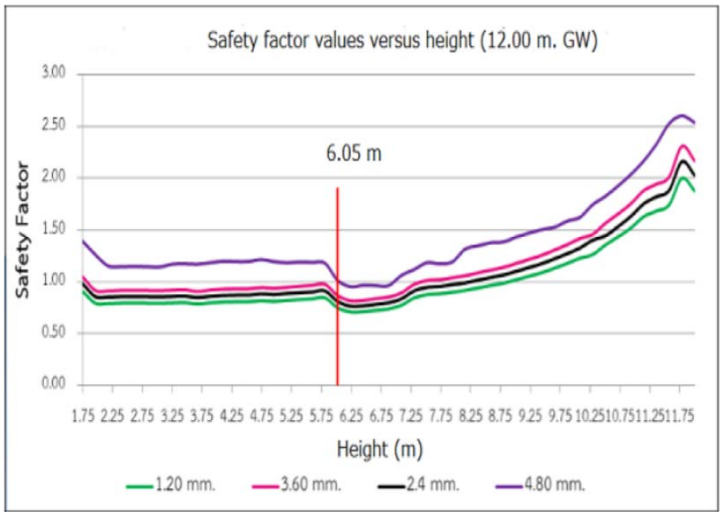

Figure 5 Safety factor values obtained along the length of pole for 12.00 m. GW model strengthen by CFRP.

It can be seen that the 4.8 mm. of CFRP thickness gives all values of safety factor greater than 1. Then, it can be concluded that to control the cracking position at 6.05 m. from the base of pole, the application of 4 wrappings of 1.2 mm. thickness of CFRP is used to fabricate.

For 69/115 KV system, 22.00 m 18 T-m model was selected to discuss and shown in figure 6. Similarly, the width of 6.0 mm, 7.2 mm and 8.4 mm of CFRP were applied to 22.00 m. model 18 T-m pole model. The 8.4 mm. of CFRP thickness gives all values of safety factor greater than 1 in the confined area beneath the height of 14.1 m. The application of 1.2 mm CFRP should be wrapped 7 times to achieve the required thickness.

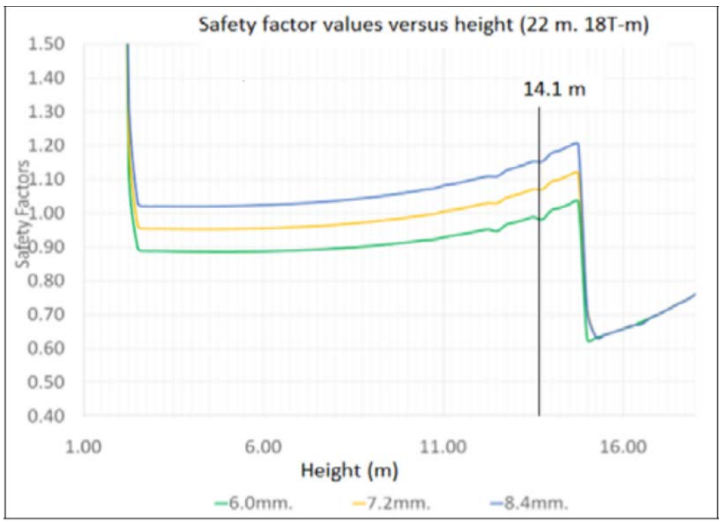

Figure 6 Safety factor values obtained along the length of pole for 22.00 m. model 18 T-m strengthen by CFRP

For the other utility poles studied in this research, the amount numbers of wrapping are concluded in table 6.

Table 6 The Amount Numbers Required for 1.2 mm. Thickness CFRP wrapping on Utility poles.

Optimum cracking height from pole base to be strengthened (m)				
12/24 KV			69/115 KV	
12.00 m.GW	12.00 m. 5 T-m	12.35 m. 6.5 T-m	22.00 m. 18 T-m	2.00 m. 25 T-m
4	4	3	7	7

2.3. FEM models to strengthen the utility poles by Steel plates

For the design criteria of utility poles in future manufacturing process, the controlling of cracking positions should be concerned to prevent progressive collapse for the toppled poles. Steel plates were introduced to strengthen the poles in this research. The material properties of steel plate had been already introduced in table 1. The sizes and weights in kg per 6 meter of chosen steel plate according to the manufacturer and are shown in table 7.

Table 7 Dimensions and weight of steel plates according to the manufacturer

Width (mm)	Thickness (mm)			
	3	4.5	6	9
12	1.7	2.5	3.4	5.1
16	2.3	3.4	4.5	6.8
19	2.7	4.0	5.4	8.1
25	3.5	5.3	7.1	10.6
38	5.4	8.1	10.7	16.1
44	6.2	9.3	12.4	18.7
50	7.1	10.6	14.1	21.2
65	9.2	13.8	18.4	27.6
75	10.6	15.9	21.2	31.8

Similar to the CFRP models, the steel plates were reinforced at the corners of the utility poles' cross sections. The specific heights of steel plate were applied to each type of the pole systems and push over analyses were carried out. The stress analyses were calculated to compare with the strength of materials as well as to define the safety of factor values. The typical cross section model is shown in figure 7 and cracking of pole is judged to present when the safety factor values is less than 1. The relationships between the height of poles versus the safety values are presented in figure 8 and figure 9 for 12.00 m. GW and 12.00 m. 5 T-m models respectively.

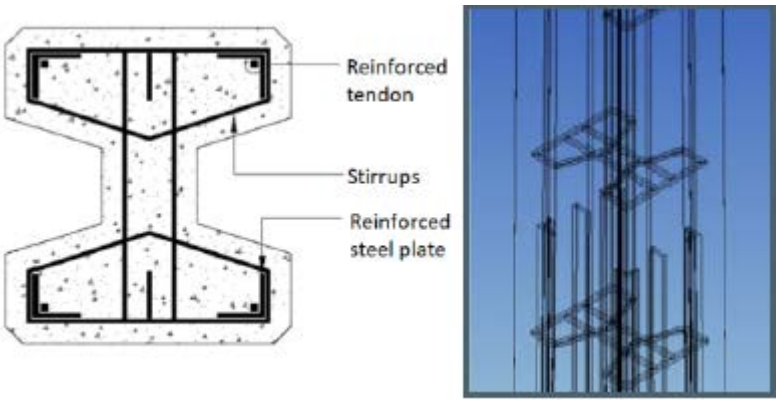

Figure 7 The typical cross section of reinforced steel plates

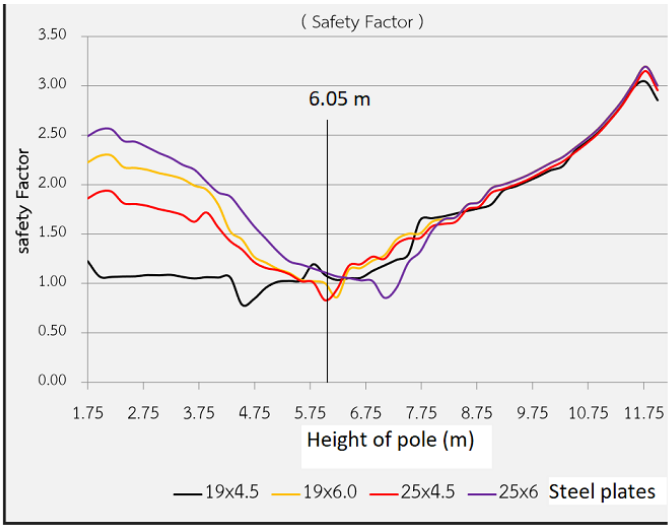

Figure 8 Safety factor values obtained along the length of pole for 12.00 m. GW model reinforced with steel plates

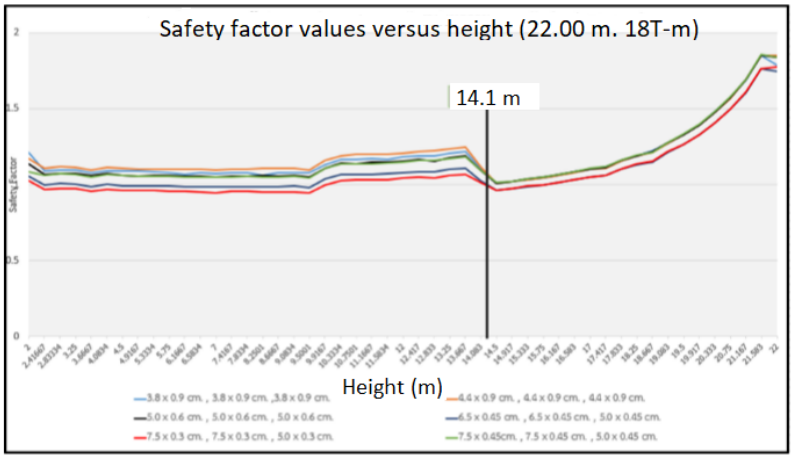

Figure 9 Safety factor values obtained along the length of pole for 22.00 m. 18 T-m model reinforced with steel plates

From these analytical results, it is indicated that for 12.00 m. GW model reinforced with the steel plate of 19x4.5 mm cannot sustain the applied push over load because the safety value less than 1 is found beneath the reinforced height of 6.05 m. It can be concluded that the least sectional area of steel plate of 25x4.5 mm or equivalent area can be applied to this type of pole to prevent the failure position until the reinforced height of 6.05 m is reached. The similar conclusion can be observed with the 22.00 m. 18 T-m model with the reinforced height is 14.1 m. The analytical results revealed that safety factor values calculated along the length of pole for 22.00 m. 18 T-m reinforced with steel plates of 65x4.5 mm and 75x3.0 mm models are lower than 1 below the reinforcement

sections. In the meanwhile, the safety factor values below the reinforcement sections are higher than 1 when the application of 50x6 mm or equivalent sectional area of steel plate are reinforced. The application of 38x9.0 mm, 44x9 mm of reinforced steel plates are also found to satisfy the safety factor values for this type of pole. The conclusions of the least sectional areas of steel plates required to satisfy the safety factor values for each type of poles are summarized in table 8.

Table 8 The least sectional area of steel plates to reinforce on utility poles.

12/24 KV			69/115 KV	
12.00 m.GW	12.00 m. 5 T-m	12.35 m. 6.5 T-m	22.00 m. 18 T-m	22.00 m. 25 T-m
25×4.5	25×4.5	19×4.5	50×6	44×4.5

3. DISCUSSIONS AND CONCLUSIONS

In this study, the proposed method to prevent the specific mode of failure of utility poles had been presented and summarized. The cause of weight above the downed position of collapsed pole above the snapped point leading to produce the tensile force in electric cables was assumed to induce the continuous collapse to adjacent poles. Two strengthen methods to increase stiffness of poles were proposed to reduce the overweight of toppled portion of collapsed poles. The optimum positions of failure to reduce the weight of toppled poles were determined beforehand. The application of CFRP was employed to existing poles while the reinforcement of steel plates was proposed for the future manufacturing process. FEM analyses were utilized to define the stress ratios in order to clarify the failure criteria. The conclusions can be summarized as the followings;

- To determine the optimum cracking positions, the pushover analysis must be carried out by subjected to the pulling forces induced by the downed pole weight, the pole is judged to sustain the weight of downed portion of adjacent pole induced through pulling load in cable lines when the stress ratio is more than 1.
- For the proposed method, CFRP and steel plates can be introduced to increase the stiffness of poles in order to control the points of failure for each type of poles. Push over analysis must be carried out subjected to the cable force at the position of electric wires. The failure is determined by obtaining the safety of factor of concrete material along the height of pole in compressive area. The cracking of pole is judged to present when the safety factors is less than 1.
- In order to control the positions of failure, decreasing the stiffness of the poles is an alternative method by reducing the moment of inertia of section or sectional area, etc.

4. ACKNOWLEDGMENT

This paper and the research behind it would not have been possible without the funding support of Metropolitan Electricity of Authority (MEA). I am also grateful for Suchat

Suwimonwan, Peerapon Annoynon, Montri Monkongkit, Kamonthip Angsirikul Thanisorn Sataporn and Nattapong Chanthananon, my graduated students at KMITL whose contribution in stimulating and encouragement, helped me to coordinate my research until completion

4. REFERENCES

[1] Metropolitan Electricity Authority, Products and Transportation Department, 2017, The Instruction of Standard Drawing of Electric Prestressed Concrete Poles 12m (GW), 12m (BM 3.5T-m.), 12.35m (BM 6.5T-m).

[2] Ministry of Interior, Department of Public Works and Urban Planning, 2008, "MorYorPhor.1508-51 The Standard of Structure Strengthening Reinforced Concrete Structures with Composite Fibre Materials", Bangkok.

[3] B. Vivek, S. Sharma, P. Raychowdhury, S.Ray-Chaudhri, "A Study on Failure Mechanism of Self-Supported Electric Poles through Full-Scale Field Testing," Engineering Failure Analysis, August, 2016, Vol.77, pp. 102–117.

[4] S. Suchat and S.Atavit, "The stress analysis is electric poles with CFRP to prevent the consecutive demolishing from car accidents" The 4th International Conference on Engineering, Applied Sciences and Technology, ICEAST 2018, pp. 1035-1038.

Thermal Property of Poly(lacticacid)/Polypropylene/Bamboo Fiber Composite for Injection Molding application

Jutamas Kordsaart[1], Weraporn Pivsa-Art[2] and Sommai Pivsa-Art1[*]

[1]*Department of Materials and Metallurgical Engineering, Faculty of Engineering, Rajamangala University of Technology Thanyaburi, Klong 6, Thanyaburi, Pathum Thani 12110, THAILAND*
[2]*Department of Chemical and Materials Engineering, Faculty of Engineering, Rajamangala University of Technology Thanyaburi, Klong 6, Thanyaburi, Pathum Thani 12110, THAILAND*

corresponding author's e-mail: sommai.p@en.rmutt.ac.th

Abstract.

Polymer composites of poly(lactic acid)/polypropylene/bamboo fibers (PLA/PP/BF) were prepared using polypropylene-graft-maleic anhydride (PP-*g*-MAH) as a compatibilizer. The ratio of PLA/PP was 40/60 by weight with 3 phr of PP-*g*-MAH. The content of BF in the composite was varied for 5, 10 and 20 phr (part per hundreds of resins). To improve the surface contact of BF and the polymer matrix, treatment of BF with alkali solution to remove lignin and hemicellulose was studied. The thermal analysis of composite was carried out using a differential scanning calorimetry (DSC) method to verify the property for injection molding application. Morphology of surface area was investigated by a scanning electron microscope (SEM). Chemical property of composite was measured to verify the functional groups by FT-IR. Crystallinity of composite was calculated from XRD analysis. Morphology of fracture structure of PLA/PP blend showed smooth surface area with clear and no phase separation between fiber and polymer matrix. The BF content of 10 phr composite showed satisfied thermal property. The interactions between BF and polymer matrix was confirmed their functional groups of PLA/PP/BF composite by FT-IR spectroscopy. The crystallinity of the composites decreased while the crystallization temperature (*Tc*) shifts to lower values with increasing BF content which indicated nucleating effect of BF.

Keywords. -

1. INTRODUCTION

Natura fibers have been used as reinforcement materials in polymers from their advantages of low specific gravity, non-abrasive and their abundant available from renewable resource. Polymer composites reinforced with natural fibers exhibit high stiffness

properties, high specific properties, easily recyclable. Unlike brittle fibers the natural fibers are not fractured during processing, low energy consumption and low cost. Wide variety of fibers are available throughout the world.

Currently bamboo is considered as an important plant natural fiber and has a great potential to be used as reinforcement materials in polymer composites. Mechanically grounded bamboo present its structure as fibers rather than particles. On the basis of BF characterization, bamboo has 60% cellulose and high lignin content. The microfibrillar angle of BF is 2–10˚, which is comparatively small. According to bamboo fiber (BF) structural variation, treatment of BF including extraction of fibers, chemical modification had made it versatile for the use in polymer composites which resulted in improvement of their mechanical and thermal properties [1-2]. The composites can be effectively applied in the automotive, building, appliance and other applications [3].

The limitation of application of natural fibers as reinforcements for polymers is their property inconsistency which depend on high moisture absorption and incompatibility with polymer matrices [4]. To overcome the above limitations, treatment the fibers surface, addition of compatibilizers and coupling agents such as maleic anhydride, acetic anhydride, and silanes have been reported to facilitate better fiber-polymer interfacial interactions and efficient load transfer [5].

Recently, biodegradable polymers have been used as composite polymer matrices with the purpose to replace the non-degradable polymers. Poly(lactic acid) (PLA) have become a topic of great interest in research and development of biobased and biodegradable polymers. PLA exhibits excellent mechanical properties such as high modulus, and biodegradability. However, PLA has disadvantages on low toughness and gas barrier properties [6].

Polypropylene (PP) is widely used for injection molding products. PP possesses applicable properties for packaging such as high heat distortion temperature, transparency, dimensional stability and outstanding flow ability. PP shows excellent characters for composite fabrication as a matrix material because PP is suitable for filling, reinforcing and blending. The study on PP reinforced with natural fibers composites was reported [7]. Zhang Ying-Chen, et al studied the blending of PLA/PP using PP-*g*-MAH as a compatibilizer. Block or graft copolymers were produced from reaction of maleic anhydride and the side chain of PLA by melt free radical copolymerization The copolymers acted as a compatibilizer for the PLA/PP blend [8]. However, the reinforcement of PLA/PP with natural fiber has not been reported.

2. EXPERIMENTAL PROCEDURE

2.1. Experimental Materials

Poly(lactic acid) (grade: 3052D, Mn 1.39 x 105, Mw 2.07 x 105, polydispersity 1.48) was purchased from NatureWorks LLC. Polypropylene (grade: HP500N) produce by HMC Polymers Company Ltd. PP-g-MAH was produced from Dupont with maleic anhydride functionalized. Bamboo fiber (BF) was purchased from Kanchanaburi province, Thailand.

2.2. Preparation of compound process

PP, PLA, PP-g-MAH, and bamboo fiber were first vacuum-dried at 80 °C for 8 h prior to mixing. The PLA/PP blending ratio was 40/60 w/w, PP-*g*-MAH compatibilizer was 3 phr, and bamboo fiber content was varied between 5, 10, and 20 phr. The blending was carried out using a twin screw extruder (CTE-D20L800) at 200°C.

2.3. Preparation of injection molding process

PLA/PP/Bamboo compounds were oven-dried at 80°C for 8 h before injection molding (Toyo Machinery & Metal Co., Ltd (TI-30F6). The configuration of injection temperature zones was 200/180/180/180/170 °C. The samples were subjected to mechanical property analysis

2.4. Morphology analysis

Samples for morphology analysis are from tensile test specimens. The morphology of polymer blends was examined by scanning electron microscopy (SEM) (JEOL, JSM-S410LV), operating at 15 kV. The samples were fixed on supports and coated with gold.

2.5. Thermal analysis

DSC scans were recorded on a differential scanning calorimeter Perkin Elmer, DSC 800 in inert atmosphere (nitrogen), with a heating rate of 10 °C/min. The samples (~10 mg) were placed into alumina crucibles. After the first heating 20 °C to 250 °C at a rate of 10 °C/min, held at that temperature for 5 min, then cooled to 20˚C with cooling rate of 10˚C/min before second step where the samples were heated again and thermograms for second heating were recorded. Glass transition temperature (T_g), cold crystallization temperature (T_c), melting temperature (T_m).

2.6. Fourier Transform Infrared Spectroscopy

FTIR spectra were recorded Nicolet iS5 FTIR Spectrometer equipped with a universal attenuated total reflectance. The spectra were recorded between 4000 and 500 cm−1 frequency ranges.

2.7. X-Ray Diffractometry (XRD) measurement

XRD analysis of PBS and its blend was performed on Panalytical X'Pert Pro (model-PW 3040/60) diffractometer with Cu Kα radiation (λ= 1.54°A) generated at voltage of 40 kV and current of 30 mA. Scanning was done in the 2θ angle of 5–80° with a scan step size and time per step of 0.01° and 0.5 s, respectively.

3. RESULTS AND DISCUSSION

3.1. Morphology (SEM)

Figure 1 shows an SEM image of fracture surface of PLA/PP (40/60 by weight) composites. PLA/PP without BF in (a) shows no phase separation which may due to the effect of a compatibilizer, PP-g-MAH (3 phr), addition. In Figure 1 (9-11) the yellow cycles indicate the bamboo fiber in matrix. With 5 and 10 phr the bamboo fibers were

found to distribute on the PLA/PP matrix. However high BF content of 20 phr, the fillers were agglomerate and phased separation of polymer matrix and BF was clearly observed.

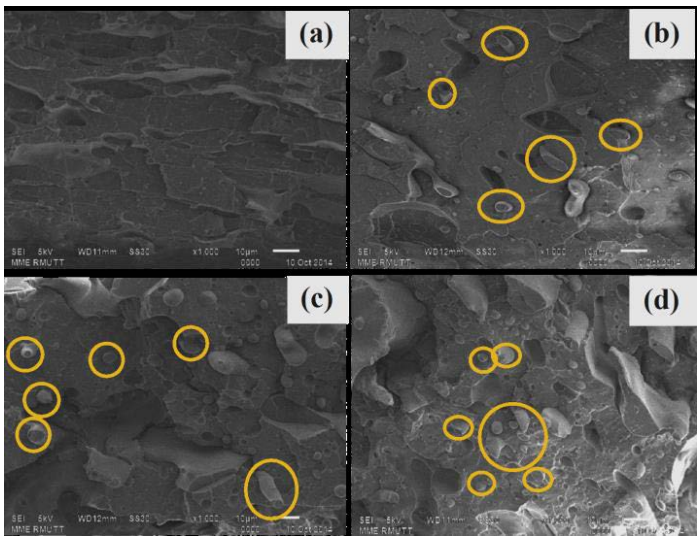

Figure 1 Morphology of PLA/PP/BF composites (3 phr PP-g-MAH) at different BF contents (a) without BF (b) 5 phr (c) 10 phr and (d) 20 phr

3.2. Chemical properties (Fourier Transform Infrared Spectroscopy, FTIR)

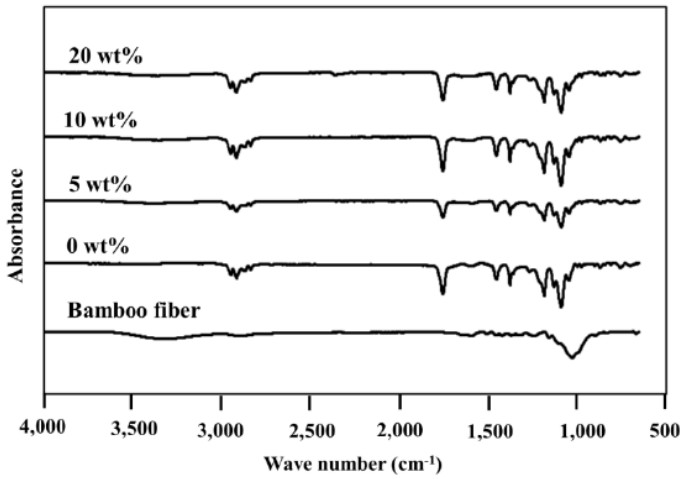

Figure 2 FT-IR spectrum of PLA/PP/BF composite at different BF content

Figure 2 exhibits the FT-IR absorptions bands of PLA/PP/BF composites. The absorbance peak at 3330 cm^{-1} of bamboo fibers represented the stretching vibration of OH and the intensity peak at 2890 cm^{-1} was attributed to the asymmetric stretching vibration of CH_2 in cellulose, hemicellulose, and lignin. The spectrum of hemicellulose (ester linkage of the carboxylic group of ferulic and p-coumaric acid of hemicellulose, C=O in hemicelluloses) of the bamboo fibers showed peak at 1735, 1596 and 1506 cm^{-1} (aromatic skeletal vibration of lignin), 1456 cm^{-1} (C-H deformation combined with aromatic ring vibration), and 1230 cm^{-1} (methoxyl groups of lignin) [10, 11]. The peak at 1735 cm^{-1}, attributed to hemicellulose, disappeared for the alkali treated BF. This disappearance of spectrum indicated that the removal of hemicellulose was successful. [10] The peak area within the region 3200–3500 cm^{-1} of the OH stretching vibration was found to be intensified after NaOH treatment. The peak located in 2922 cm^{-1} is attributed to a hydrocarbon (C–H) stretching vibration. The typical absorption peaks of cellulose are observed at 1422 and 1159 cm^{-1}. It could be highlighted that the peak was shifted to the lower value of 1032 cm^{-1} which derived from C–O and C–C stretching vibration, which may be expected as a result of alkaline treatment for the change in molecular orientation [12-13].

The FT-IR spectrum of PP observed at 2956, 2910, and 2830 cm^{-1} are attributed to –CH_2– and –CH_3 groups. The absorption bands at 1452 and 1377 cm^{-1} are attributed to -CH- and –CH_2– groups [14]. PLA shows characteristic frequencies at 1746, 2995, 2946 and 1080 cm^{-1} for C=O, –CH_3 asymmetric, –CH_3 symmetric, and C–O stretching, respectively [15-17].

For the composites, after addition of BF into PLA/PP, the O-H stretching vibration at 3657 cm^{-1} was shifted to 3650 cm^{-1}, which indicated the interactions between the BFs and polymer matrix. Treatment of BF surface by NaOH resulted in removals of the impurities which led to smaller sized and higher crystallinity of the cellulosic fibers and increased the fiber surface area [18].

3.3. Crystallinity of composites (XRD)

Figure 3 shows the XRD pattern of PLA/PP/BF composites at difference BF contents. Bamboo fiber displayed XRD peaks at 2θ 14.9°, 16.1°, 22.1°, and 34.5°, are corresponding to the (101), (110), (200), and (004) crystallographic planes, respectively [19-21]. The intensity of reflections at the angular positions 14.2°, 16.8°, 18.6° of 2θ are in agreement with the (110), (040) and (130) planes of PP [8, 22-24]. The peaks at 16.7o, 19.1o of 2θ are corresponding to the (110) and (020 plane of PLA [24]. The XRD patterns of PLA/PP/BF composites with difference bamboo fiber content was not change but the reduction of peak intensity was observed, The crystallinity of the composite was found to decreased when the amount of bamboo fibers increased. The results may arise from restriction to deformation capacity of the matrix in the elastic zone [25].

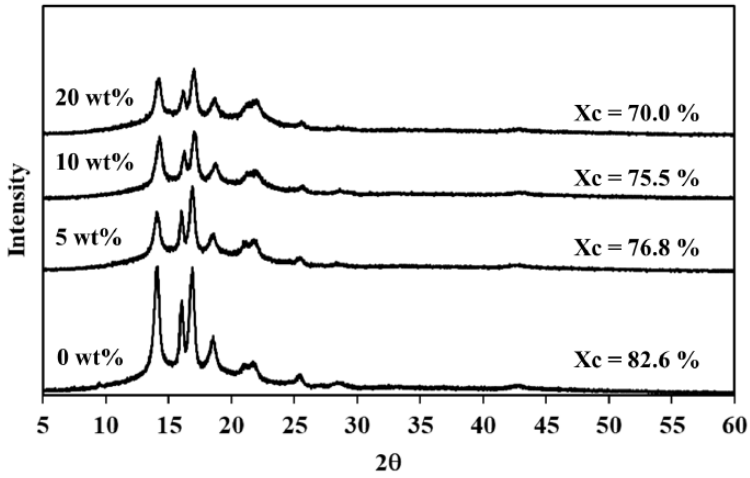

Figure 3 XRD pattern of of PLA/PP/BF composite at different BF content

3.4. Thermal property analysis

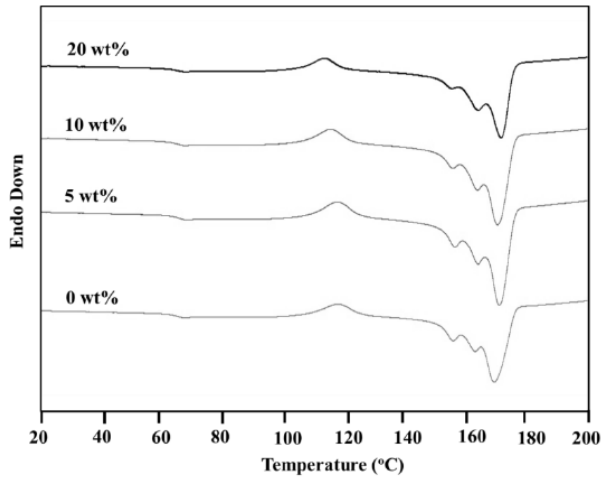

Figure 4 DSC thermogram of PLA/PP/BF composite at different BF content

Figure 4 and Table 1 depict the DSC thermogram of composites of PLA/PP (40/60 by weight) at difference BF contents. The melting temperature (T_m) of PP and PLA of all samples are not significantly changed. Two melting peaks of PLA in the composites are observed which are attributed to size distribution of crystalline lamella if the melting points are not produced due to the matrix polymorphism [26-27]. The peak of crystallization temperature (T_c) of composite was shifted to lower values with increasing the bamboo fiber contents. The results indicated the nucleating effect of BF [5] and the

presence of a transcrystalline zone form at the BF-PP interface [26]. The enthalpy of melting (ΔH_m) of main crystalline parts of PLA is in agreement with the nucleating effect of BF.

Table 1 Thermal property of PLA/PP/Bamboo fiber composites

BF (wt%)	T_g (°C)	T_c (°C)	ΔH_c (g/J)	PLA				PP	
				T_m1 (°C)	ΔH_m (g/J)	T_m2 (°C)	ΔH_m (g/J)	T_m (°C)	ΔH_m (g/J)
0	63.29	116.83	6.57	154.46	11.25	160.92	7.59	167.80	109.87
5	64.64	116.74	6.39	153.91	10.33	161.60	13.97	169.43	113.39
10	64.53	114.30	5.02	153.60	8.05	161.92	14.10	168.76	112.18
20	63.91	112.43	3.99	153.33	4.00	161.98	16.17	169.94	85.67

4. CONCLUSION

This research study the production of green composites from poly(lactic acid) (PLA) and polypropylene (PP) blend reinforced with bamboo fibers using an injection molding process. The polymer blend ratio of PLA/PP was 40/60 by weight with addition of polypropylene-grafted-maleic anhydride (PP-g-MAH) for 3 phr as a compatibilizer. The contents of BF reinforced in the PLA/PP blend were varied from 5, 10 and 20 phr. The composites were subjected to morphology of surface area by SEM, chemical property as a functional group by FT-IR, crystallinity of composite calculated from XRD and thermal property was analyzed by DSC. Morphology of fracture structure of PLA/PP blend showed smooth surface area with clear and no phase separation between fiber and polymer matrix which may due to addition of polypropylene-grafted-maleic anhydride (PP-g-MAH) for 3 phr as a compatibilizer. However, increasing the BF content to 20 phr the agglomeration of fiber and phased separation were occurred. FTIR spectrum confirmed functional group of PLA/PP/BF composite which indicated the interactions between the BFs and matrix. The XRD patterns of PLA/PP/BF composite with difference bamboo fiber contents were not changed but the intensity of peak was reduced. The crystallinity of the composite decreased with increasing BF content which may due to restriction to deformation capacity of the matrix in the elastic zone. Addition of bamboo fiber has no effect to melting temperature (Tm) of composites but the crystallization temperature (Tc) shifts to lower values with increasing the bamboo fiber contents. The results indicated nucleating effect and the presence of a transcrystalline zone form at the BF-PP interface.

5. REFERENCES

[1] H. P. S. A. Khalil, I. U. H. Bhat, M. Jawaid, A. Zaidon, D. Hermawan, Y. S. Hadi, “Bamboo fibre reinforced biocomposites: A review.,” Materials & Design, 42, 353-368, 2012.

[2] S. Amada, Y. Ichikawa, T. Munekata, Y. Nagase, H. Shimuzu. “Fiber texture and mechanical graded structure of bamboo,” Composites Part B: Engineering 28, no. 1-2 (1997): 13-20, 1997.

[3] Q. Tarrés, F. Vilaseca, P. J. Herrera-Franco, F. X. Espinach, M. Delgado-Aguilar, and P. Mutjé, "Interface and micromechanical characterization of tensile strength of bio-based composites from polypropylene and henequen strands," Industrial Crops and Products, 132, 319-326, 2019.

[4] J. E. Riccieri, L. H. D. Carvalho, A. V´azquez, “Interfacial properties and initial step of the water sorption in unidirectional unsaturated polyester/vegetable fiber composites,” Polymer Composites, 20(1), 29-371999.

[5] S. O. Han, M. Karevan, I. N. Sim, M. A. Bhuiyan, Y. H. Jang, J. Ghaffar, K. Kalaitzidou, “Understanding the reinforcing mechanisms in kenaf fiber/PLA and kenaf fiber/PP composites: A comparative study,” International Journal of Polymer Science, 2012.

[6] Y. N Wang, Y. X Weng, L. Wang, “Characterization of interfacial compatibility of polylactic acid and bamboo flour (PLA/BF) in biocomposites,” Polymer testing, 36, 119-125, 2014.

[7] Q. T. Shubhra, A. K. M. M. Alam, and M. A. Quaiyyum, “Mechanical properties of polypropylene composites: A review,” Journal of thermoplastic composite materials, 26(3), 362-391, 2013.

[8] Z. Ying-Chen, W. Hong-Yan, and Q. Yi-Ping, “Morphology and properties of hybrid composites based on polypropylene/polylactic acid blend and bamboo fiber,” Bioresource Technology, 101(20), 7944-7950, 2010

[9] H. Peltola, E. Pääkkönen, P. Jetsu, and S. Heinemann, “Wood based PLA and PP composites: Effect of fibre type and matrix polymer on fibre morphology, dispersion and composite properties,” Composites Part A: Applied Science and Manufacturing, 61, 13-22, 2014

[10] J. Xie, C. Y. Hse, F. Cornelis, T. Hu, J. Qi, and T. F. Shupe, “Isolation and characterization of cellulose nanofibers from bamboo using microwave liquefaction combined with chemical treatment and ultrasonication,” Carbohydrate polymers, 151, 725-734, 2016.

[11] G. Li, W. Lao, T. Qin, and L. Huang, “Rapid determination of biomass and polypropylene in three types of wood plastic composites (WPCs) using FTIR spectroscopy and partial least squares regression (PLSR),” Holzforschung, 69(4), 399-404, 2015.

[12] K. Zhang, F. Wang, W. Liang, Z. Wang, Z. Duan, and B. Yang, “Thermal and mechanical properties of bamboo fiber reinforced epoxy composites,” Polymers, 10(6), 608, 2018.

[13] X. Zhang, F. Wang, and L. M. Keer, “Influence of surface modification on the microstructure and thermo-mechanical properties of bamboo fibers,” Materials, 8(10), 6597-6608, 2015.

[14] H. Ren, Z. Liu, H. Zhai, Y. Cao, and S. Omori, “Effects of lignophenols on mechanical performance of biocomposites based on polyhydroxybutyrate (PHB) and polypropylene (PP) reinforced with pulp fibers,” BioResources, 10(1), 432-447, 2015.

[15] B. W. Chieng, N. A. Ibrahim, W. M. Z. W. Yunus, and M. Z. Hussein, “Poly (lactic acid)/poly (ethylene glycol) polymer nanocomposites: effects of graphene nanoplatelets,” Polymers, 6(1), 93-104, 2014.

[16] W. H. Hoidy, M. B. Ahmad, E. J. Al-Mulla, and N. A. B. Ibrahim, “Preparation and characterization of polylactic acid/polycaprolactone clay nanocomposites,” Journal of Applied sciences, 10(2), 97-106, 2010.

[17] L. Zhang, S. Lv, C. Sun, L. Wan, H. Tan, and Y. Zhang, “Effect of MAH-g-PLA on the properties of wood fiber/polylactic acid composites,” Polymers, 9(11), 591, 2017.

[18] T. Lu, S. Liu, M. Jiang, X. Xu, Y. Wang, Z. Wang, and Z. Zhou, “Effects of modifications of bamboo cellulose fibers on the improved mechanical properties of cellulose reinforced poly (lactic acid) composites,” Composites Part B: Engineering, 62, 191-197, 2014.

[19] A. D. French, “Idealized powder diffraction patterns for cellulose polymorphs,” Cellulose, 21(2), 885-896, 2014.

[20] J. Xie, C. Y. Hse, F. Cornelis, T. Hu, J. Qi, and T. F. Shupe, “Isolation and characterization of cellulose nanofibers from bamboo using microwave liquefaction combined with chemical treatment and ultrasonication,” Carbohydrate polymers, 151, 725-734, 2016.

[21] Y. Li, L. Jiang, C. Xiong, and W. Peng, “Effect of different surface treatment for bamboo fiber on the crystallization behavior and mechanical property of bamboo fiber/nanohydroxyapatite/poly (lactic-co-glycolic) composite,” Industrial & Engineering Chemistry Research, 54(48), 12017-12024, 2015.

[22] S. Ummartyotin, and C. Pechyen, “Microcrystalline-cellulose and polypropylene based composite: A simple, selective and effective material for microwavable packaging,” Carbohydrate polymers, 142, 133-140, 2016.

[23] H. Ren, Z. Liu, H. Zhai, Y. Cao, and S. Omori, “Effects of lignophenols on mechanical performance of biocomposites based on polyhydroxybutyrate (PHB) and polypropylene (PP) reinforced with pulp fibers,” BioResources, 10(1), 432-447, 2015.

[24] R. Bouza, C. Marco, Z. Martin, M. A. Gómez, G. Ellis, and L. Barral, “Dynamic crystallization of polypropylene and wood-based composites ,” Journal of applied polymer science, 102(6), 6028-6036, 2006.

[25] X. Li, B. Lei, Z. Lin, L. Huang, S. Tan, and X. Cai, “The utilization of bamboo charcoal enhances wood plastic composites with excellent mechanical and thermal properties,” Materials & Design, 53, 419-424, 2014.

[26] A. R. Sanadi and D. F. Caulfield, “Transcrystalline interphases in natural fiber-PP composites: effect of coupling agent,” Composite Interfaces, 7(1), 31-43, 2000.

[27] W. Pivsa-Art, K. Fujii, K. Nomura, Y. Aso, H. Ohara, and H. Yamane, “The effect of poly (ethylene glycol) as plasticizer in blends of poly (lactic acid) and poly (butylene succinate),” Journal of Applied Polymer Science, 133(8), 2016.

Study of lactic acid production from invert sugar with ion exchange membrane electrodialysis

R Sirisangsawang[1] and P Kitchaiya[1,2]

[1]*Department of Chemical Engineering, Faculty of Engineering, King Mongkut's Institute of Technology Ladkrabang, Bangkok, 10520, Thailand*

[2]*prakob.ki@kmitl.ac.th*

Abstract.

Lactic acid is an important raw material for biodegradable production. This work was studied to lactic acid production from invert sugar. First step, the invert sugar was reacted with sodium hydroxide by alkaline degradation. Semi-batch reactor was used because it can controlled concentration of raw material and temperature. The yield of lactic acid from semi-batch was higher than batch reactor. It can produce high yield of lactic acid about 60%. Second step, the product from alkaline degradation was used for raw material for electrodialysis. For this experiment, the sodium lactate from alkaline degradation was changed to lactic acid with this technique. The constant voltage was applied at 4, 6 and 8 volts. When cation exchange membrane was used and voltage increased, the recovery of lactic acid decreased. It could recover about 50% lactic acid. Moreover, it can recycled sodium hydroxide for alkaline degradation.

Keywords.-

1. INTRODUCTION

The problem of waste in the world, mostly it due to plastic waste which made from petroleum industry. The campaign, stop the use of plastic, occurred. However, people still need plastic for many applications such as packaging. An attractive material which was alternative and can used to replace plastic called biodegradable plastic. Polylactic acid (PLA) was an interested biodegradable plastic. Polylactic acid was produced from polymerization of lactic acid. Lactic acid (CH3CHOHCOOH) was monomer of polylactic acid. It can produced from renewable resource such as corn, cassava, sugar. It can produce from either fermentation or chemical synthesis. The fermentation can got high yield, more than 90% depend on fermentation process or type of microorganism [1]. However, fermentation is difficult to control microorganism and takes a long time to ferment. Lactic acid from chemical synthesis got lower yield than fermentation. But it is easy and does not take a long time reaction. In the past, alkaline degradation of sugar was studied by many

researcher. This process was simple to produced salt of hydroxy acid and the main product was sodium lactate that can changed to lactic acid [2-4].

Many techniques can be used for convert sodium lactate to lactic acid such as adsorption, reactive distillation, and electrodialysis [5-7]. Electrodialysis is the technique which ion-exchange membrane can change from salts to acid under the driving force of electrical potential. The electrodialysis is an interested method because it was friendly environment and it didn't produce waste. This research study the feasibility of lactic acid production from invert sugar. First, study the alkaline degradation from invert sugar after that convert sodium lactate to lactic acid by using electrodialysis technique with ion exchange membrane.

2. MATERIAL AND METHODS

2.1. Material

Sucrose was purchase in supermarket in Thailand. After that, it was hydrolyzed with sulfuric acid at 65°C for 6 hours to invert sugar. Sodium hydroxide (NaOH) and sulfuric acid were analytical grade.

2.2. Method

2.2.1. Sodium lactate production from alkaline degradation

For semi-batch reactor, invert sugar was periodically added in desired sodium hydroxide solution in in-house double jacketed glass reactor. The temperature of solution in the reactor was controlled by flowing of water from circulating bath at 50°C. Sodium lactate was the main product from alkaline degradation was produced. Sample was analyzed in the percentage of lactic acid yield with High Performance Liquid Chromatograph (HPLC). After that, repeated experiment was study in batch reactor.

2.2.2. Electrodialysis

The single-state in-house electrolytic cell was use for convert sodium lactate to lactic acid. It consisted of power supply, pump and container with cation exchange membrane or anion exchange membrane. The membrane with the effective area of 144 cm2 was set in the middle of cell between catholyte and anolyte. The type of cation and anion exchange membrane was CSO and AMV respectively from AGC Engineering Ltd, Japan. The two electrodes were made of stainless steel.

Sodium lactate which was produced by alkaline degradation was added with CO2 until pH 8-9. After that it was added in anode side and low concentration of sodium hydroxide were added in cathode side for cation exchange membrane. The voltage was supplied and the sample were taken for analysed. The reaction will stopped when pH of anolyte was lower than 2.5.

After that the experiment was set up with anion exchange membrane. The sodium lactate and low concentration of lactic acid were added in catholyte and anolyte, respectively. Repeated the same experiment as before.

2.2.3. Analytical procedure:

The sample of sodium lactate was taken and acidified until pH about 2. After that lactic acid concentration was analysed by HPLC of Thermo Spectra SYSTEM with Platisil 5 µm ODS column using UV-VIS detector at 210 nm. The mobile was 5 mmol sulfuric acid at flowrate 0.8 ml/min. The concentration of sodium hydroxide was analysed with titration with 0.01 M hydrochloric acid.

3. RESULTS AND DISCUSSIONS

3.1. The study of alkaline degradation of sodium lactate

When the invert sugar was added into sodium hydroxide, the salt of hydroxy acid was produced. The main product from this reaction was sodium lactate. The reaction of alkaline degradation was studied in batch and semi-batch reactor at temperature 50°C. The results showed in Table 1.

Table 1 The yield of lactic acid in batch and semi-batch reactor

Experiment	Initial concentration of sodium hydroxide (M)	Time (hr)	Yield of lactic acid (%)
Batch	8.5	2	57.2
		4	57.4
		8	59.5
Semi-batch	3.5	8	48.1
	6.0	8	64.2
	8.5	8	64.5

From the result, it showed that the yield from the semi-batch reaction was higher than batch reactor. In the semi-batch reactor, the invert sugar was slowly added into the sodium hydroxide, in batch reactor the two solutions was mixed immediately. Therefore, the concentration of invert sugar in semi-batch reactor was kept lower than in batch all the time of reaction. On the contrary, the concentration of sodium hydroxide was high in semi-batch reactor. Low concentration of sugar and high concentration of sodium hydroxide will support the lactic acid yield and decrease other products such as acetic acid, formic acid and glycolic acid [8]. Moreover, the temperature in batch reactor will increased rapidly due to exothermic reaction. In this experiment, temperature increased from 50 to 58°C, while semi-batch can controlled temperature and the temperature of solution was not changing 1°C. Batch is not good for large scale, it will produce very high temperature, that it is not safety. Therefore, semi-batch was suitable for this reaction at high both concentration of raw material. The concentration of alkaline effected on the yield of lactic acid [8]. The initial concentration of sodium hydroxide at 3.5, 6 and 8.5 M was studied. When high

concentration of sodium hydroxide was use the yield of lactic acid will increased. The yield were 48.1, 64.2 and 64.5% at 3.5, 6.0 and 8.5 M of sodium hydroxide, respectively. High initial concentration of sodium hydroxide improved lactic acid yield. From the result, 6M of sodium hydroxide was suitable for further study.

3.2. The study of electrolysis with cation exchange membrane/ anion exchange membrane

Sodium lactate from invert sugar was prepared. The invert sugar was reacted with 6 M sodium hydroxide at 50°C in semi-batch reactor. After that the solution was added with CO_2 and filter. The filtrate was added in single-stage electrolyzer with cation exchange membrane. Anolyte and catholyte was sodium lactate and sodium hydroxide, respectively. The results with cation exchange membrane were applied. The results were shown in the Figure 1

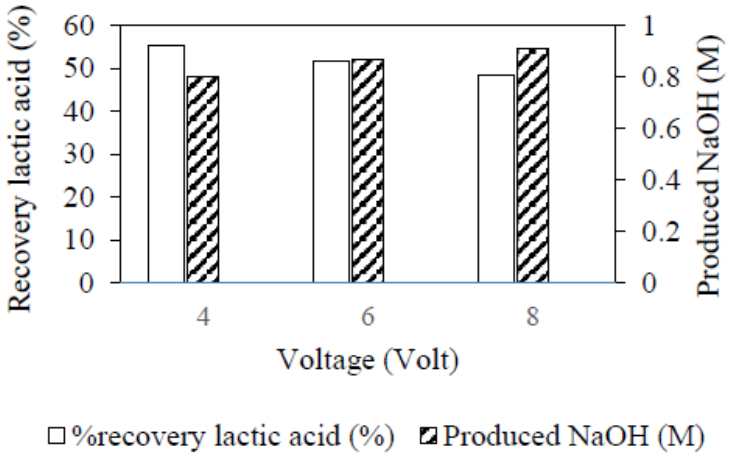

Figure 1 The recovery of lactic acid and produced sodium hydroxide at 4, 6 and 8 volts when using cation exchange membrane

When the voltage was applied, sodium lactate in anode side will dissociate and sodium ion (Na^+) was transferred pass cation exchange membrane to cathode. At cathode side the reduction occurred, H_2O received electron and the hydroxide ion (OH^-) and H_2 (g) was produced. Na^+ will change to sodium hydroxide at cathode side. Therefore the sodium hydroxide will increased as time increased. As voltage increased, sodium hydroxide were produce as 0.80 0.87 and 0.91 M at 4, 6 and 8 volts, respectively. At anode side the oxidation occurred, H_2O was oxidized to hydrogen ion (H^+) and O_2 (g). Lactate ion (La^-) in anode side will form with H^+ to lactic acid, so the lactic acid will increased at this side. The recovery of lactic acid were 55.5 51.7 and 48.6% at 4, 6 and 8 volts, respectively. The recovery of lactic acid at high voltage was lower than at low voltage. At high voltage lactate ion might be oxidized to proton and pyruvate ion, so the lactic acid yield was

decreased and the recovery of lactic acid was decreased. After that the anion exchange membrane was used replace to cation exchange membrane. The sodium lactate was added in cathode side and low concentration of lactic acid was added in anode side. After voltage was applied, the yield of lactic acid was decrease with time as shown in Fig.2. It decreased more than 95%. These results showed that the lactic acid wasn't produced with single anion exchange membrane, lactate ion pass through membrane difficultly. While pH of solution at this side slightly increased, it showed that hydroxide ion (OH-) from cathode side may pass through membrane to anode side. Thus only single anion exchange membrane was not suitable for lactic acid production in this condition.

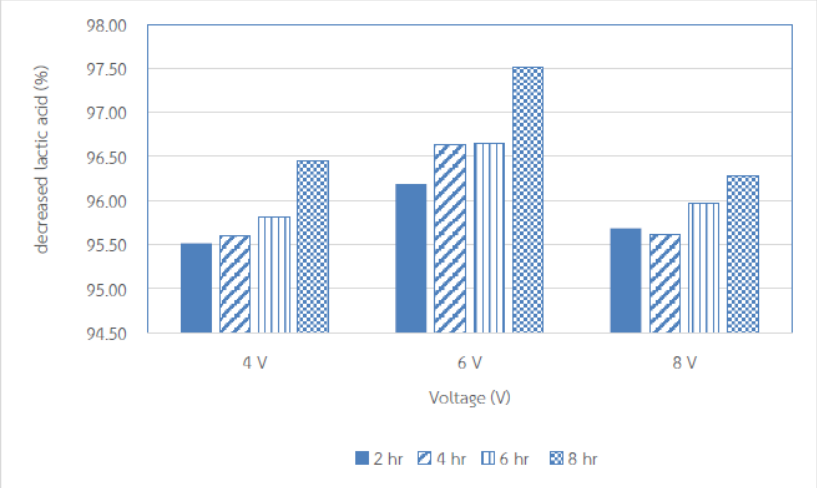

Figure 2 The decreasing lactic acid when using anion exchange membrane at 4, 6 and 8 volts

The lactic acid production from invert sugar with alkaline degradation and electrodialysis is advantage. Sucrose and sodium hydroxide were cheap and easy to found in Thailand. The process is easy and low temperature reaction was used and low energy cost too. Moreover, the yield was quite high.

After that, sodium lactate from alkaline degradation can convert to lactic acid by using electrolysis technique with cation exchange membrane. It can recovery lactic acid more than 50%, and it enable efficiency sodium hydroxide recycling as using raw material for alkaline degradation. This process was shown in Fig.3. This process was good for environment because no waste from this process and didn't used chemical. However, this process used only cation exchange membrane, so it took high energy consumption.

4. CONCLUSIONS

The semi-batch reactor was suitable for lactic acid production with alkaline degradation. When high concentration of sodium hydroxide was used, the lactic acid yield was high. For cation exchange membrane electrolysis, the voltage has effected on the recovery lactic acid and this process can got sodium hydroxide which can recycle for alkaline degradation. The recovery of lactic acid was about 50-55% and could produce 0.8-0.9 M sodium hydroxide at this conditions.

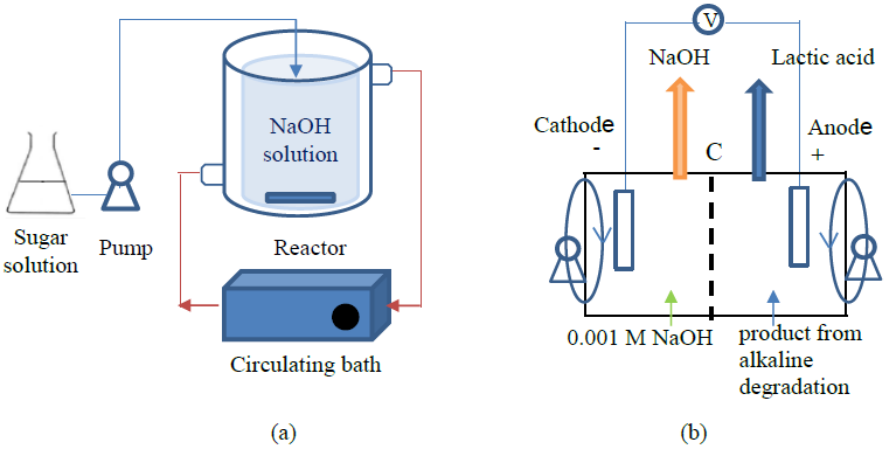

Figure 3 The process of lactic acid production from invert sugar with cation exchange membrane electrolysis (a) alkaline degradation (b) Electrodialysis with cation exchange membrane; C: cation exchange membrane

5. REFERENCES

[1] L. Ye, X. Zhou, M. S. B. Hudari, Z. Li, and J. C. Wu, "Highly efficient production of L-lactic acid from xylose by newly isolated Bacillus coagulans C106," Bioresource technology, 132, 38-44, 2013.

[2] P. A. Shaffer, and T. E. Friedemann, "Sugar activation by alkali I. Formation of lactic and saccharinic acids," Journal of Biological Chemistry, 86(1), 345-374, 1930.

[3] B. Y. Yang, and R. Montgomery, "Alkaline degradation of glucose: effect of initial concentration of reactants," Carbohydrate Research, 280(1), 27-45, 1996.

[4] B. Y. Yang, and R. Montgomery, "Alkaline degradation of fructofuranosides," Carbohydrate Research, 280(1), 47-57, 1996.

[5] E. N. Kaufman, S. P. Cooper, and B. H. Davison, "Screening of resins for use in a biparticle fluidized-bed bioreactor for the continuous fermentation and separation of lactic acid," Applied Biochemistry and biotechnology, 45(1), 545-554, 1994.

[6] Y. Seo, W. H. Hong, and T. H. Hong, “Effects of operation variables on the recovery of lactic acid in a batch distillation process with chemical reactions,” Korean Journal of Chemical Engineering, 16(5), 556-561, 1999.

[7] A. Saxena, G. S. Gohil, and V. K. Shahi, “Electrochemical membrane reactor: single-step separation and ion substitution for the recovery of lactic acid from lactate salts,” Industrial & engineering chemistry research, 46(4), 1270-1276, 2007.

[8] J. M. De Bruijn, A. P. G. Kieboom, and H. Van Bekkum, “Alkaline degradation of monosaccharides III. Influence of reaction parameters upon the final product composition,” Recueil des Travaux Chimiques des Pays-Bas, 105(6), 176 -183, 1986.

A Study of Recycle Cellular Lightweight Concrete as Coarese Aggregates in Concrete Bricks.

Amphon Jarasjarungkiat[1], Setsawat Chuaisrinual[2]

[1,2]Department of Civil Engineering, Faculty of Engineering, King Mongkut's institute of Technology Ladkrabang, Bangkok, Thailand.

[1]Corresponding author; E-mail address: amphon.ja@kmitl.ac.th

Abstract.

This research aims to apply the aggregate material in concrete blocks with Cellular Lightweight Concrete (CLC), which is a waste from CLC manufacturing. Even though, this type of lightweight concrete has less compressive strength than ordinary concrete block. But it has advantageous properties such as heat insulation, Sound insulation, light weight, and ability to trimmed. Moreover, recycling the waste can reduce the impacts on environment. By experiment the ratio of CLC concrete fragment in concrete blocks as a coarse aggregate. The researchers compared the properties of ordinary concrete blocks with CLC mixed concrete blocks according to the non-load-bearing concrete standards (TIS 58-2533) [1]. The results show that dry unit weight is inversely variation to specimens (1) ordinary concrete block, (2) concrete block with CLC passed sieve no. 4 and (3) no. 8 respectively. Compressive strength is directly variation to dry unit weight. And water absorption is inversely variation to dry unit weight. Finally, the specimens that passed the standard criterias are ordinary and mixed CLC passed sieve no. 4. There are samples also can be improved in construction technology and reduce environmental impact.

Keywords. concrete block, lightweight concrete, recycled material, cellular, CLC

1. INTRODUCTION

Lightweight concrete is a concrete that has less unit weight than general concrete. Lightweight concrete is a new product manufactured from natural raw materials as portland cement, lime sand, gypsum, water, air entraining admixtures and design admixtures in a unique formula. Normally, the concrete has a unit weight around 2300 kg/m3 in dry conditions. But lightweight concrete such as Cellular Lightweight Concrete (CLC) has dry unit weight between 600 - 1600 kg/m3. [2]

Cellular Lightweight Concrete (CLC) is now widely used in construction engineering. Because it has better properties than general concrete such as heat insulation, sound insulation and lightweight. For these reasons, CLC concrete is more widely accepted in

modern construction than general concrete. In addition, many manufacturing processes of CLC yield that significant CLC concrete waste.

For this reason, the researchers realized the importance of recycling the concrete fragment as coarse aggregate materials used in concrete blocks to bring the benefits of CLC to develop new concrete blocks as an alternative for construction materials.

2. METHOD

This study compares the properties of concrete blocks and CLC mixed concrete fragment. The specimen's dimension of tested specimens is specified as a cube with the size of 15 cm × 15 cm × 15 cm. The specimens of concrete block have admixture ratio as cement per sand per stone equals to 1: 1: 1. And the sample with CLC have admixture ratio as cement per sand per stone per CLC fragment equal to 1: 1: 1: 1. Water cement ratio of both specimens is 0.4. Mixed samples are separated into 2 cases with the size remaining on sieve no. 4 and no. 8. Then all specimens be compared with the non-load-bearing concrete standards (TIS 58-2530), to confirm that the concrete block passed the standard criteria for construction.

Table 1 Compressive strength of non-load-bearing concrete standards (TIS 58-2533)

Minimum of Compressive strength Mpa. (ksc.)	
Averrage from 5 block.	For each block.
2.5 (25.5)	2.0 (20.4)

Table 2 Water absorption of non-load-bearing concrete standards (TIS 58-2533)

Long side shrinkage percent	Maximum humidity Percentage of water absorption (Average 5 concrete blocks)		
	Average annual humidity percent		
	<50	50≤ W ≤75	75 <
≤ 0.03	35	40	45
0.03 < L ≤ 0.45	30	35	40
0.45 ≤	25	30	35

2.1. The manufacturing process of concrete block.

1 Mixing cement, sand, stone and water with the specified ratio.

2 Grinding CLC fragment with the Los Angeles Abrasion Machine. Then sieve the fragment to select the remaining fragment on sieve number 4 and 8.

3 Producing CLC foam from foaming agent with foam generator machine and air pump. Immediately leaving the generator, the smooth foam must be used rapidly since deterioration after mixed exposure to the environment.

Figure 1 CLC fragment recycled remain on the sieve.

4 Mixes admixture together as specific ratio. For general concrete block used ratio 1: 1: 1. And for mixed CLC concrete block used ratio 1: 1: 1: 1.

5 After a proper mixing. the concrete is casted into the formwork and finishing the surface with a trowel. Then surface is sealed with plastic to prevent water evaporation.

6 Curing CLC in the formwork for 24 hours. Then remove from formwork. And curing the samples in water.

7 By the age 7 days old, the specimens were brought out of the water. Wiping the skin to dry, then the specimens were weighted. Then baked for 24 hours to completely dry. And measure the size on both sides of the length with the vernier caliper and then tested to compressive strength.

2.2. Water absorption

The specimens were brought out from curing then drying the skin and weighted the samples to collect the saturated condition weight. Then drying the samples in the oven for 24 hours to completely dry and collect the absolute dry condition weight. After that calculating the water absorption from the formula below.

$$\%\mathrm{W} = \left[\frac{SW - DW}{DW}\right] \times 100\% \quad (1)$$

- SW : Saturated weight, kg

- DW : Dry weight, kg
- %W : Water absorption, %

2.3. Compressive Strength

1 Measuring samples in width, length and height by vernier caliper.

2 Weighing samples and taking notes.

3 installing samples into the concrete compression testing machine.

4 Applying the compression to the specimens at a constant rate in the range of 0.14 - 0.34 Newton per square millimeter per second to the point of failure. And collecting compressive strength data to calculate compressive stress from formula below. (TIS 409-2525)[3]

Calculation

$$\sigma = F/(L \times W) \tag{2}$$

- W : Width of the sample(cm.)
- L : Length of the sample(cm.)
- H : Height of the sample (cm.)
- F : Compressive force (kg.)
- σ : Compressive strength (ksc.)

Figure 2 General concrete block specimen.

2.4. Analysis results

From the experiments, the properties were compared with concrete block criteria (TIS 58-2533). Specimens which pass the standard shall be considered for engineering construction.

3. RESULT AND ANALYSIS

From the testing results, the density of specimens show that density is inversely proportional to percentage of foam.

Table 3 Comparison of properties of concrete specimens.

Average properties		General	CLC sieve no.4	CLC sieve no.8
Dry Unit Weight	kg/m3	1870.65	1579.52	1406.83
Comp. strength	ksc	75.44	36.36	10.50
Water absorption	%	4.05	9.91	12.24

From table 3, the weight of the samples containing CLC decreased. Because the aggregate mass added has a pore structure inside that make the concrete block has more lightweight than general.

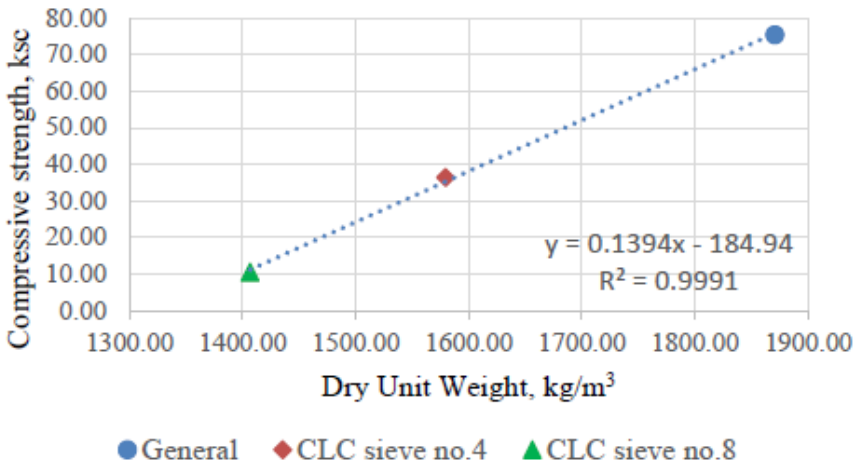

Figure.3 Relationship between dry unit weight and compressive strength

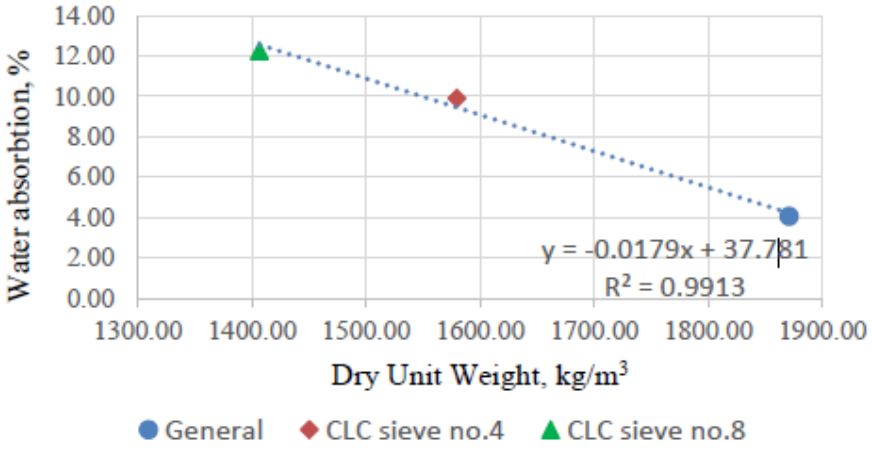

Figure 4 Relationship between dry unit weight and water absorption

From Figure 3 compressive test show that, the weight of the concrete is reduced because the combination of CLC and the compressive strength. The compressive strength of concrete blocks decreases varies with decreasing of weight. From concrete blocks with compressive strength 75.44 ksc. To only 10.50 ksc. In the case of mixed with CLC passed sieve no.8.

From Figure 4 water absorption test show that, water absorption is inversely proportional with dry unit weight. Concrete block with CLC passed sieve no.8 specimen has more pore structural than the other. That cause this sample has the most water absorption (12.24%).

4. CONCLUSION

The specimens which passed all criteria can be classified in non-load-bearing concrete standards. From the analysis, general concrete block has average compressive strength at 75.44 ksc being above the standard. For specimens with CLC passed sieve no.4 is 36.36 ksc that higher than the compressive standard.

Moreover, water absorption test of all specimens has water absorption under the standard criteria (from table 2 the lowest value is 25%). Every samples pass this criterion.

However, concrete block with CLC passed sieve no.8 has compressive strength under criteria value (from table 1 minimum average compressive load is 25.5 ksc.). Because this admixture has too much pore structure and reduced compressive strength.

Finally, the specimens pass the standard criteria and can be an optional of construction are ordinary concrete block and concrete block with CLC passed sieve no.4.

5. ACKNOWLEDGMENT

The author would like to send gratitude to support this research. especially, the professors for advising to improve this project.

6. REFERENCES

[1] *The non-load-bearing concrete standards,* TIS 58-2533. December 2019. [Online]. Available: https://cpacacademy.com /download/cpacacademy.com/b-pc026.pdf.

[2] A. Jarasjarungkiat & S. Chuaisrinual. October 2019. "Development of Effective Lightweight Material for Construction Building. In IOP Conference Series: Materials Science and Engineering," Vol. 639, No. 1, p. 012034. IOP Publishing.

[3] *Standard test method for compressive strength of concrete specimens,* TIS 409-2525. December2019. [Online]. Available: http://www.fio.co.th/web/tisi_fio/full text/TIS409-2525.pdf.

[4] N. Tanpaiboonkul, "Replacing Cement by Dust from Rock Crushing Plant in Interlocking Block Production," M.S. thesis, Eng., Princess of naradhiwas Univ., 2017.

[5] P. Khembubpha. "A Study of General Properties of Concrete Using Recycled Concrete Coarse Aggregate Having Different Compressive Strengths," M.S. thesis, Engi., Kasetsart Univ., 2005.

[6] T. Saisut. Recycled Coarse Aggregate by Residual Concrete Piles. M.S. thesis, Eng., KMUTT., 2012.

[7] K. Sutthiphan. "Light weight concrete for the construction of physics and engineering," December 2019. [Online]. Available: http://www.dss.go.th/images/st-article/pep-11-2557-Concrete.pdf.

[8] N. Tengsiritum. "An Optimization Model for a Prediction on mix proportion of Cellular Lightweight Concrete," M.S. thesis, Eng., KMITL., 2015.

[9] Z. M. Yaseen, R. C. Deo, A. Hilal, A. M. Abd, L. C. Bueno, S. Salcedo-Sanz and M. L. Nehdi, "Predicting compressive strength of lightweight foamed concrete using extreme learning machine model. Advances in Engineering Software," 115, 112-125, 2018.

[10] T. Nguyen. 2018. 3D Meso-Scale Modelling of Foamed Concrete Based on X-Ray Computed Tomography. (Science direct research paper, Department of Infrastructure Engineering, The University of Melbourne, Melbourne, Australia).

[11] K. T. Wan. 2018. Development of Low Drying Shrinkage Foamed Concrete and Hygro-Mechanical Finite Element Model for Prefabricated Building Façade Applications. (Department of Civil and Environmental Engineering, Brunel University London, UK).

[12] P. Damrongchai. 1999. Construction Materials. (1th ed.). Khonkaen: Department of Civil Engineering Faculty of Engineering Khonkaen University.

[13] W. Chowichian, Concrete technology. 2001. (9th ed.). Khonkaen: Bangkok. Sampanpanit.

[14] S. Taitachang. "The Study of Aluminum Dross Effect on Refractory Brick Properties," M.S. thesis, Eng., RMUTT., 2010.

[15] S. Chaichana. 1999. Concrete Technology Laboratory. (2th ed.). Bangkok. VJ Printing., Ltd.

[16] S. Santadwattana. 2011. Prediction on the Properties of Cellular Light Weight Concrete from Concrete Density. (Bachelor project, Faculty of Engineering, King Mongkut's Institute of Technology Ladkrabang).

[17] *Standard test method for compressive strength of cylindrical concrete specimens*, TIS. 409-2525. June 2018. [Online]. Available: http://research.rid.go.th/vijais/moa/.

[18] *Industrial product standards for Cellular Lightweight Concrete*, TIS. 2601-2556. June 2018. [Online]. Available: http://research.rid.go.th/vijais/moa/

[19] J. Phaiphuphim. “Stress-Strain Curve of Cellular Lightweight Concrete,” M.S. thesis, Eng., Ubon Ratchathani Uni., 2014.

[20] P. Orathaiwan, S. Chuaisrinual and I. Sirikul. 2017. Study on Properties of Lightweight Concrete Mixing with Recycled Glass Bead after Configuration. (Bachelor project, Faculty of Engineering, King Mongkut's Institute of Technology Ladkrabang).

[21] A. Chalermwong. “Study of Compressive Strength and Sound Absorption of Cellular Lightweight Concrete with Superplasticizer,” M.S. thesis, Eng., Ubon Ratchathani Univ,. 2013.

Risk factors affecting conflict management for construction government project in Thailand

Bancha Teanngen[1], Wuttipong Kusonkhum[2], Surapong Liwthaisong[3],Tanayut Chaitongrat[4] and Korb Srinavin[5]

[1,2]Doctoral degree student, Department of Civil Engineering, Faculty of Engineering, Khon Kaen University, Khon Kaen, Thailand.

[3,4]Lecturer, Faculty of Architecture, Urban Design and Creative Arts, Mahasarakham University, Mahasarakham, Thailand.

[5] Ascociate Professsor, Department of Civil Engineering, Faculty of Engineering, Khon Kaen University, Khon Kaen, Thailand.

Krobsri@kku.ac.th

Abstract.

Risk management has been widely used in project management to reduce the delay of projects or the loss from a granted budget. However, conflict is one of many causes which increases risk, affect timeline and budget of the project. Therefore, this research study aims to study the important risks which should be handled at most. The study tool was a questionnaire and the data were collected from 454 government projects which all project officer responded 100%. The data had taken into qualitative risk analysis and the results had found that there were 12 risk factors of conflict which affected cost management of the project, and also 8 risk factors of conflict which affected time management of the project.

Keywords. -

1. INTRODUCTION

Conflict and defectiveness in construction industry are unavoidable. They could happen in different procedures in construction works [1]. In addition, the conflict will affect time and cost of the project [1- 4]. Further, the construction project has lost 32.2 million US dollars in finance division also wasted time of resolving disputes 13 months in average [5].

A construction project has a clear scope of operations as the agreement and conditions of stakeholders [1-4]. The success of a construction project consists of project cost management, project time management, and project quality management [6]. Additionally, one of the knowledges applied in construction management for an effective and successful

project is risk analysis, which affects time and cost of the project. Moreover, a conflict of a project is also considered as a risk. The tool which is used to handle with construction project conflict could analyze the risk. Thus, this research study would present qualitative risk analysis [7] to find factors of conflict which affect time and cost of a project and to increase efficiency of conflict management.

2. LITERATURE REVIEW

The successful conflict management is to understand the different aspects of conflicts includes how the conflicts happen. Conflicts can be classified as follows; 1) Intrapersonal Conflict, 2) Interpersonal Conflict, 3) Intragroup Conflict [9]. According to the related studies, factors of conflicts could be summarized as in picture number 1.

Table 1 Summary of factors of construction conflict

Factors of Conflict Which Lead to Disputes	Related Studies (Key Support)
1.Conflicts Which Affect the Time	
1.1 Authority of the project owner [1,3,10-12]	Jaffar, N., Tharim, A. A., & Shuib, M. N. (2011), Pétursson, B. K. (2015), H. J. Thamhain and D. L. Wilemon. (1975), Acharya, N. K., Dai Lee, Y., & Man Im, H. (2006), Acharya, N. K., Dai Lee, Y., & Kim, J. K. (2006), Yates, J. K., & Epstein, A. (2006)
1.2 An unclear scope of project [1,3,11,12]	Jaffar, N., Tharim, A. A., & Shuib, M. N. (2011), Pétursson, B. K. (2015), Acharya, N. K., Dai Lee, Y., & Man Im, H. (2006), Yates, J. K., & Epstein, A. (2006)
1.3 Site condition [1- 3,13-15]	Jaffar, N., Tharim, A. A., & Shuib, M. N. (2011), Pétursson, B. K. (2015), San Loke, Y. (2013), Khahro, S. H., & Ali, T. H. (2014), Acharya, N. K., Dai Lee, Y., & Man Im, H. (2006), Acharya, N. K., Dai Lee, Y., & Kim, J. K. (2006), Yates, J. K., & Epstein, A. (2006), Zidane, Y., & Andersen, B. (2018)
1.4 Neglect or negative attitude of the project's members [2,11]	Jaffar, N., Tharim, A. A., & Shuib, M. N. (2011), Acharya, N. K., Dai Lee, Y., & Man Im, H. (2006)

Table 1 Continued

Factors of Conflict Which Lead to Disputes	Related Studies (Key Support)
1.5 Deviation of the project's documents [3,11]	Jaffar, N., Tharim, A. A., & Shuib, M. N. (2011), Acharya, N. K., Dai Lee, Y., & Man Im, H. (2006)
1.6 Conflict of the locals [3,11,16]	Jaffar, N., Tharim, A. A., & Shuib, M. N. (2011), Acharya, N. K., Dai Lee, Y., & Man Im, H. (2006), Maemura, Y., Kim, E., & Ozawa, K. (2018)
1.7 Confused desire of the project owner [3,11]	Jaffar, N., Tharim, A. A., & Shuib, M. N. (2011), Acharya, N. K., Dai Lee, Y., & Man Im, H. (2006)
1.8 A change of work [2-3,11-12,14-15]	Jaffar, N., Tharim, A. A., & Shuib, M. N. (2011), Pétursson, B. K. (2015), San Loke, Y. (2013), Khahro, S. H., & Ali, T. H. (2014), Acharya, N. K., Dai Lee, Y., & Man Im, H. (2006), Acharya, N. K., Dai Lee, Y., & Kim, J. K. (2006), Yates, J. K., & Epstein, A. (2006), , Zidane, Y., & Andersen, B. (2018)
1.9 Late attendance [1-3,11-12]	Jaffar, N., Tharim, A. A., & Shuib, M. N. (2011), Pétursson, B. K. (2015), San Loke, Y. (2013), Acharya, N. K., Dai Lee, Y., & Man Im, H. (2006),Yates, J. K., & Epstein, A. (2006)
1.10 Narrow constructionsite [1,3,11]	Jaffar, N., Tharim, A. A., & Shuib, M. N. (2011), Pétursson, B. K. (2015),Acharya, N. K., Dai Lee, Y., & Man Im, H. (2006)
1.11 Shortage ofmaterials [3,11-12]	Jaffar, N., Tharim, A. A., & Shuib, M. N. (2011), Acharya, N. K., Dai Lee, Y., & Man Im, H. (2006), Yates, J. K., & Epstein, A. (2006), Zidane,Y., & Andersen, B. (2018)
1.12 Late decision making of the project owner [1,3,11-12,14,16]	Jaffar, N., Tharim, A. A., & Shuib, M. N. (2011), Pétursson, B. K. (2015), , H. J. Thamhain and D. L. Wilemon. (1975), Acharya, N. K., Dai Lee, Y., & Man Im, H. (2006), Acharya, N. K., Dai Lee, Y., & Kim, J. K. (2006), Maemura, Y., Kim, E., & Ozawa, K. (2018), Yates, J. K., & Epstein, A. (2006), Zidane, Y., & Andersen, B. (2018)
1.13 The delay of delivering construction site to a contractor [3,11]	Jaffar, N., Tharim, A. A., & Shuib, M. N. (2011), Acharya, N. K., Dai Lee, Y., & Man Im, H. (2006)

Table 1 Continued

Factors of Conflict Which Lead to Disputes	Related Studies (Key Support)
1.14 Shortage of machines [3,11-12,14]	Jaffar, N., Tharim, A. A., & Shuib, M. N. (2011), Acharya, N. K., Dai Lee, Y., & Man Im, H. (2006), Yates, J. K., & Epstein, A. (2006), Zidane,Y., & Andersen, B. (2018)
1.15 The delay of contractor's work [3,11-12]	Jaffar, N., Tharim, A. A., & Shuib, M. N. (2011), Acharya, N. K., Dai Lee, Y., & Man Im, H. (2006), Yates, J. K., & Epstein, A. (2006)
1.16 A contractor with work inefficiency [1,3]	Jaffar, N., Tharim, A. A., & Shuib, M. N. (2011), Pétursson, B. K. (2015), , Acharya, N. K., Dai Lee, Y., & Man Im, H. (2006), Yates, J. K., & Epstein, A. (2006), Zidane, Y., & Andersen, B. (2018)
1.17 A subcontractor with work inefficiency [1,3]	Jaffar, N., Tharim, A. A., & Shuib, M. N. (2011), Pétursson, B. K. (2015), , Acharya, N. K., Dai Lee, Y., & Man Im, H. (2006), Yates, J. K., & Epstein, A. (2006), Zidane, Y., & Andersen, B. (2018)
1.18 Strikes of workers [3,11]	Jaffar, N., Tharim, A. A., & Shuib, M. N. (2011), Acharya, N. K., Dai Lee, Y., & Man Im, H. (2006)
1.19 Natural disaster [3,11]	Jaffar, N., Tharim, A. A., & Shuib, M. N. (2011), Acharya, N. K., Dai Lee, Y., & Man Im, H. (2006)
1.20 The delays of other parties involved in the project [1,3,10-11]	Jaffar, N., Tharim, A. A., & Shuib, M. N. (2011), Pétursson, B. K. (2015), , H. J. Thamhain and D. L. Wilemon. (1975), Acharya, N. K., Dai Lee, Y., & Man Im, H. (2006)
1.21 The lack of Communication [1,3,11,13-14,17]	Jaffar, N., Tharim, A. A., & Shuib, M. N. (2011), Pétursson, B. K. (2015), Khahro, S. H., & Ali, T. H. (2014), Huo, X., Zhang, L., & Guo, H. (2016), Acharya, N. K., Dai Lee, Y., & Man Im, H. (2006), Zidane, Y., & Andersen, B. (2018)
1.22 An accident in the project [3,11]	Jaffar, N., Tharim, A. A., & Shuib, M. N. (2011), Acharya, N. K., Dai Lee, Y., & Man Im, H. (2006)

Table 1 Continued

Factors of Conflict Which Lead to Disputes	Related Studies (Key Support)
1.23 Shortage of manpower [1-3,10-13]	Jaffar, N., Tharim, A. A., & Shuib, M. N. (2011), Pétursson, B. K. (2015), , San Loke, Y. (2013), Khahro, S. H., & Ali, T. H. (2014), H. J. Thamhain and D. L. Wilemon. (1975), Acharya, N. K., Dai Lee, Y., & Man Im, H. (2006), Yates, J. K., & Epstein, A. (2006)
1.24 Too many numbers of other participants involved in the project [3,11]	Jaffar, N., Tharim, A. A., & Shuib, M. N. (2011), Acharya, N. K., Dai Lee, Y., & Man Im, H. (2006)
1.25 The involved participants lack of management and supervision the project [3,11]	Jaffar, N., Tharim, A. A., & Shuib, M. N. (2011), Acharya, N. K., Dai Lee, Y., & Man Im, H. (2006)
1.26 Precipitation orsuspension of work [3,10-11,17]	Jaffar, N., Tharim, A. A., & Shuib, M. N. (2011), Huo, X., Zhang, L., & Guo, H. (2016), H. J. Thamhain and D. L. Wilemon. (1975), Acharya, N. K., Dai Lee, Y., & Man Im, H. (2006)
2. Conflicts Which Affect the Cost Factors of Conflict Which Lead to Disputes	Related Studies (Key Support)
2.1 A contractor with work inefficiency [1,3]	Jaffar, N., Tharim, A. A., & Shuib, M. N. (2011), Pétursson, B. K. (2015), , Acharya, N. K., Dai Lee, Y., & Man Im, H. (2006), Yates, J. K., & Epstein, A. (2006), Zidane, Y., & Andersen, B. (2018)
2.2 A subcontractor with work inefficiency [1,3,12,14]	Jaffar, N., Tharim, A. A., & Shuib, M. N. (2011), Pétursson, B. K. (2015), , Acharya, N. K., Dai Lee, Y., & Man Im, H. (2006), Yates, J. K., & Epstein, A. (2006), Zidane, Y., & Andersen, B. (2018)
2.3 A change of work [1-3,11-14]	Jaffar, N., Tharim, A. A., & Shuib, M. N. (2011), Pétursson, B. K. (2015), , San Loke, Y. (2013), Khahro, S. H., & Ali, T. H. (2014), Acharya, N. K., Dai Lee, Y., & Man Im, H. (2006), Acharya, N. K., Dai Lee, Y., & Kim, J. K. (2006), Yates, J. K., & Epstein, A. (2006), , Zidane, Y., &Andersen, B. (2018)

Table 1 Continued

Factors of Conflict Which Lead to Disputes	Related Studies (Key Support)
2.4 Work does not meet the requirements [1-3]	Jaffar, N., Tharim, A. A., & Shuib, M. N. (2011), Pétursson, B. K. (2015), , San Loke, Y. (2013), Khahro, S. H., & Ali, T. H. (2014), Acharya, N. K., Dai Lee, Y., & Man Im, H. (2006)
2.5 The involved participants lack of management and supervision the project [2-3,11,13-14]	Jaffar, N., Tharim, A. A., & Shuib, M. N. (2011), San Loke, Y. (2013), Khahro, S. H., & Ali, T. H. (2014), Acharya, N. K., Dai Lee, Y., & Man Im, H. (2006), Zidane, Y., & Andersen, B. (2018)
2.6 Defectiveness of work [2-3,14-15]	Jaffar, N., Tharim, A. A., & Shuib, M. N. (2011), , San Loke, Y. (2013), Acharya, N. K., Dai Lee, Y., & Man Im, H. (2006), Yates, J. K., & Epstein, A. (2006), Zidane, Y., & Andersen, B. (2018)
2.7 Precipitation orsuspension of work [3,10,11,17]	Jaffar, N., Tharim, A. A., & Shuib, M. N. (2011), Huo, X., Zhang, L., & Guo, H. (2016), H. J. Thamhain and D. L. Wilemon. (1975), Acharya, N. K., Dai Lee, Y., & Man Im, H. (2006)
2.8 A change of work [2-3,11-12,14-15]	Jaffar, N., Tharim, A. A., & Shuib, M. N. (2011), Pétursson, B. K. (2015), , San Loke, Y. (2013), Khahro, S. H., & Ali, T. H. (2014), Acharya, N. K., Dai Lee, Y., & Man Im, H. (2006), Acharya, N. K., Dai Lee, Y., & Kim, J. K. (2006), Yates, J. K., & Epstein, A. (2006), , Zidane, Y., & Andersen, B. (2018)

3. RESEARCH METHODOLOGY

Population in the study were 454 construction government projects which were supervised in all kind [18]. And data had been collected from those 454 construction projects. In addition, the representatives from each project were the engineers who experienced government construction management. Data collection had been done with questionnaire which were separated into 2 parts; (1) general information of a participant and (2) issues of contract conditions for a creator and a construction supervisor, the questions used were rating scale questions with 5 levels. The mentioned questionnaire had passed the quality inspection for research tools with Index of Item-Objective Congruence (IOC) by 3 experts [19-20]. Furthermore, the questionnaire was tested to find its reliability, which Cronbach's Alpha accounted for 0.967. After that, the questionnaire was sent to the population which they have the period of one month to respond, and the population responded at 100%.

Data analysis part was separated into 2 parts; (1) general information of a participant, this part was analyzed by statistics: frequency and percentage and (2) Qualitative risk analysis, which was done by taking chance of conflict score, cost, time and quality impact scores and calculating with Probability and Impact Matrix as shown in a picture no. 1 [4].

Probability and Impact Matrix

Probability	Threats				
0.90 Very High	0.05	0.09	0.18	0.36	0.72
0.70 High	0.04	0.07	0.14	0.28	0.56
0.50 Moderate	0.03	0.05	0.10	0.20	0.40
0.30 Low	0.02	0.01	0.06	0.12	0.24
0.10 Very Low	0.01	0.10	0.02	0.04	0.08
	0.05 Very Low	0.10 Low	0.20 Moderate	0.40 High	0.80 Very High
Impact (numerical scale) on an objective (e.g., cost, time, scope or quality)					
Impact thresholds are established according to organizational risk tolerances. **Note:** numerical precision is NOT intended ; these scores simply provide a means of relative comparison.					

Figure 1 Probability and Impact Matrix Risk [4].

4. CONCLUSION AND DISCUSSION

The results had found that there were 62 administrators who administrated 454 construction projects under government agencies in Thailand. In addition, those projects were many types including building constructions, highway construction, bridge construction, square pipe construction, and irrigation construction. More than a half of the projects, projects values were less than 50 million.

4.1. Result of Qualitative Risk Data Analysis

The results had found that risk factors of conflict affecting cost of the project at most was a subcontractor with work inefficiency, which its risk score made up for 6.46. The study showed that an inefficiency subcontractor came from ineffective selection by the main contractor or the financial conflict between the main contractor and the subcontractor [21]. The following risk factor of conflict was the delay of contractor's work which its risk score made up for 6.08. From the study, the delay of work affecting cost of the project was from the dispute of the project's owner as followed; 1. The delay of the owner's payment, 2. No compensation for a change from the owner, 3. The owner's standard of payment. Those conflicts affected the delay of projects and the expensive costs [22]. And the last one was a contractor with work inefficiency, which its risk score made up for 5.94. Risk factors of a contractor could be divided into 4 categories: 1. Social Politic, 2. Government Regulation, 3. Natural Disaster, and 4. Monetary. Further, the risk factors affecting cost of the project the most was the increased gas price and economic crisis [23]. The data showed in table 2 and picture number 2 in cost part.

However, the risk factors of conflict affecting the delay of payment was separated as followed: 1. Lack of Funds, 2. Poor Financial Projection on the Client Side, 3. Inadequate Contract Provision for Enforcement of Timely Payment, 4. Delay Originating from Evaluation Process of the Contractors by the Consultants. Those affected cost project management [24].

The result had found that risk factors affecting conflict of time of the project at most was a subcontractor with work inefficiency, which its risk score made up for 6.52. The subcontractor was selected inefficiently [21], which mostly because of the main contractor's administration. In addition, it had not only affect the main contractor [21], but also all stakeholders of the project [4]. The following risk factor of conflict was a contractor with work inefficiency, which its risk score made up for 5.89. From the research study, it showed that a contractor with work inefficiency would extend the period of time and cause conflict in a contract if the contact had unclear indication of the penalty and fines in case of the delay of construction [25]. And the third one was a change of work, which its risk score accounted for 5.24. Additionally, it had found from the study that the incomplete construction drafting affected the delay of construction project and additional cost continuously [22-23]. It caused a mistaken draft and incorrect cost [24] which might come from the unclear contract between partners [26] respectively. The data showed in the table 2 and picture number 3 in time part

On the other side, it had mentioned that the delay from the conflicts could be managed correctly if there was a proper solution [27]. There were steps and procedures of conflicts management as followed; 1. Withdrawing or Avoiding, 2. Smoothing or Accommodating, 3. Compromising or Reconcile and 4. Forcing or Directing [4,8]..

Table 2 The result of data analysis of risk factors affecting conflict of cost and time of a project.

Factor	Description	Opportunity	Impact	Risk scoring
The risk factors affecting conflict of cost for a project.				
Cost 1	A subcontractor with work inefficiency	2.52	2.57	6.46
Cost 2	The delay of contractor's work	2.36	2.57	6.08
Cost 3	A contractor with work inefficiency	2.41	2.47	5.94
Cost 4	A change or work	2.26	2.40	5.41
Cost 5	A fine for contract cancellation	2.24	2.37	5.30
Cost 6	Precipitation or suspension of work	2.36	2.22	5.24
Cost 7	The request for extending construction period of time	2.37	2.17	5.16
Cost 8	Error cost estimation	2.27	2.26	5.14
Cost 9	No payment for a contractor or a subcontractor	2.23	2.27	5.06
Cost 10	An error drafting	2.09	2.37	4.95
Cost 11	The failure of the owner's money management	2.06	2.20	4.53
Cost 12	Work does not meet the requirements	2.03	2.22	4.50
The risk factors affecting conflict of time for a project.				
Time 1	A subcontractor with work inefficiency	2.61	2.50	6.52
Time 2	A contractor with work inefficiency	2.39	2.46	5.89
Time 3	A change or work	2.24	2.34	5.24
Time 4	Work does not meet the requirements	2.27	2.25	5.12
Time 5	The involved participants lack of management and supervision the project	2.17	2.23	4.84
Time 6	Defective work	2.19	2.18	4.77
Time 7	Precipitation or suspension of work	2.16	2.18	4.70
Time 8	Quality of construction materials or machines	2.13	2.20	4.68

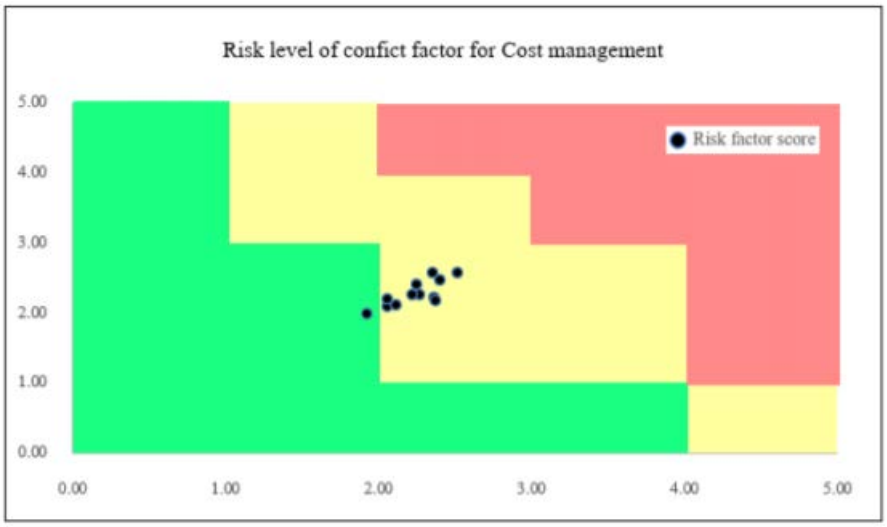

Figure 2 Risk factors of conflict affecting cost of construction government projects.

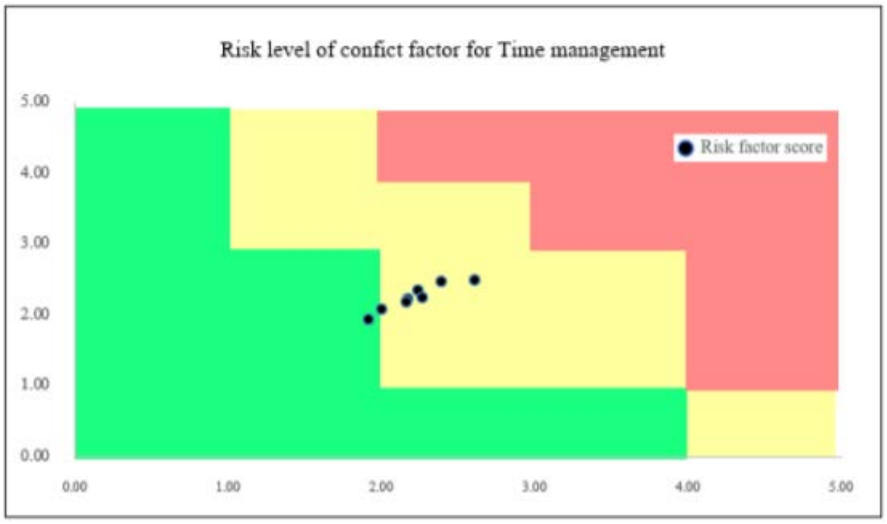

Figure 3 Risk factors of conflict affecting time of construction government projects.

5. CONCLUSION

From the scores of risk factors affecting conflict of government constructions in Thailand, it is found that the factors of conflict in cost management, which is at the highest risk, consist of a subcontractor with work inefficiency respectively. Moving on for the factors of conflict in time management, the highest risk factors of conflicts consist of a

subcontractor with work inefficiency, a contractor with work inefficiency, and a change of work respectively. Those factors affect directly to the cost and time of the government construction projects.

6. ACKNOWLEDGEMENT

I would like to express my deepest appreciation to the department of Civil Engineering, faculty of Engineering, Khon Kaen University, Faculty Architecture, Urban Design and Creative Arts, Mahasarakham University, and government officers for the opportunities and mercy that provided me to study and develop construction management in order to avoid conflicts which would cause troublesfor the government properties.

7. REFERENCES

[1] B. K. Petursson, “Disputes and Conflicts within Construction Contracts in the Icelandic Construction Industry,” Thesis of 30 ECTS credits submitted to the School of Science and Engineering at Reykjavík University in partial fulfillment of the requirements for the degree of Master of Science in Construction Management, 2015.

[2] Y. San Loke “A Study of Causes and Effects of Conflict in Construction Industry (Doctoral dissertation, UMP),” Report submitted in partial fulfillment of the requirements of the requirements for the award of the degree Bachelor of Project Management with Honours Faculty of Technology UNIVERISTY MALAYSIA PAHANG, 2013.

[3] N. Jaffar, A. Tharim, M. N. Shuib, “Factors of conflict in construction industry: a literature review,” The 2nd International Building Control Conference 2011, Procedia Engineering, vol. 20, pp 193 – 202, 2011.

[4] A. PMI, “Guide to the project management body of knowledge (PMBOK guide),” in Project Management Institute, vol. 5, 2013.

[5] K. A. Shami, “Investigating the use Building Information Modeling (BIM) in Managing Construction Claims,” PM World Journal, vol 7, 2018.

[6] K. K. Chitkara, “Construction project management,” Tata McGraw-Hill Education, 1998.

[7] R. Burke, “Risk Management: Tricks of the Trade® for Project Managers: a Coursein a Book [trademark Symbol],” 2003.

[8] R. Burke, “Project management: planning and control techniques,” New Jersey, USA, 2013.

[9] N. Swanstrom and M. Weissmann, “Conflict, Conflict Prevention and Conflict Management and beyond: a conceptual exploration,” CACI & SRSP, Washington & Uppsala, 2005.

[10] H. J. Thamhain and D. L. Wilemon, “Conflict management in project life cycles,” Sloan Management Review, 1975.

[11] N. K. Acharya, Y. D. Lee and H. M. Im, “Conflicting factors in construction projects: Korean perspective,” Engineering, Construction and Architectural Management, 2006.

[12] J. K. Yates and A. Epstein, “Avoiding and minimizing construction delay claim disputes in relational contracting,” Journal of Professional Issues in Engineering Education and Practice,” pp 168-179, 2006.

[13] S. H. Khahro and T. H. Ali, “Causes leading to conflicts in construction projects: a viewpoint of Pakistani construction industry,” In International Conference on challenges in IT, Engineering and Technology (ICCIET’2014) July, pp 17-18, 2014.

[14] Y. Zidane and B. Andersen, “Causes of delay and their cures in major Norwegianprojects,” 2018.

[15] N. K. Acharya, Y. D. Lee and J. K. Kim, “Critical construction conflicting factors identification using analytical hierarchy process,” KSCE Journal of Civil Engineering, vol.10, pp 165-174, 2006.

[16] Y.Maemura, E. Kim and K. Ozawa, “Root causes of recurring contractual conflicts in international construction projects: Five case studies from Vietnam,” Journal of Construction Engineering and Management, 2018.

[17] X. Huo, L. Zhang and H. Guo, “Antecedents of relationship conflict in cross-functional project teams,” Project Management Journal, pp 52-69, 2016.

[18] CGD, ““The Government Procurement and Supplies Management Act B.E. 2560,” The Comptroller General’s Department, 2017

[19] S. Kangpheng, S. Gunlong and D. Kaewin, “Mixed Methods: Paradigms of Research for the 21st Century,” Khon Kaen: Apichat, 2016

[20] S. Vorakitkasemsakul, “Applied Statistics for Behavioral and Social Science Research,” Udon Thani: Aksonsin, 2011.

[21] B. M. Jervis and P. Levin, “Construction law, principles and practice,” McGraw-Hill College, 1998.

[22] S. Trangkanont, T.Wichaiphruek and P.Uttaraphon, “IMPACTS OF DISPUTE ON PROJECT COST: CONTRACTORS’PERSPECTIVE,” International Journal pp 210-221, 2018.

[23] S. H. Mubarak and M. Oktaviati, “External risk factors affecting construction costs,” In AIP Conference Proceedings, no.110005, 2017

[24] S. H. Khahro and T. H. Ali, “Causes leading to conflicts in construction projects: a viewpoint of Pakistani construction industry,” In International Conference on challenges in IT, pp 17-18, 2014.

[25] A. Rauzana, “Causes of conflicts and disputes in construction projects,” Journal of mechanical and civil engineering, pp 44-48, 2016.

[26] P. I. Cakmak, “Causes of disputes in the Turkish construction industry: Case of public sector projects,” Istanbul Technical University, pp 109-118, 2016

[27] A. M. Al-Ashwal and M. H. Al-Sabahi, “Risk factors in construction projects during unrest period in Yemen,” Journal of Construction in Developing Counties, pp 43-62, 2018.

Biodegradation of POM/PLA Multifilament in Sea Water

A Wongkorn[1], W Pivsa-Art[2] and S Pivsa-Art1, [3]

[1]*Department of Materials and Metallurgical Engineering, Faculty of Engineering, Rajamangala University of Technology Thanyaburi, Klong 6, Thanyaburi, PathumThani 12110, THAILAND*

[2]*Department of Chemical and Materials Engineering, Faculty of Engineering, Rajamangala University of Technology Thanyaburi, Klong 6, Thanyaburi, PathumThani 12110, THAILAND*

[3]*sommai.p@en.rmutt.ac.th*

Abstract.

Multifilaments of POM/PLA (70/30 by weight) were produced using a melt spinning process. The effect of addition of additives, PEG and EBS (0.5, 1 and 1.5 phr) to improve the flexibility and reduce the static electricity on the fiber. The tenacity and percent extension at break of multifilaments were measured. POM/PLA/PEG exhibits good results of polymer high tenacity and extension at break. Increasing the additive contents improved the mechanical property of multifilaments. High mechanical property POM/PLA with addition of 1 phr PEG exhibit satisfy mechanical property. The degradation test of multifilaments was carried out in sea water compared with in tap water for 120 days. The degradation of multifilaments in was observed to be higher than in tap water. The rate of degradation increased after 90 days. High and more than 10 % of weight loss was observed after 120 days. The fiber size of POM/PLA/PEG (1 phr) by SEM measurement.

Keywords. -

1. INTRODUCTION

The environmental concerns on wastes from non-degradable petroleum-based plastic have been recognized as they are harmful to sea animals. As a result it is needed to develop the industrial manufacturing of biodegradable polymers to replace the conventional polymers. The investigation on development of biobased and biodegradable polymers has been continuously reported [1-4]. Poly (lactic acid) (PLA) is the best known biodegradable polymer made from renewable resources such as corn, tapioca and sugar cane [5,6]. PLA has high mechanical property but its glass transition temperature (Tg) is high (ca 55 oC). Then, PLA is rigid and brittle at room temperature [6]. This drawback limits the PLA applications including extrusion and fiber products. To improve the mechanical property of PLA, copolymerized lactide with other monomers have been reported. However, the

scale-up of copolymerization processes has not reported due to unprofitable reasons [7-10]. Blending of PLA with other polymers or copolymers that have the recompensed properties of PLA was reported. This method could moderately improve the mechanical properties of the polymer [11-20].

In a fishing net or seine manufacturing process, conventional polymers used to produce the nets are polypropylene (PP) and nylon 6. They exhibit high mechanical property and good processability for fiber fabrication. But PP and nylon 6 are non-degradable polymers and their wastes are not degraded and floating on the sea surface. These wastes are harmful to sea animals. Decompose of nets under severe environment is a source of microplastic pollutions. Therefore, investigation of new materials that their wastes can be degraded to replace PP and Nylon 6 is the eminent problem solving method.

Polyoxymethylene (POM) is an engineering plastics used in automotive industry due to their high mechanical property, high fracture toughness and crystallinity, excellent abrasion and fatigue resistance [21-23]. Goossens et al. reported the study on improvement of physicochemical properties of epoxy/POM blends [24]. For the textile industry POM must be modified by copolymerize the oxymethylene monomer with oxyethylene to increase the polymer toughness and flexibility

Furthermore, due to the high capacity of fishing net utilization the application of POM for seine manufacturing with modification the mechanical and physical property by blending POM with biodegradable polymer, PLA will produce the partly biodegradable polymer for seine production. We have reported the production of POM/PLA multifilament that exhibited excellent elongation.

In the melt spinning process of POM/PLA blend, the electrostatic from the fiber flowing through the air produced repulsion force is the difficulty problem of multifilament winding. In the polyethylene (PE) and polypropylene (PP) melt spinning process, oil spraying to fiber extruded prior to the winder as antistatic materials has been used to solve the electrostatic. However, oil spray could not apply to PLA for anti-electrostatic additive due to oil affects the crystallinity and stability of polymer chain.

In this research we studied the fabrication process of multifilament from POM/PLA blends. The ratio of POM/PLA was 70/30 [25]. The effect of 2 types of additives: poly (ethylene glycol), PEG and N,N’-Ethylene bis-stearamide, EBS, as anti-electrostatic additive to solve the processing problems was investigated. There are 2 types of mechanical properties tests: normal and knot. Then select good formula for degradation measurement. We studied degradation of POM/PLA fiber in sea water and tap water. Compare morphology of fiber before and after degradation test. For the actual application of multifilament for seine fishing in the sea, the biodegradation of fishing net was evaluated. The results will be significant to the application of POM/PLA blends as an environmental friendly material for seine production. The fiber fabrication process and effect of POM on product property was measured.

2. EXPERIMENTAL PROCEDURE

2.1. Experimental Materials

Poly(lactic acid), (PLA), grade TP4000 was purchased from Unitika Ltd., Japan, (Density = 1.25 g/cm3). Polyoxymethylene (POM), Iupital V20-HE, (Density = 1.39 g/cm3) were produced by Mitsubishi Gas Chemical Corporation, Japan. Poly(ethylene glycol), (PEG, MW 20,000) was purchased from Sanyo Chemical Industries Company Ltd., Japan. N,N'-Ethylene bis-stearamide (EBS) was purchased from Tarak Chemicals Company Ltd., China.

2.2. Multifilament preparation

The POM and PLA pellets were first dried in an oven at 80°C for 8 h prior to processing. Multifilament yarns of polyoxymethylene (POM) and poly(lactic acid) (PLA) blends were prepared by a melt-spinning method using single screw extruder (ThermoHaake Polydrive) equipped (Figure 1). The ratios of the POM/PLA fibers studied were 70/30 by weight with additives (PEG and EBS) 0.5, 1.0 and 1.5 wt%. The polymers and additive were mixed together and processed with dry blend method. The spinning conditions are as follows table 1. After that, the final multifilament was subjected to secondary winding to make extension of the fiber for 6.5 and 7.5 times (6.5x and 7.5x).

Table 1 The melt spinning conditions of POM/PLA multifilament

Die	24 holes (diameter has 0.32 mm/hole)
Temperature (^{o}C)	180, 190, 200 (Zone Extruder) 210 (Connecter) and 210 (Die)
Screw speed	8 rpm
Winding speed (m/min)	500

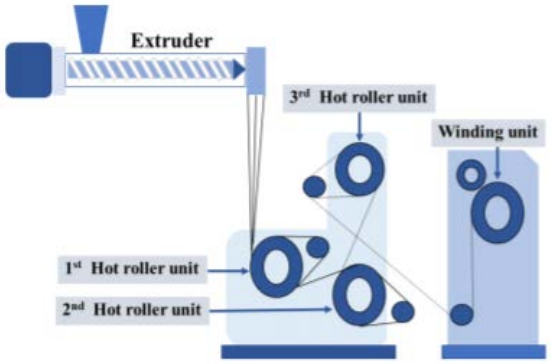

Figure 1 Fiber melt spinning process

2.3. Thermal property analysis

Thermal analysis of multifilament was recorded on a differential scanning calorimeter, Perkin Elmer, DSC 8000 under nitrogen atmosphere with a heating rate of 10°C/min from 30 to 250°C.

2.4. Tensile property measurement

The tensile strength and elongation at break (%) of the fiber were measured using an Instron universal testing machine (INSTRON5569) according to the ASTM standard method D3822-01. The mechanical property of the fiber was testing with a load cell of 50kN with gauge length of 25 mm and test speed of 50 mm/min. Figure 2 show 2 types of fiber test: normal type and knot type.

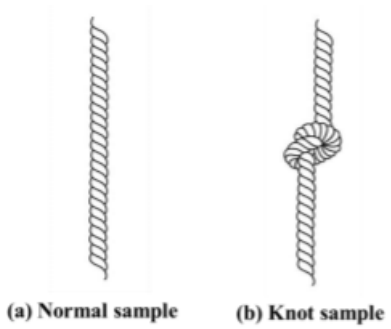

Figure 2 Tensile test samples

2.5. Degradability of POM/PLA multifilaments

Multifilaments of POM/PLA blend produced by a melt spinning process was cut for 30 cm length. The fibers were packed in a nylon tea bags. For the biodegradability test of multifilaments in sea water, natural sea water was collected at 1 m depth from the sea surface from Laem Chabang Port, Chon Buri, Thailand. The salinity was 30 ppt. The degradation test of multifilament was carried out compared with the tap water. The sample bag was soaked in the test sink. The sampling of test samples was done after 15, 30, 60, 90 and 120 days. The temperature, salinity and pH of the solution was recorded daily. The samples taken from each period were dried and weighed to calculate the percent weight loss.

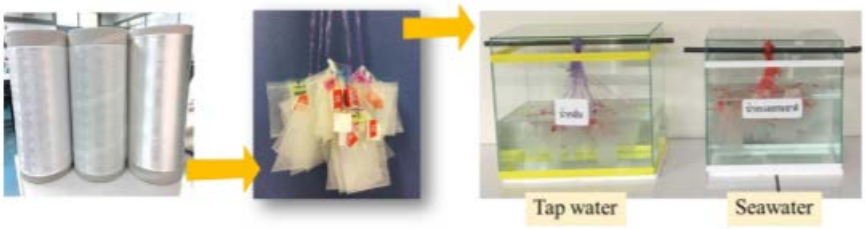

Figure 3 Degradability of POM/PLA fibers in sea water and tap water

3. RESULTS AND DISCUSSION

3.1 Thermal property analysis

The thermal property analysis of POM/PLA (70/30 w/w) blend with and without additive was carried out using a DSC analysis. The results are shown in Figure 4, 5 and Table 1.

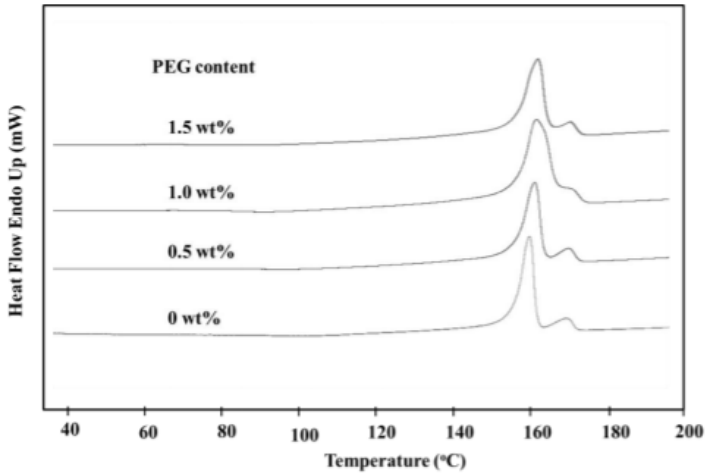

Figure 4 DSC Thermogram of POM/PLA fiber with PEG (winding speed 500 m/min)

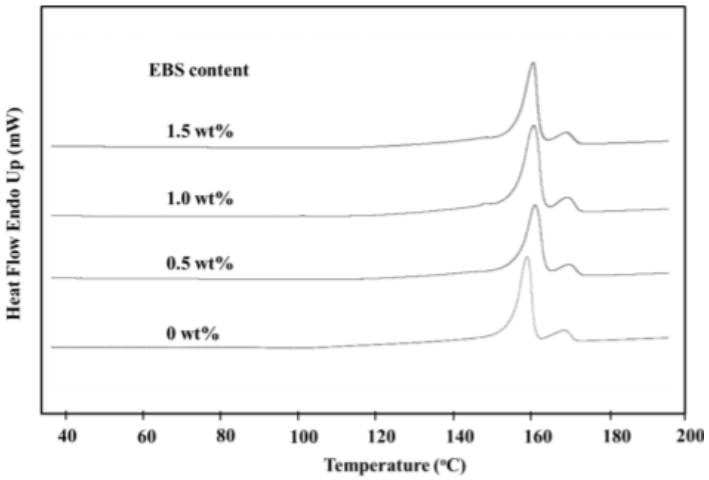

Figure 5 DSC Thermogram of POM/PLA fiber with EBS (winding speed 500 m/min)

Table 2 DSC Thermogram data of POM/PLA fiber at winding speed 500 m/min

Sample	Plasticizers (phr)		Tm POM (°C)	ΔHm POM (J/g)	Tm PLA (°C)	ΔHm PLA (J/g)	Xc POM (%)	Xc PLA (%)
POM	-		160.27	68.82	-	-	21.11	-
PLA	-		-	-	175.47	32.75	-	35.22
POM/PLA (70/30)	-		159.28	59.22	169.95	7.23	18.17	7.77
	PEG	0.5	160.52	48.95	169.52	6.23	15.02	6.70
		1	161.11	45.92	170.69	5.83	14.09	6.27
		1.5	161.57	42.98	170.05	3.67	13.18	3.95
	EBS	0.5	161.41	49.37	170.25	6.30	15.14	6.77
		1	161.02	48.44	169.84	5.39	14.86	5.80
		1.5	160.96	45.63	169.70	5.17	14.00	5.56

Figure 4 and 5 show DSC thermogram of POM/ PLA fiber with PEG and EBS, respectively. The increasing of additive contents shows no significant effect on melting temperature of POM/PLA fiber. The enthalpy of melting and percent crystallinity were calculated and showed in Table 2. The degree of crystallinity (Xc) of POM and PLA was determined by using Eq (1)

$$Xc = \frac{\Delta H_m}{\Delta H_m^0} \times 100\% \quad (3.1)$$

where ΔH_m is the heat of fusion of POM or PLA sample measured, ΔH_m^0 is the heat of fusion of 100% crystalline POM (326.3 J/g) or PLA (93 J/g) [25]. Table 2 shows DSC

thermogram data of POM/PLA fiber with PEG and EBS additive. The melting temperature (Tm) of neat POM, neat PLA was observed at 160 and 175 °C. For the POM/PLA fiber without additive, Tm of POM not change but Tm of PLA reduced may be POM molecules enhanced the mobility of PLA molecules. The Tm of POM and PLA blend show two melting peaks confirmed the phase separation of the two polymers. Due to the polymer blends of POM and PLA at low temperature are miscible in the melt state. [26, 27] The immiscibility of POM and PLA is accounted for by the weak interactions between the carboxyl groups of PLA and the methylene groups of POM [25]

3.2. Mechanical Properties

The tenacity and extension at break of POM/PLA multifilament with PEG and EBS addition at drawing extension of 6.5 and 7.5 times compare normal and knot test are shown in Figure 6 and 7. For normal test the tenacity (Figure 6) of 7.5 times extension is higher than 6.5 times and PEG shows higher tenacity than EBS. For knot test, the drawing 7.5 times is slightly higher than 6.5 times extension but the PEG and EBS additives are not significantly different. The percent extension at break measurement in Figure 7 shows contrast results of normal test. Drawing at 6.5 times exhibits higher percent extension at break than 7.5 times. The knot test also shows similar trend but lower value. The effect of PEG and EBS was not clearly observed. For effect of the additive contents for both PEG and EBS shows similar tendency of increasing the tenacity and extension at break while increasing the additive contents from 0.5 to 1.5 phr. It was found that PEG has higher effect than EBS.

3.3 Degradation of Multifilament in Sea Water

The degradation of POM/PLA/PEG (1 phr) multifilament in sea water and tap water was carried out for 120 days. The fibers were soaked in the solution medium and sampling at 15, 30, 60, 90 and 120 days. Weight loss of fibers was calculated to compare the percent of degradability. Slow degradation of fibers in tap water was observed while the degradation rate increased after 90 days. The degradation of fibers in sea water was much higher than tap water which indicated the effect of salinity to the ester scission. Rate of degradation in sea water was clearly observed after 90 days. The results verified that the POM/PLA/PEG multifilaments were degraded under the sea water condition.

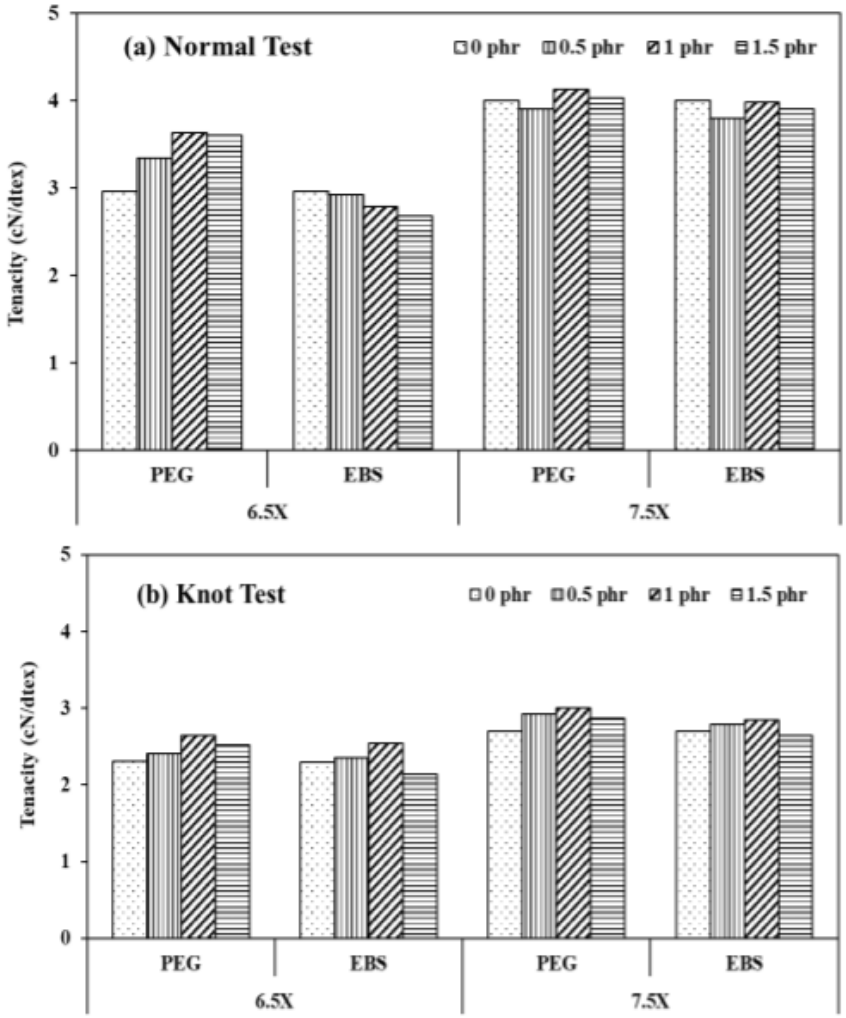

Figure 6 Tenacity of POM/PLA fibers with PEG and EBS additives at 6.5 and 7.5 times extension.

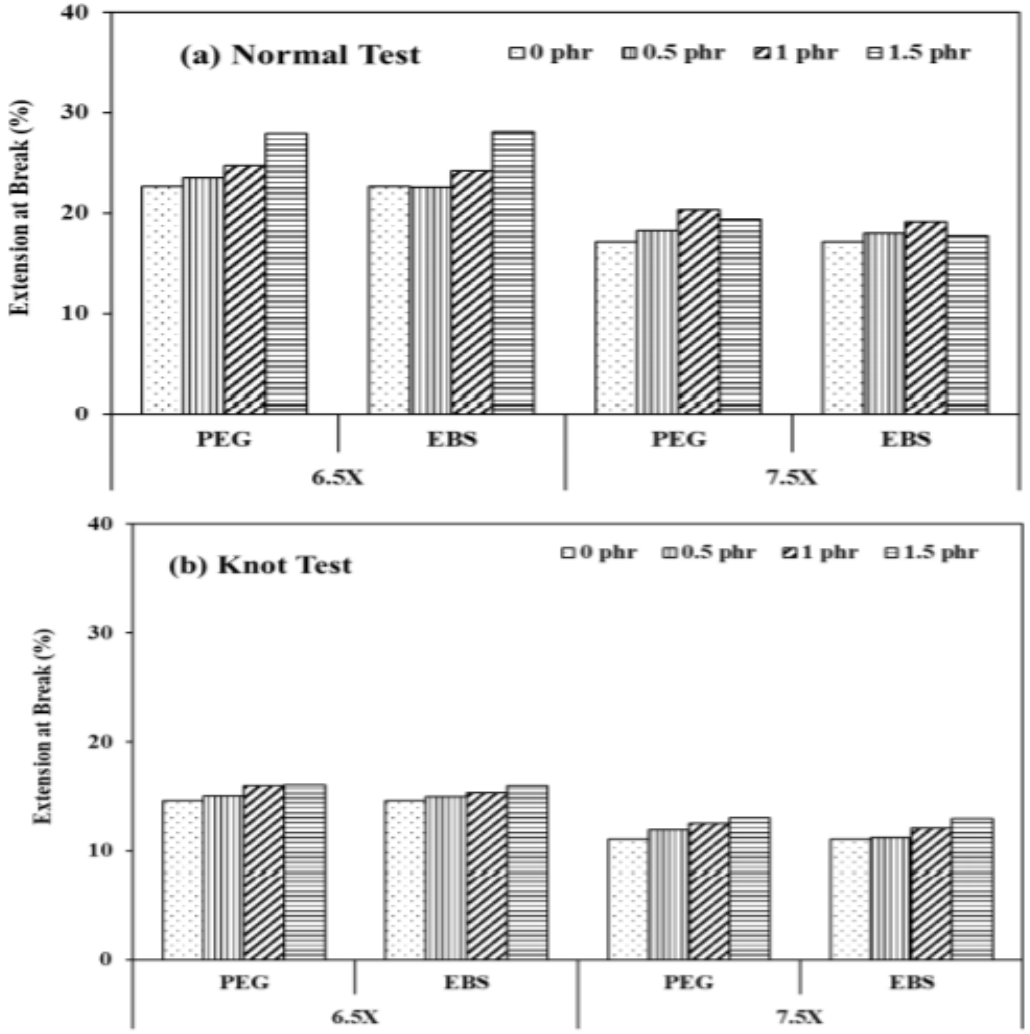

Figure 7 Extension at break of POM/PLA fiber with PEG and EBS additives at 6.5 and 7.5 times extension

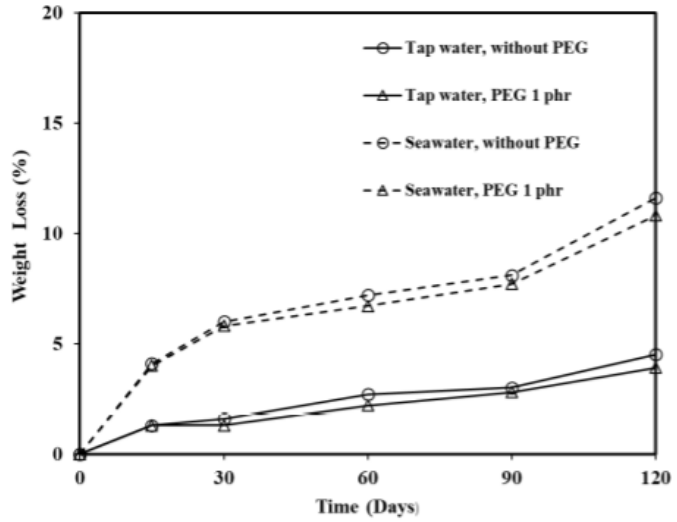

Figure 8 Degradation of POM/PLA/PEG (1 phr) multifilament in sea water and tap water

3.4 Degradation of Multifilament in Sea Water

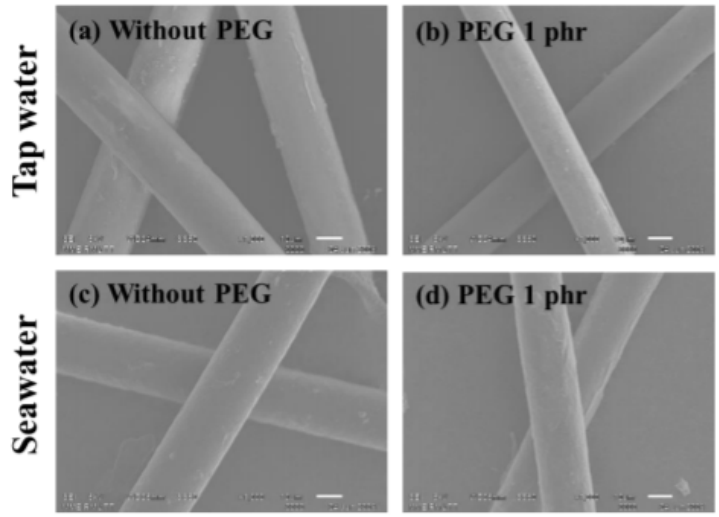

Figure 9 SEM image of fiber after 4 months in water

The SEM image of morphology of POM/PLA/PEG (1 phr) multifilament are shown in Figure 9. The diameter and surface of fibers with addition of PEG (1 phr) show decrease in

diameter and the surface is rough due to surface degradation. The results are in agreement with the weight loss measurement in Figure 8.

4. CONCLUSION

Multifilaments of POM/PLA with addition of additives, PEG and EBS, were produced using a melt spinning process. PEG exhibits high tenacity and extension at break. The additive contents improve the mechanical property of multifilaments. The addition of 1 phr PEG to POM/ PLA exhibit satisfy mechanical property. The degradation of multifilaments in sea water was observed to be higher than in tap water. The rate of degradation increased after 90 days and more than 10 % of weight loss was observed after 120 days. The fiber surface shows decrease in fiber size for POM/PLA/PEG (1 phr) which verified by SEM measurement.

5. ACKNOWLEDGEMENT

The authors would like to acknowledge the Thai Polycarbonate Co., Ltd. and MEP Technical Center Asia Ltd. for materials support. Research and Researchers for Industries-RRI, The Thailand Research Fund (TRF) Contract number MSD60I0121.

6. REFERENCES

[1] R. U. S. T. G. I. Chandra and R.Rustgi, “Biodegradable polymers,” Progress in polymer science, 23(7), 1273-1335, 1998.

[2] J. J. Grodzinski, “Biomedical application of functional polymers,” React. Funct. Polym., 39, pp. 99-138, 1999.

[3] I. Vroman and L. Tighzert, “Biodegradable Polymers,” Materials pp. 2-307, 2009.

[4] H. N. Rabetafika, M. Paquot and P. Dubois “Biotechnol Agron Soc Environ,” pp. 10-96, 2006.

[5] D. Garlotta, “A literature review of poly (lactic acid),” Journal of Polymers and the Environment, 9(2), 63-84, 2001.

[6] L. T. Lim, R. Auras and M. Rubino, “Processing technologies for poly (lactic acid),” Prog Polym Sci, vol. 33, pp. 52, 2008.

[7] Z. Zhu, C. Xiong, L. Zhang, M. Yuan, and X. Deng, “Preparation of biodegradable polylactide-co-poly (ethylene glycol) copolymer by lactide reacted poly (ethylene glycol),” European polymer journal, 35(10), 1821-1828, 1999.

[8] F. Tasaka, H. Miyazaki, Y. Ohya, and T. Ouchi, “synthesis of comb-type biodegradable polylactide through depsipeptide− lactide copolymer containing serine residues,” Macromolecules, 32(19), 6386-6389, 1999.

[9] J. K. Kim, D. J. Park, M. S. Lee and K. J. Ihn, “Synthesis and crystallization behavior of poly (l-lactide)-block-poly (ϵ-caprolactone) copolymer,” Polymer, 42(17), 7429-7441, 2001.

[10] X. Chen and R. A. Gross, “Versatile copolymers from [L]-lactide and [D]-xylofuranose,” Macromolecules, 32(2), 308-314, 1999.

[11] I. Ohkoshi, H. Abe and Y. Doi, “Miscibility and solid-state structures for blends of poly [(S)-lactide] with atactic poly [(R, S)-3-hydroxybutyrate],” Polymer, 41(15), 5985-5992, 1999.

[12] M. R. Lostocco, A. Borzacchiello and S. J. Huang, “Binary and ternary poly (lactic acid)/poly (ϵ□caprolactone) blends: The effects of oligo□ϵ□caprolactones upon mechanical properties,” In Macromolecular Symposia Vol. 130, No. 1, pp. 151-160, 1998.

[13] A. M. Gajria, V. Dave, R. A. Gross and S. P. McCarthy, “Miscibility and biodegradability of blends of poly (lactic acid) and poly (vinyl acetate),” Polymer, 37(3), 437-444, 1996.

[14] N. S. Choi, C. H. Kim, K. Y. Cho and J. K. Park, “Morphology and hydrolysis of PCL/PLLA blends compatibilized with P (LLA-co-□CL) or P（LLA-b-□CL），” Journal of applied polymer science, 86(8), 1892-1898, 2002.

[15] H. Tsuji, T. Yamada, M. Suzuki and S. Itsuno, “Blends of aliphatic polyestersPart 7. Effects of poly (L-lactide-co-ϵ-caprolactone) on morphology, structure, crystallization, and physical properties of blends of poly (L-lactide) and poly (ϵ-caprolactone),” Polymer international, 52(2), 269-275, 2003.

[16] S. Aslan, L. Calandrelli, P. Laurienzo, M. Malinconico and C. Migliaresi, “Poly (D, L-lactic acid)/poly (∈-caprolactone) blend membranes: preparation and morphological characterisation,” Journal of materials science, 35(7), 1615-1622, 2000.

[17] M. L. Focarete, M. Scandola, P. Dobrzynski and M. Kowalczuk, “Miscibility and mechanical properties of blends of (L)-lactide copolymers with atactic poly (3-hydroxybutyrate),” Macromolecules, 35(22), 8472-8477, 2002.

[18] N. Ogata, T. Tatsushima, K. Nakane, K. Sasaki and T. Ogihara, “Structure and physical properties of cellulose acetate/poly (l-lactide) blends,” Journal of applied polymer science, 85(6), 1219-1226, 2002.

[19] J. W. Park and S. S. Im, “Phase behavior and morphology in blends of poly (L-lactic acid) and poly (butylene succinate),” Journal of applied polymer science, 86(3), 647-655, 2002.

[20] T. Komatsu, S. Enoki and A. Aoshima, “The effects of pressure on drawing polyoxymethylene: 1. Processing,” Polymer, 32(11), 1983-1987, 1991.

[21] D. L. Long, R. Tsunashima and L. Cronin, “Polyoxometalates: building blocks for functional nanoscale systems,” Angewandte Chemie International Edition, 49(10), 1736-1758, 2010.

[22] D. E. Katsoulis, “A survey of applications of polyoxometalates,” Chemical Reviews, 98(1), 1998.

[23] S. Goossens and G. Groeninckx, “Mutual influence between reaction-induced phase separation and isothermal crystallization in POM/epoxy resin blends,” Macromolecules, 39(23), 8049-8059, 2006.

[24] S. Goossens, B. Goderis, and G. Groeninckx, “Reaction-induced phase separation in crystallizable micro-and nanostructured high melting thermoplastic/epoxy resin blends,” Macromolecules, 39(8), 2953-2963, 2006.

[25] W. Pivsa-Art and S. Pivsa-Art, “Multifilament yarns of polyoxymethylene/poly (lactic acid) blends produced by a melt-spinning method,” Textile Research Journal, 90(3-4), 294-301, 2020.

Applying Image Processing and Edge Computing for Plant Growth Monitoring in Smart Farm

K Namee[1], J Polpinij[2] and G M Albadrani[3]

[1]*King Mongkut's University of Technology North Bangkok, Thailand*

[2]*Mahasarakham University, Thailand*

[3]*Princess Nourah Bint Abdulrahman University, Saudi Arabia,*

Khanista.N@fitm.kmutnb.ac.th

Abstract.

In the history of development economics, smart farming has been thought of as a key factor in agriculture more efficiently. It is necessary to integrate various technologies to deploy in the process of production and cultivation. The aim of this study was to apply and evaluate information technology technique with agricultural engineering in order to reduce the monitoring process for farmers. This research was applying Image Processing techniques to assist in cultivation by measuring plant growth and plant health through webcam. The image of plant will calculate on Edge Computing in Raspberry Pie 3. The results will be displayed as a percentage of plant growth. In addition, this process can be performed the Smart Farming through the Internet of Things (IoT) technology and Edge Computing. The system will control the environment such as temperature, humidity, light, heat, pH in the greenhouse is appropriate for the growth of plant automatically. The results of this study indicate that plants growing faster is to increase productivity and reduce workload for farmers. The current findings add substantially to our understanding of techniques for processing plant growth from low resolution images in order to be suitable for real farmers' use. The results from the research are satisfactory. The evidence from this study indicates that 80.95% accurate for low resolution images.

Keywords. -

1. INTRODUCTION

Agriculture in many countries around the world are still agriculture based on human labor. It is also a dependency on the environment, climate factors, mainly external factors which will affect the product received. Many counties want to change from traditional agriculture today to modern agriculture that focuses on management and technology become Smart Farming. In order to develop farmers to be able to do agriculture more efficiently, have more labor-saving devices, reduce work procedures for farmers and increase productivity.

It is necessary to bring various technologies to modify in the process of production and cultivation. This research is applying information and communication technology including the knowledge of agricultural technology to developagriculture as much as possible. In order to reduce the processes in working for farmers. This research applied the Image Processing techniques to monitor with cultivation by measuring plant growth and plant health through Webcam. It will show the results as a percentage of growth. This result can be connected to the Smart Farm through the Internet of Things (IoT) to help control the environment in greenhouse. For example, controlling the temperature, humidity, light, heat, pH in the greenhouse is suitable for the growth of that plant automatically. Resulting in plants growing faster, this increase productivity and reduce workload for farmers to become Smart Farmer. The knowledge gained from this research will be process the growth of plants from low resolution images. The rest of this paper is organized as follows. Section 2 provides a brief overview of some theory and related works which had to be implemented within this research. Then, in Section 3, the system designs of hardware and software components are presented in detail. The experimental deployment is presented in Section 4 to demonstrate the design. Including the measurement results and performance are presented. Finally, conclusions are drawn in Section 5 and following with acknowledgement section.

2. RELATED WORKS

Research that has been processed to increase agricultural productivity is divided into 4 main areas as follows.

1. Checking for the Plant Growth
2. Checking for the Plant Health.
3. Plant Disease Detection
4. Pest Detection and Identification

The image analysis and processing system has a high potential for evaluating plant growth and health with high accuracy. Automatic image analysis system is flexible to use. In the development of automated inspection tools for plant growth and health assessments. The image analysis is often included in mechanical equipment to replace manual assessments by humans [1]. Also, to control the operation of the machine. There are 5 main steps in image analysis: image recording, preanalysis, segmentation, detection and classify [1] Image processing can reduce the total data of the image to a manageable level. By adding edges and making geometric corrections before analysis, measurement, and specifying some specific details such as size, area, and shape [6]. The most important benefit of image analysis is able to see specific areas and contrasting colors. This helps with visual explanation and interactive analysis by computer. The images that are analyzed can also be stored in a large memory. When computers are connected to the internet, it becomes very easy to transfer data between scientists from cities or countries [6].

Leister [2] was using digital video and visual analysis that shows to determine the size of plants without destroying by measuring the leaf area. The system provides non-destructive methods for evaluating plant growth and growth rates by examining and

quantifying plant parameter parameters. Other studies, such as plant growth and health in a controlled environment, are continuously monitored by Kacira and Ling, [5] were using visual inspection methods. The back area is also an important variable related to plant growth. In addition, the growth of plants is clearly associated with dry weight. Measuring the area of the bushes of plants or in other respects covered by image processing methods can provide valuable information for monitoring plant growth [3].

Trimi Neha Tete and Sushma Kamlu [10] have used image processing techniques for the detection and classification of different leaf diseases that exist. This system helps to detect and analyze plant diseases automatically. By using images to inspect organisms such as fungi, bacteria, viruses, etc. In order to help farmers, reduce costs in the analysis of diseases and causes of that plant disease.

2.1. Image Processing

Image Processing is the image to be processed or calculated using a computer to get the information we need both in terms of quality and quantity. There is an important step that are to make the image sharper, eliminating noise from images. The segmentation of the object that interests us from the image. In order to take the picture of the object to analyze for quantitative data such as the size, shape and the direction of movement of the object in the picture. Then we can analyze these quantitative data and create a systematic to use in various fields such as grading or quality grading systems for agricultural crops. It can be seen that these systems require a lot of image processing and is a process that must be repeated in the most original form which works in these ways if human beings analyze themselves often requires a lot of time and labor. Also, if it is necessary to analyze a large number of images. The image analyzer may be tired. It can result in errors. Therefore, computers play an important role in performing these functions on behalf of humans. It is also known that the computer has the ability to calculate and process huge amounts of data in a short time [4]. Therefore, it is very useful in increasing the efficiency of image processing and analyzing the data obtained from the images in various systems mentioned above.

2.2. Edge Computing

Edge Computing is data processing that is as close as possible to data sources. In the form of data analysis statistical data processing which instead of taking a large amount of data to process on the Cloud, it takes that data to process at the source closest to the data source or edge itself. The main reason why the processing needs to be at the edge is latency. Edge Computing has the advantage of speed in data transfer, bandwidth and privacy & security. [9]. To monitor and control the Smart Farm, we work as Edge Computing technique for processing on Raspberry Pi3.

2.3. Internet of Things (IoT)

IoT means many "things" connected to the internet so they can share information with other things - IoT applications, connecting devices, industrial machines, and more. Built-in sensors to collect information and in some cases do so devices and machines that connect IoT can improve the way people work and live [7]. For example, the Internet of Things in the real-world ranges from smart homes that automatically adjust heat and light to intelligent factories that monitor industrial machinery for finding the problem, then adjust automatically to avoid failure [8]. Many sensors had been added in this research.

3. SYSTEM DESIGN AND ARCHITECTURE

3.1. System Architecture

Detailed information about the microcontroller board, its features, and the capabilities of each model. In this research has 3 microcontroller boards consist of Arduino UNO R3, Node MCU ESP8266 and Raspberry Pi 3 which are designed to be suit for each function.

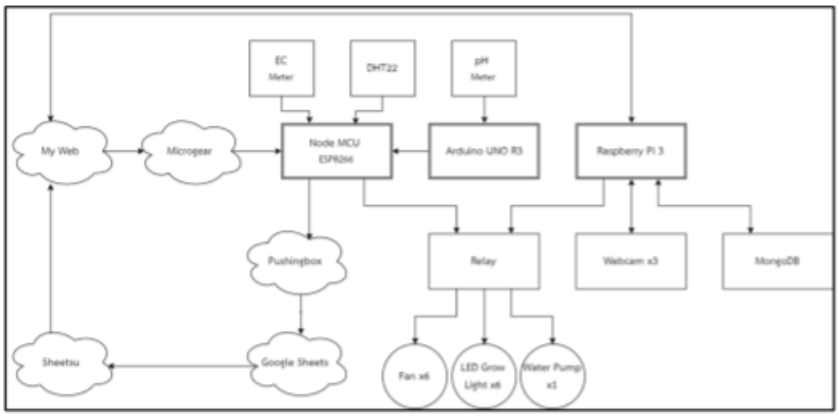

Figure 1 System Architecture

3.2. System Design

These three boards have different capabilities, such as the Node MCU ESP8266 has the ability to connect to Wi-Fi, but the problem is that there is only one analog channel. Arduino UNO R3 boards are required to receive the analog value and then sent to the Node MCU ESP8266 board for storage at the Google Sheets, but the two boards mentioned above. There is also a downside: there is no USB port for this, which requires a USB port for taking pictures of plants in a greenhouse using a webcam.

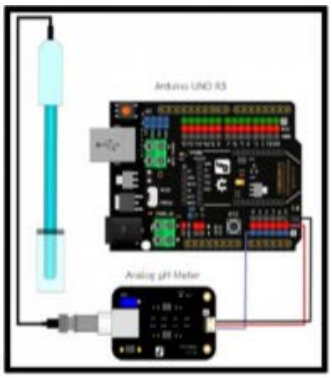

Figure 2 Analog pH Meter Connection

Analog pH meter is a pH sensor that measures the pH of a solution in the range 0-14. The output is analog (0 - 1023) 5v. Analog EC Meter is a sensor for measuring the electrical conductivity of soil nutrients for soil tillers. The web page can also display the values stored on Google Sheets. It can also instruct the Node MCU ESP8266 board to send the value received from the sensor to Google Sheets by pressing the button from the page. The webpage will send a working order to the Microgear. The Microgear will then send the order to the Node MCU ESP8266 board. For detecting plant growth, the system will be taking a photo on a web page. The webpage will send a photo order to the Raspberry Pi 3 board. The Raspberry Pi 3 board will then take a picture using the three webcams connected. Then take the image to be stored on the memory card of the Raspberry Pi 3 board itself, which web pages will be called photos stored on the Raspberry Pi 3 board to display on another page. This is a process of Edge computing.

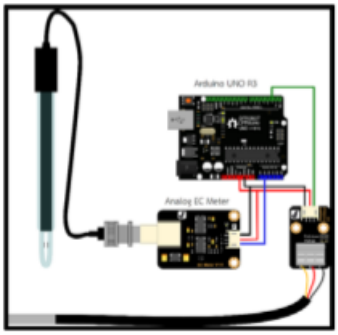

Figure 3 Analog EC Meter connection

3.3. Image Processing Methodology

Detailed information about the microcontroller board, its features, and the capabilities of each model. In this research has 3 microcontroller boards consist of Arduino UNO

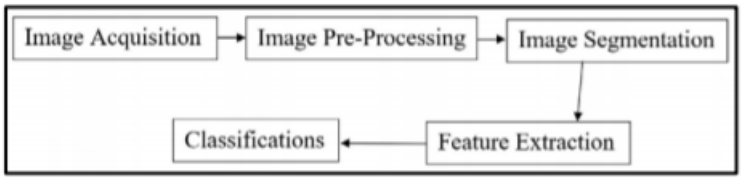

Figure 4 Image Processing Methodology

First, the images of plants are acquired using a WebCam. Then image processing techniques are applied to the acquired images to extract useful features that are necessary for further analysis. These images are in the form of RGB (Red, Green, and Blue). Second, pre-processing is a progress of the image data that enhances some image feature necessary for the next processing. In this process, image enrichment is done for increasing the contrast of the image. Colour conversion of RGB to Gray image is done using following equation:

$$f(x) = r * 0.2989 + g * 0.5870 + b * 0.114 \quad (1)$$

For image segmentation can be done using Thresholding, K-mean cluster, converting RGB to HIS (hue, saturation, intensity) colour model. Image thresholding is an effortless and efficient way of distribute an image into a foreground and background. Then, masking the green pixels, the green coloured pixels mostly represent the healthy and growth area of the plant. The next step is counting the green pixels and calculate the growth percentage.

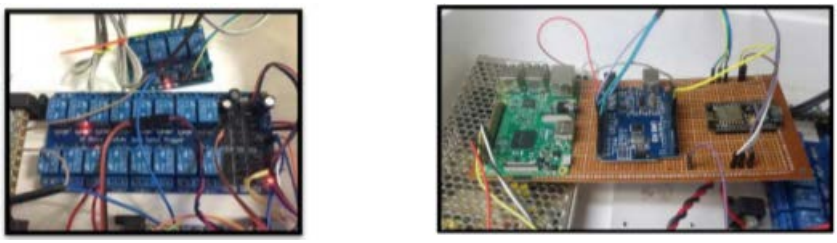

Figure 5 The sensor circuit and IoT controlling

4. RESULTS

The results of the sensor circuit and IoT controlling part are shown in the Fig 5. The circuit connected to the pH sensor and the sensor circuit used for conductivity measurement (EC) and the relay connection to control the operation of various electrical equipment. Once it has started, the microcontroller will execute commands on the various devices and sensors used. The system can be monitored by observing the operation of the LED grow light or other electrical equipment of the system, with the timing of the device through the relay. Relay is in the control of the microcontroller.

The image from the webcam will be processed at Raspberry Pie 3. The image processing procedure is described in Section 3.3. The result of the processing will be as shown in Fig. 6. The image on the left was an RGB image obtained from the camera. The image on the right is the image after processing.

Figure 6 Output of image processing method

Due to this research aims to use image processing to analyse the percentage of plant growth, therefore, in Fig.7 it shows the results when the plant grows which the processing steps will remain the same.

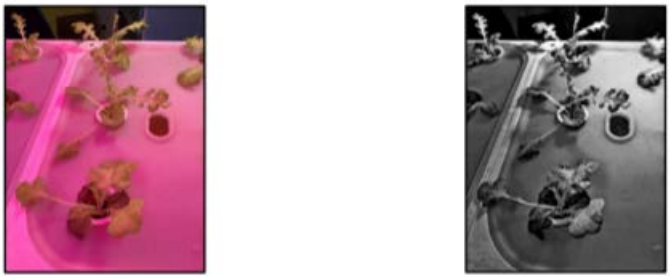

Figure 7 Output result of image processing method

In this experiment, the webcam is set to automatically take a picture to be processed once a day at 1 pm every day and then calculate the percentage of growth. The information obtained will be displayed on the website as shown in Fig 8.

For supporting smart farming, the operation of the equipment will be automated such as the operation of LED Grow Light, which will be scheduled to work. Also, it stops working like the ventilator, and the water pump will work according to the conditions set. Sensor values will be measured and send the data up to Google Sheets. Fig 9 and 10 show the result from Google Sheets.

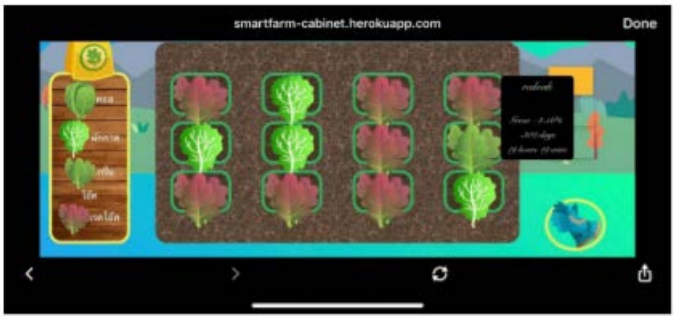

Figure 8 The percentage of growth display on the website

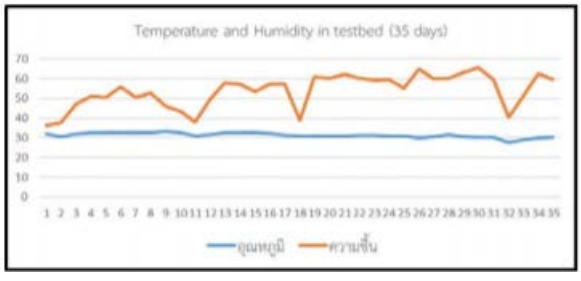

Figure 9 Show the result of Temperature and Humidity

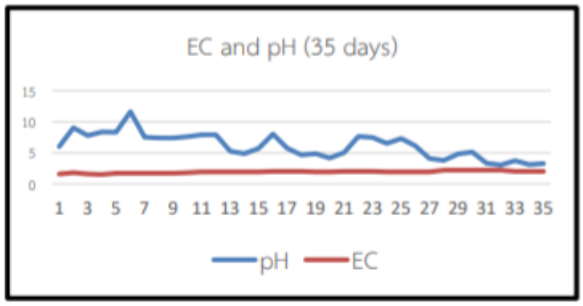

Figure 10 Show the result of pH and EC

5. CONCLUSION

This research was applying Image Processing techniques to assist in cultivation by measuring plant growth and plant health through webcam. The image of plant will calculate on Edge Computing in Raspberry Pie 3. The results will be displayed as a percentage of plant growth. The system will control the environment via IoT such as temperature, humidity, light, heat, pH in the greenhouse is appropriate for the growth of plant automatically. The current findings add substantially to our understanding of techniques for processing plant growth from low resolution images in order to be suitable for real farmers' use. The results from the research are satisfactory. The output results, there were 240 errors from a total of 1260 times. The evidence from this study indicates that 80.95% accurate for low resolution images.

6. ACKNOWLEDGMENTS

This research was funded by King Mongkut's University of Technology North Bangkok. Contract no KMUTNB-63-DRIVE-17. We would like to deliver our greatest appreciation for their support.

7. REFERENCES

[1] C. Du and D. Sun 2004 "Recent developments in the applications of image processing techniques for food quality evaluation Trends in Food Science Technology," vol. 15(5), pp. 230-249.

[2] D. Leister, C. Varotto, P. Pesaresi, A. Niwergall and F. Salamini. 1999. “Large-Scale evaluation of plant growth in arabidopsis thaliana by non-invasive image analysis Plant Physiology and Biochemistry,” vol. 37(9), pp. 671-678.

[3] M. Bhangea, and H. A. Hingoliwalab. 2015. “Smart Farming: Pomegranate Disease Detection Using Image Processing Second International Symposium on Computer Vision and the Internet (VisionNet’15) Procedia Computer Science,” vol. 58, pp. 280 – 288.

[4] K. Namee. 2009. “Performance Evaluation of Multimedia Application QoS over Wireless and Wired IPv6 Networks International Conference on Communication Software and Networks, Macau,” pp. 629-633. DOI: 10.1109/ICCSN.2009.158.

[5] M. Kacira and P. P. Ling. 2001. “Design and development of an automated and non-contact sensing system for continuous monitoring of plant health and growth Transactions of the ASAE,” vol. 44(4), pp. 989-996.

[6] H. E. Nilsson. 2009. “Remote-Sensing and image-analysis in plant pathology Annual Review of Phytopathology” 33, pp. 489-527

[7] K. Namee and G. M. Albadrani. 2019. “Applying IoT,” Web Real-Time Communication and Cloud Computing to Maximize Emergency Medical Service (EMS) Efficiency The 3rd International,” Conference on Big Data and Internet of Things (BDIOT 2019), La Trobe University, Melbourne, Australia pp. 115-119 DOI:https://doi.org/10.1145/3361758.3361777.

[8] P. Serikul, N. Nakpong and N. Nakjuatong. 2018. “Smart Farm Monitoring via the Blynk IoT Platform : Case Study: Humidity Monitoring and Data Recording The 16th International,” Conference on ICT and Knowledge Engineering (ICT&KE), Bangkok pp 1-6 DOI:10.1109/ICTKE.2018.8612441.

[9] K. Namee, N. Panong and J. Polpinij. 2019. “Integration of IoT, Edge Computing and Cloud Computing for Monitoring and Controlling Automated External Defibrillator Cabinets in Emergency Medical Service The 5th International,” Conference on Information Management (ICIM2019), The Trinity Hall, University of Cambridge, UK pp 237-241 DOI: 10.1109/INFOMAN.2019.8714717.

[10] T. N. Tete and S. Kamlu. 2017. “Plant Disease Detection Using Different Algorithms Proceedings of the Second International Conference on Research in Intelligent and Computing in Engineering,” pp. 103-106 ACSIS, Vol. 10 ISSN 2300-5963.

Fully Autonomous Drug and Food Delivery Robot for Hospital and Patient Care Logistic Management based on Artificial Intelligence

Antica Eam opha[1], Sittikorn Titaviriya[2] and Wibool Piyawattanametha[3]

[1]*Biomedical Engineering Department Faculty of Engineering King Mongkut's Institute of Technology Ladkrabang Ladkrabang, anticae11@gmail.com*

[2]*Biomedical Engineering Department Faculty of Engineering King Mongkut's Institute of Technology Ladkrabang Ladkrabang, project.liew@gmail.com*

[3]*Biomedical Engineering Department Faculty of Engineering King Mongkut's Institute of Technology Ladkrabang Ladkrabang and Institute for Quantitative for Health Sciences and Engineering Michigan State University, East Lansing, wibool@gmail.com*

Abstract.

We developed a fully autonomous drug and food delivery robot for hospital and patient care logistic management based on an artificial intelligence. This robot will act as an intermediary in delivering food, medicine, and medical supplies among the departments themselves or departments and patients, which will be controlled via a very intuitive software that enables navigation technology with intelligent coordinate systems by simulating the use area as a map to control the movement of the robot. The intelligent coordinate navigation technology for this robot will be integrated with a depth camera, and a LIDAR sensor operating on an robot operating system melodic for Simultaneous Localization and Mapping allowing robots to recognize objects or people in the environment. The robot achieves the maximum traveling speed of 0.2 m/s and can operate for 2 hrs with a fully charged battery.

Keywords. Logistics in hospital, autonomous robot, SLAM, LiDAR, depth camera, ROS, RealSense.

1. INTRODUCTION

The hospital is an organization with a complex internal management system. Therefore, it needs high accuracy and high precision in managing information, devices, materials, or medical products including drug, medical supplies, medical equipment, food, and patients. These materials and medical products are the last mile in hospital logistics that could help determine the life and death of each patient. The flow of information among these

responsible areas in this last mile is fractured and unorganized resulting in very poor resource and supply management which could be very costly.

The drug and medical management system are one of the most important systems in the hospital which can demonstrate the potential of communication management and coordination of various departments related to medical and medical supplies in the hospital. To achieve maximum efficacy, accuracy, completeness, and timeliness on time which these activities show the performance, safety, reliability Including the availability of medical services in the hospital. Because the delivery system needs to be done through the medical personnel of different departments, which means it may cause delays and errors from the steps, wastes the time and human resources, as well as increasing unnecessary workloads for hospital staffs. For this reason, the automation system began to support the increasing number of patients and to ensure the smooth operation of medical units.

At present, various automatic robots are used in hospitals. With the expectation that the robots will replace the hospital personnel in complicated, redundant tasks and require high accuracy. There are advantages in reducing the cost of hiring non-essential personnel. To shorten the working time to reduce errors and increase the efficiency of work. Including in the field of treatment to increase the ability to support patients who need treatment which is likely to increase from the number of elderlies in the future.

The purpose of a fully autonomous drug and food delivery robot for hospital and patient care logistics management based on artificial intelligence is to reduce the unnecessary workload of hospital personnel. The robot allows the person to focus on working with patient care to their full potentials The use of robots will help increase patients' security, reduce the risk of errors, reduce time and costs in terms of hiring personnel for unnecessary long-term workloads. Furthermore, it can help in reducing the amount of waste generated by the tracking system, forwarding, and reporting in the old document formats including more efficiency in easy in following up and traceable medicines and medical supplies in case that the medical product has a problem or needs to be recalled. There, we aimed to develop a delivery robot that can achieved the aforementioned tasks at an affordable price point with great versatility and utility.

BACKGROUND

1.1. Logistics in a hospital

Patient safety is very important for medical care, with each step of the procedure being at risk for errors. The hospital is an organization that has medical products such as medicines and medical supplies, medical equipment, etc., which are important resources that affect the lives of patients receiving medical care. However, the material flow of people and the information in the hospital is complicated causing each department in the hospital to not yet be able to connect to the data between each other effectively. As a result, the system does not have data to track and trace medicines and medical supplies in the case that a medical product has a problem or requires product recall.

Logistics is a flow science. Stock and Lambert define this flow in 3 ways:

1. Product / Service Flow is a flow in the form of Physical Movement.
2. Information Flow is the flow of information for communication such as product needed, cost, etc.
3. Financial Flow such as goods or services must be paid in exchange for goods and the resulting flow focuses mainly on the product or service with the aim of how to flow the most effective,

Therefore, to meet this efficiency, the logistics system is built based on 13 activities as shown in Figure 1 [1].

Figure 1 The basis of 13 activities in the logistics system

1.2. SLAM – Simultaneous Localization and Mapping

SLAM is a process to create maps of the environment as robots are moving and identifying their locations at the same time, with no information about the environment before. SLAM is very important for robots that need instant interaction [2].

Mapping of the environment is the process in which measurement data that can be measured from the environment. From various sensors that are combined to create a data structure to describe the environment in that area. The localization is a description of the position of the robot or various objects that we are interested in the map which may be predefined or created while specifying the position.

In the operation of the robot specifying locations and creating maps localization and mapping is an important task for robots. Because the robot needs to use map data together with the location data of the robot to plan activities to respond to the environment, such as the movement of the automatic survey robot, rescue robot, robot housekeeper, or even to pick up things, robots also need to know the location of items to be picked up and the position of robot's hand too.

There are many types of maps used to describe the robot environment, using patterns that humans may understand or not, explaining the environment with a large number of points (Point Cloud), explaining environment by arranging content that robots are interested in or describing things surrounded by the relationship structure of the environment is possible (Topology).

1.3. LIDAR - Light Detection and Ranging Data

The working principle of Light Detection and Ranging system is quite simple. It generates a laser pulse train, which sent to the surface/target to measure the time and it takes to return to its source. The actual calculation for measuring how far a returning light photon has traveled to and from an object is calculated by:

$$\text{Distance} = \left(\text{Speed of Light x Time of Flight}\right) / 2. \quad (1)$$

The laser instrument fires rapid pulses of laser light at a surface, some at up to 150,000 pulses per second. A sensor on the instrument measures the amount of time it takes for each pulse to reflect. Light moves at a constant and known speed so the LIDAR instrument can calculate the distance between itself and the target with high accuracy. By repeating this in quick progression the instrument builds up a complex 'map' of the surface it is measuring [2].

1.4. Three-dimension (3D) Depth sensing: Intel Realsense camera

The cameras can calculate the distance between objects, separating objects from the background layers. This gives much better object, facial and gesture recognition than a traditional camera.

Mapping and navigation: A RealSense SLAM uses a fisheye camera, accelerometer, gyroscope, and depth camera to track a system's movement in 6DoF. It also allows a location that was mapped previously to be recognized, which is known as re-localization. Tracking and re-localization allow robots to build and share knowledge about the environment.

Facial recognition/person tracking: identify faces in the camera's range of facial features on an individual face.

Obstacle avoidance: The RealSense camera can help robots identify and autonomously avoid objects. The RealSense camera can calculate the distance between object and separate objects from the background layers behind them [3].

1.5. ROS – Robot Operating system

The Robot Operating System (ROS) is not an actual operating system, but a framework and set of tools that provide the functionality of an operating system on a heterogeneous computer cluster. Its usefulness is not limited to robots, but the majority of tools provided are focused on working with peripheral hardware.

ROS provides functionality for hardware abstraction, device drivers, communication between processes over multiple machines, tools for testing and visualization, and much more.

The key feature of ROS is the way the software is run and the way it communicates, allow to design complex software without knowing how certain hardware works. ROS provides a way to connect a network of processes (nodes) with a central hub. Nodes can be

run on multiple devices, and they connect to that hub in various ways as shown in Figure 2.

The main ways of creating the network are providing requestable services or defining publisher/subscriber connections with other nodes. Both methods communicate via specified message types. Some types are provided by the core packages, but message types can be defined by individual packages [4-5].

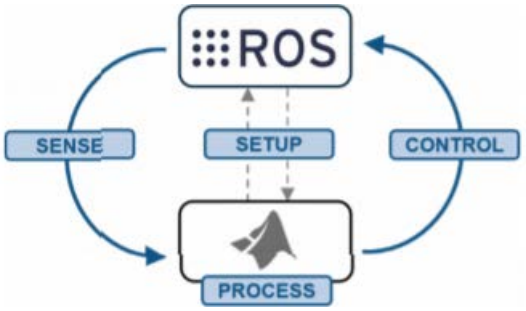

Figure 2 Working principle of ROS

2. METHODS

The work is divided into 3 main parts namely sub-system design, robot design, and software design. Each part is described in detail below.

2.1. Sub-system design

This part separates into 4 sub-system as shown in Figure 3.

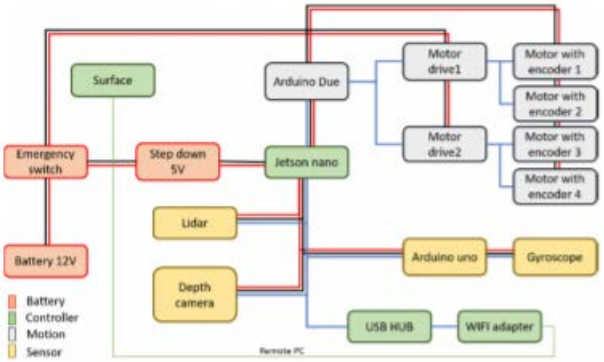

Figure 3 Hardware system diagram

Our delivery robot needs a 12-volt 30-Ah batteries split them into 2 outputs. The first one goes to drive 2 motor. The second one is used as an input to step voltage down to 5

volts for supplying to the a Nvidia Jetson (version Jetson nano) used to control robot's four sub-systems. Those are:

1. Battery sub-systems: this part consists of a step down 5 volts, an emergency switch, and a 12-volt Lithium-ion battery.
2. Controller sub-systems: this part used a Jetson nano as a microcontroller to control the robot, software, and hardware. The Microsoft Surface pro 5 computer (Model: Surface Pro) was used to enter commands and to display information about the robot.
3. Motion sub-systems: the motion of the robot consists of 2 driving motors, 4 motors, and 4 wheels.
4. . Sensor sub-systems: A Lidar and a depth camera (3D sensing sensor) for image processing are utilized to avoid obstacles in real-time.

In motion sub-system part, we used both a Lidar and a depth camera as 3D sensing elements. The depth camera will be used to acquire 3D images and process them in high resolution 3D images. However, it has a short operating scan range (0.1-10 meters). The lidar will acquire images in series of 2D planes and will process them into 3D images with low resolution due to its long operating scan range (0.12-18 meters). The chosen Lidar and depth camera are a RPLidarA2 and an Intel RealSense D435 for positioning and map creation, respectively. By combining both sensing elements, the overall system will achieve a higher resolution wither moderately long operating scan-range. The specifications of both sensors are listed on Table 1 and Table 2.

Table 1 Depth camera specifications.

Depth camera operational specifications: the Intel RealSense D435	
Operating Range (Min-Max)	0.1 m – 10 m
Depth Resolution and FPS	1280 x 720 @ 90fps
Depth Field of View	82.5 x 58

Table 2 Lidar specifications.

Lidar operational specification: RPLidarA2	
Distance range	0.12-18 m
Angular range	0-360 deg
Distance resolution	<1% Dis.range
Angular resolution	0.9 deg
Sample duration	0.25 ms
Sample Freq.	2000-4000-8000 Hz
Scan rate	10 Hz
Weight	190 g
Height	41 mm
Width	76 mm

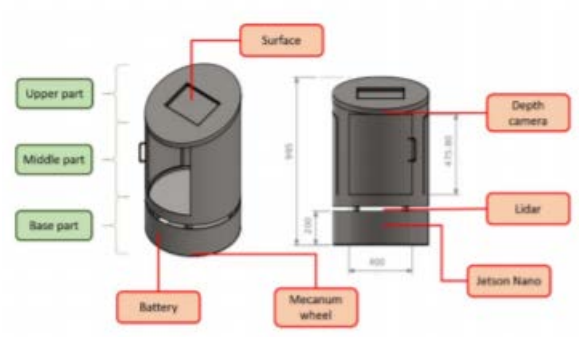

Figure 4 All components in the 3D model

2.2. Robot design

Our delivery robot shell was designed with the Solidworks 2018 program which has the following characteristics:

- Base part: the robot shell has a cylindrical shape with a diameter of 606 millimeters and its backside height of 995 millimeters. It has 4 wheels controlled by 4 motors and 2 dual-motor driving boards. The bottom compartment of the base contains a robot's microcontroller system and other electronics circuit boards. The top compartment contains a circularshape slot for Lidar laser scanning for a mapping process.

- Middle part: this part is a storage area for food, drug, or any medical supplies. This part adds an additional height of about 500 millimeters from the base part. This part is allocated for both a space shelf installation and a mounted weight sensor to check overall load limits. The front area above the door is for a depth camera installation for both a distance measurement and as a 3D scene scanner.

- Upper part: this part adds an additional height of approximately 150 millimeters with an oblique cut from the middle part. It is a part of the display screen and was cut obliquely for visibility. The Microsoft Surface pro 5 computer was used to both inputting commands and displaying robot information.

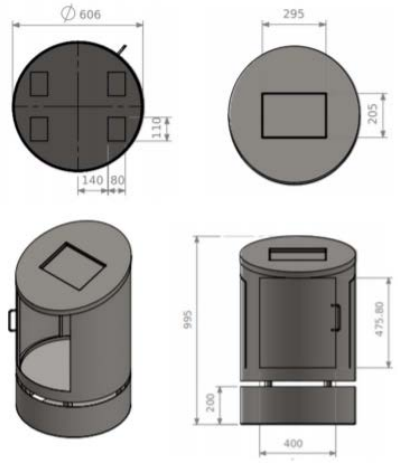

Figure 5 Our delivery robot design: bottom view (top left), top view (top right), side view (bottom left), and front view (bottom right).

2.3. Software design

The Jetson nano operating system was installed with the Ubuntu 18.04 and the ROS melodic for controlling the robot. Figure 6 shows the ROS diagram. An arduino due (Microcontroller AT91SAM3X8E) was employed to both read the encoder value from the motors and to control their speeds by varying pulse frequencies. Then, we used command from rosserial packages to communicate with the motor controller while the ROS was used to control the motor via a keyboard. Integration of both a Lidar with a depth camera were used for a gmapping node and a navigation node, respectively. A 3-axis accelerometer/Gyro module (MPU 6050) we employed for a gyroscopic function for the base controller. Finally, the base controller was calibrated with all acquired data to be ready for an operation.

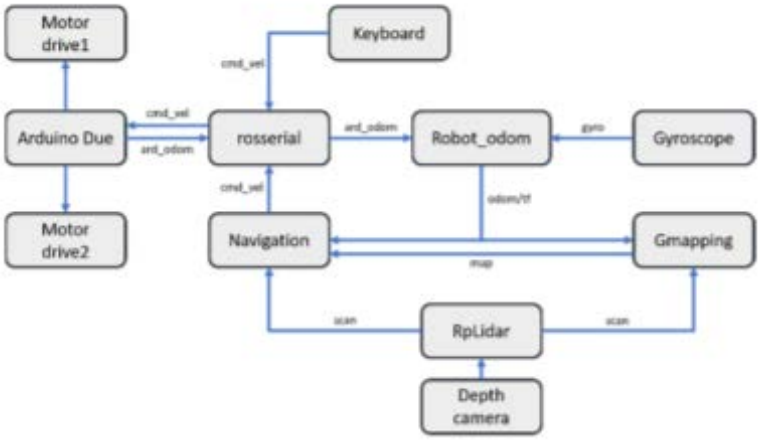

Figure 6 ROS diagram

3. RESULT

3.1. Aluminum Robot Frame

The robot frame is shown in Figure 7 consisting 3 main compartments as mentioned in previous section. The robot is designed to support the maximum load of 30 kgs.

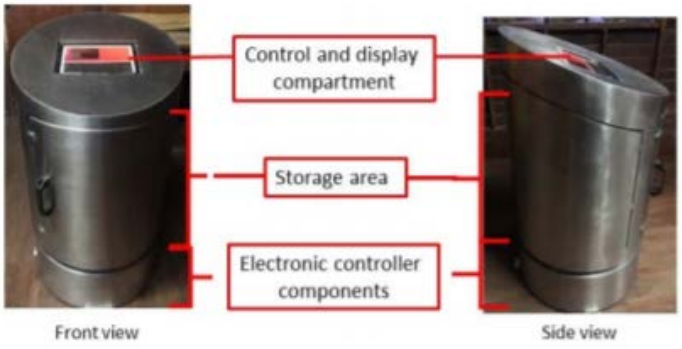

Figure 7 An aluminium robot frame

3.2. The interface of depth camera: Intel RealSense D435

The RealSense camera run on the Ubuntu 18.04 operating system was connected via a USB port. Then, the camera processing software controlled the RealSense Viewer program can display video streams in 3 types including a red-green-blue (RGB) video stream, an infrared (IR) video stream, and a depth video stream. The software combined all imaging data namely left RGB camera, right RGB camera, and an infrared camera to improve both depth resolution and image accuracy. Figure 8 shows the RealSense Viewer software interface with images acquired from the aforementioned cameras.

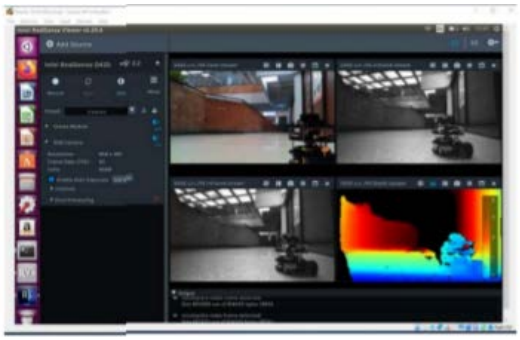

Figure 8 An interface of the RealSense Viewer and displayed images: RGB (top left), IR (top right and bottom left), and depth (bottom right)

3.3. Mapping on ROS visualization (rviz)

To collect mapping data from a Lidar sensor commanded via the ROS, both a slam node and a teleoperation node need to be manually controlled for a mapping process first. Figure 7 shows an example of mapping data file that control and display through the rviz program on the ROS. Therefore, this interface shows environments around the robot, location, a path of the robot, and a target position that the robot will navigate to. This information is applied for the navigation system in next part.

Moreover, the rviz connects to the RealSense camera and displays on the same interface of this program as shown at the bottom left pictures (RGB and IR camera streams) in Figure 9.

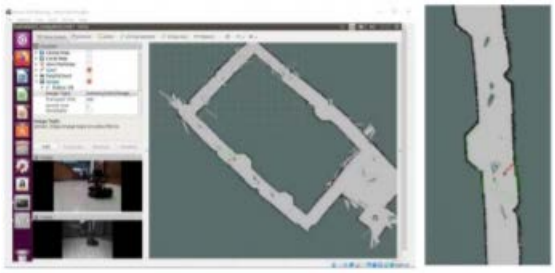

Figure 9 Show the interface environment around the robot

3.4. Navigation system

Navigation node operated on the rviz is a tool of the ROS. This software system communicates with the robot to visualize, detect, and locate the position of the robot. Then, the system will send an exact position to be displayed on the interface program.

To use the navigation system, an operator needs need to first point to a target on the map. Then, the robot will automatically process and create the shortest route to travel to that location.

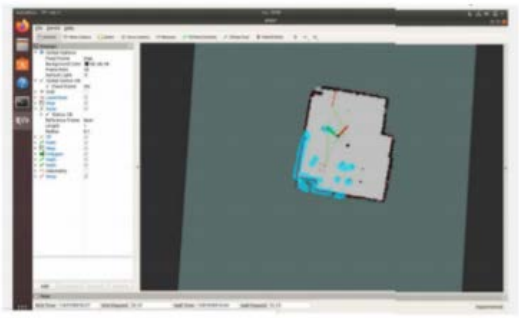

Figure 10 An interface of our navigation program

4. DISCUSSION AND CONCLUSIONS

A fully autonomous drug and food delivery robot has been developed. Mapping generation and shortest path can be automatically generated by utilizing SLAM to specify the location of the robot. Besides, additional navigational maps are derived by various packages of ROS applied on 2D and 3D data obtained from sensing elements to increase the efficiency of the mapping, including the system that can avoid obstacles by itself. The delivery bot can travel at the maximum travel speed of 0.2 m/s for 2 hrs. We anticipate a broad set of robot utility in the transportation of medicines, food, and medical supplies in the hospital, to reduce management problems and reduce unnecessary workloads of medical personal

5. ACKNOWLEDGEMENT

This work is partially supported by grants from the King Mongkut's Institute of Technology Ladkrabang Research Fund, Thailand; the National Research Council of Thailand; the Thailand Science Research and Innovation; the Newton Fund Researcher Links, British Council, UK; the Fraunhofer-Bessel Research Award, Alexander von Humboldt Foundation, Germany.

6. REFERENCES

[1] K. Duangpun, et al., "Hospital Logistic" in *Title of HOSPITAL LOGISTICS*, Thailand: LogHealth, Mahidol university, 2016, ch. 1, pp. 2-4.

[2] M. Mahrami, M. N. Islam, and R. Karimi, “Simultaneous localization and mapping: issues and approaches,” *International Journal of Computer Science and Telecommunications*, 4(1), 2013.

[3] Intel Realsense, "Capabilities of intel realsense" in *Title of Intel RealSense Brings 3D Vision to Robots [whitepaper]*, Robotics Bussiness Review, ch. 2, pp. 7, 2017.

[4] P. YoonSeok, C. HanCheol, J. RyuWoonand, L. TaeHoon, "Important Concepts of ROS" in *Title of ROS Robot Programming*, Korea: ROBOTIS Co.,Ltd., 2017, ch. 4, pp. 41-89.

[5] A. Adnan, “An Introduction to Robot Operating System: The Ultimate Robot Application Framework.” Toptal.com. https://www.toptal.com /robotics/introduce tion-to-robot-operating-system (accessed Oct. 24,2019).

CFD based Improvement of Thai Irrigation Pump

Kittipass Wasinarom[1], Dachdanai Boonchauy[2] and Jarruwat Charoensuk[3]

[1]*School of International and Interdisciplinary Engineering Programs Faculty of Engineering, King Mongkut's Institute of Technology Ladkrabang Bangkok, Thailand, kittipass.wa@kmitl.ac.th*

[2]*Seagate Technology (Thailand) Ltd. Teparak, Samutprakarn ,Thailand, dachdanai.boonchauy@seagate.com*

[3]*Department of Mechanical Engineering Faculty of Engineering, King Mongkut's Institute of Technology Ladkrabang Bangkok, Thailand, jarruwat.ch@kmitl.ac.th*

Abstract.

Evaluation phase which was partial fulfilment of the beginning phase of "Development of Performance test rig and Efficiency improvement of impeller in Thai irrigation pump project" is presented in this paper. Overall flow field in the pump system that consisted of inlet, impeller and stator vane of the available pump was analyzed using commercial Computational Fluid Dynamics (CFD) code. The goal of this investigation is to obtain more understanding of energy dissipation which results from shear stress that developed within the flow field in each section of the pump. The improvement measure is then conducted with the concern of manufacturing difficulties. High dissipation flow structure was observed around the impeller outlet. Jet-wake and recirculation flow were observed. The first improvement measure was conducted by adding the bluff body in the flow channel to alleviate jet-wake structure and delay flow separation. After the implementation of the optimized bluff body around the impeller exit, CFD results indicated around 3-8% improvement compared with the CFD results of the available pump for the entire range of operating conditions.

Keywords. CFD, turbo-machine, pump, improvement.

1. INTRODUCTION

The irrigation pump is a small portable pump unit (Figure1). It is typically developed by local technicians. The improvement focused on the increasing volume flow rate rather than the energy efficiency. Therefore, generally the energy efficiency of this kind of pump is very low. The test of the available pump shows that the obtained peak efficiency was around 40% [1] which there is high potential to conduct energy efficiency improvement projects. There are a lot of different conditions between development of Thai irrigation pumps and the industrial pumps. Irrigation pumps are forced to use simple manufacturing

techniques because of its low capital cost. Domestic human resources are used in this development rather than the world's leading turbomachines

In this project progress, CFD simulation of the flow inside the pump system was conducted. Energy dissipation which results from shear stress that developed within the flow field of each section of the baseline pump was analyzed in order to point out the improvement opportunity in specific sections. The results showed that there was the jet-wake, recirculation and flow separation at the impeller outlet area which were considered high internal dissipation flow structure at the impeller outlet. The first improvement measure was implemented by adding the bluff body profile at the impeller outlet (behind the impeller). By this action, it was expected to alleviate jet-wake structure and delay the separation flow. After performing CFD simulation of the improved version, it was found that recirculation disappeared and the jet-wake flow structure was significantly reduced.

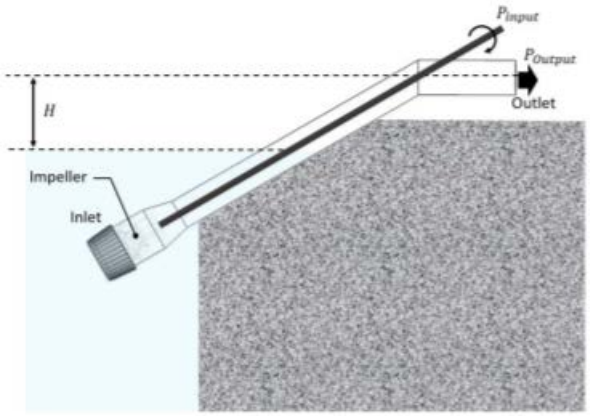

Figure 1 Thai irrigation pumps used in flooding application

2. METHODOLOGY

Energy dissipation is the process that leads to the conversion of useful mechanical energy (flow energy) to non-useful heat energy (internal energy). It can be described by the first law of thermodynamics for SteadyState, Steady Flow Process (SSSF). The equation can be developed for turbo-machine equipment as shown in (4). The isentropic process which is the ideal case, it considers non-dissipation occurs between inlet and outlet of turbomachine. The process occurs following the line that starts at point 1 to point 2s as seen in Figure 3. The energy efficiency is 100 percent in the isentropic process. In the other words, all of the input mechanical shaft energy can be converted to useful flow energy at outlet (state2). While in actual situations, some input shaft energy is converted to heat by fluid friction or so called energy dissipation which resulted in less useful flow energy at outlet regarding to the equation (4). This process is also known as internal irreversibility since the dissipation occurs inside the fluid medium itself.

The efficiency can be calculated as the equation (1)

$$n = \frac{p_{output}}{p_{input}} \tag{2.1}$$

Where η is the calculated efficiency, Poutput is the flow energy at the pump outlet which can be calculated as the equation (2)

$$P_{output} = p \times g \times Q \times H \tag{2.2}$$

Where ρ is water density, g is the gravitational acceleration, Q is volume low rate and H is lifted head as indicated by Figure 1.

P_{input} can be calculated by equation (3)

$$P_{input} = Tshaft \times \omega \tag{2.3}$$

P_{input} is the shaft mechanical energy. ω is the shaft rotational speed and *Tshaft* is the torque.

$$P_{output} = P_{input} + Internal\ dissipation \tag{2.4}$$

Flow dissipation is generated by the presence of velocity gradient (shear layer) which has a specific magnitude in particular location of the flow domain. The developed shear stress is directly proportional to the velocity gradient in Newtonian fluids [5]. The most basic illustration of the situation is the laminar flow in a simple circular pipe. Shear stress is proportional to the velocity gradient magnitude which in this case, it depends on y location as shown in Figure 2. It has only shear stress in x direction in this case. Flow structure in a turbomachine is much more complicated than the flow within a circular pipe. The fluid elements usually possessed 3D of viscous shear force.

In order to conduct energy efficiency improvement activity in turbo machinery, it is necessary to be able to visualize detailed fluid dynamics within the flow passage. Therefore, viscous shear stress at specific locations in the system can be quantified or at least estimated. Then the improvement measure is implemented with the expectation of reduced shear flow. The optimization process may incorporate the validated CFD simulation code to minimize cost and time consumed and also allow high ability to analyze. Finally, the experimental test must be performed. Flow visualization technique is the key to this process. CFD is an interesting method to obtain detailed flow visualization. Many researchers employed CFD as a tool [2, 3, 4]. However, it has to calibrate and validate with the experimental result in order to justify the obtained flow field.

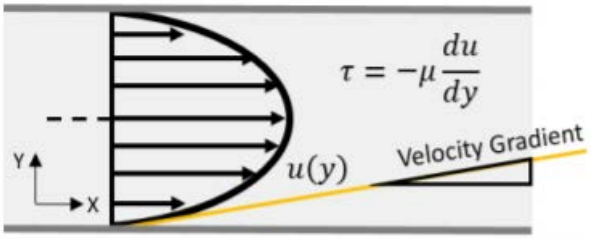

Figure 2 Viscous shear stress relates to velocity profile of the Newtonian fluids in circular pipe

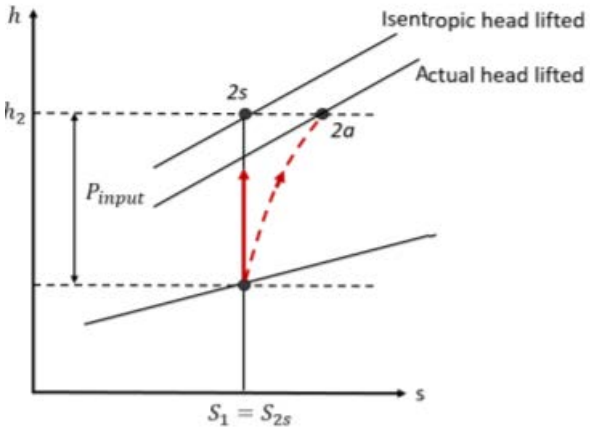

Figure 3 Example of Ideal (isentropic) and actual pump process of the same flow rate and input shaft energy

CFD has become an important tool to explore the flow field inside the flow channel of turbomachinery. The obtained results then analyzed by focusing on shear stress occurred in the fluid element at the particular location of flow domain

3. MODELING

Commercial CFD code was used in this work. The simulation of available Thai irrigation pumps was performed throughout the flow rate of 0.01 to 0.1 m^3/s while speed was kept constant at 900 rpm. CFD results were validated with experimental results from a test rig at King Mongkut's University of Technology Thonburi (KMUTT). The test rig was conforming to grade 1 according to the applicable JIS standard (JIS B 8301, 8302) [1]. Flow channel, impeller and stator vane of the available pump was reproduced by CAD program as shown in Fig. 4. The flow channel was divided into 8,000,000 control volumes. Then this geometry file was imported to the ANSYS CFX solver [6]. The flow model was RANS (Reynolds Averaged Navier Stokes) with SST turbulence model. The boundary

condition and all necessary parameters were set regarding Table 1. Iterative solution procedure of inter-link between discretized momentum equation, continuity equation, turbulence kinetic energy and turbulence dissipation equation was executed. It continued until calculated normalized residual was below 10^{-4} Finally the last updated pressure and velocity field was considered as the simulation results.

Figure 4 CAD geometry of the irrigation pump system

Table 1 Boundary condition and input parameter used in CFD simulation

Analysis type	Steady Stat
Mesh	8,000,000 elements
Turbulence model	SST
Fluid domain	Water
Moving Reference Frame (MRF)	900 RPM
Inlet	Total pressure 1 atm
Outlet	Desire flow rate
Convergence residual	10^{-4}

Figure 5 Cross Section A-A of the pump system

4. RESULT

Model validation of the available Thai irrigation pump showed the acceptable agreement with the experimental results throughout the flow rate between 0.01 to 0.1 m^3/s which covered all operation range of the pump [1].

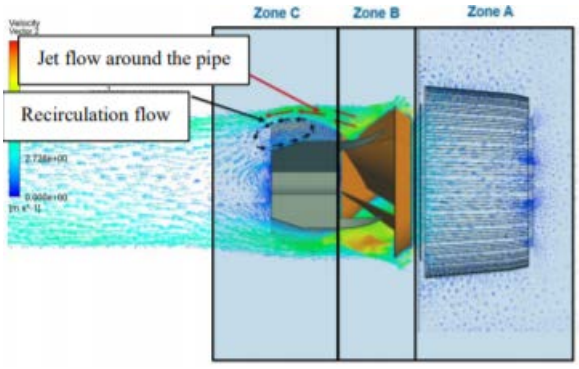

Figure 6 Jet flow and recirculation flow at the peak efficiency condition of available version

General flow structure around peak efficiency condition (0.05 m^3/s) was analyzed. The flow domain was divided into 3 sections as shown in Figure 6. They were composed of 1.) Inlet region 2.) Impeller and 3.) Behind impeller. All of the demonstrated flow fields in this paper were on the cross-section in A-A planar as shown in Figure 5. It was found that, at the inlet region, flow entered the impeller with considerable low velocity as indicated by blue velocity vector and the flow was nearly uniform with only low velocity gradient presented. The flow inside the impeller was highly complex but it was beyond scope of discussion in this paper. At section 3 (behind impeller), evidence of high shear flow was observed. High velocity flow at the impeller exit impinged on the pipe wall which resulted in the formation of high velocity-jet flow around the pipe rim, while the low velocity-wake flow was found at the inner core of section C as shown in Figure 6 Highly shear flow of this jet-wake structure will result in massive energy dissipation in this section.

First improvement measures focused on the area around the impeller exit (section 3 or Zone C in Figure 6 even though there was also considerable shear flow observed inside the impeller passage. This is because any change in impeller manufacturing is a complicated task. The impeller improvement will be performed in the later phases.

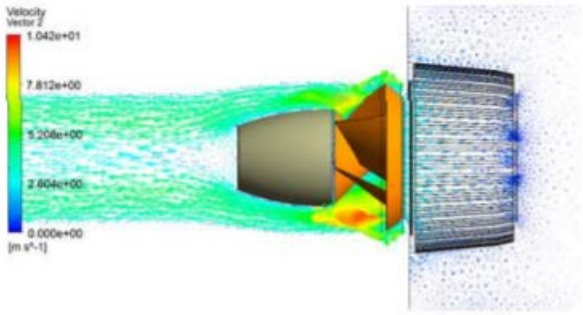

Figure 7 An improved version A

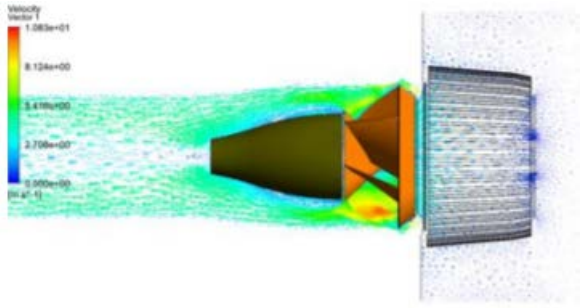

Figure 8 An improved version B

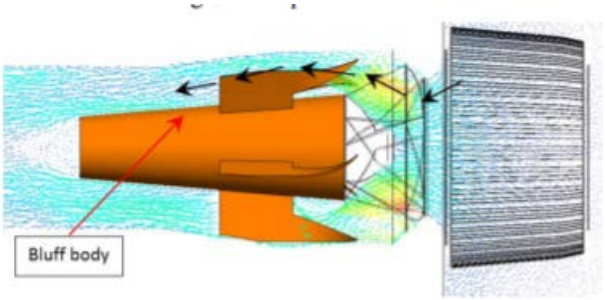

Figure 9 The final improved version

The first improvement measure is to add the bluff body profile behind the impeller. It proposed to prevent abrupt expansion of the flow cross-sectional area at the impeller exit. This expansion flow cross-sectional area will result in a wake region at the inner core behind the impeller as shown in Figure 6. Where both recirculation and separation flow were observed. Various profile shapes were trialed by CFD simulation (Figure 7 and 8). The profile shape was optimized in this process. It was improved by analyzing the velocity field which related to the cross-area of the flow channel that developed by the bluff body.

The profile of the bluff body should be allowed as low as possible of the averaged flow velocity while still absent of jet-wake flow or any flow separation. However, the curved profile was transformed to conical shape at the end (Figure 9) for the ease of manufacturing reason. After this action, CFD results indicated around 3-8% improvement compared with the CFD results of available pumps for the entire range of operating conditions as shown in Figure 10.

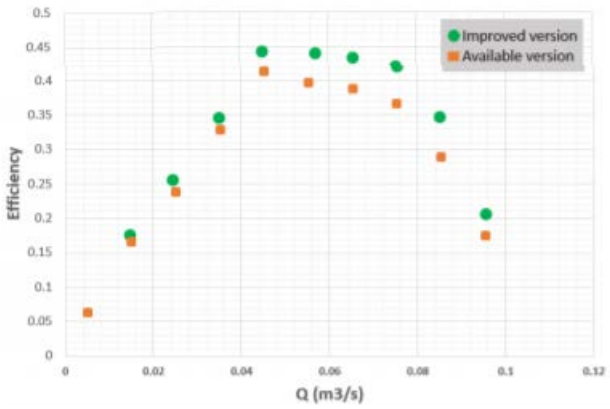

Figure 10 Efficiency of available pump and improved pump (bluff body installed) by CFD

5. CONCLUSION

Overall flow field in the available irrigation pump system that consisted of inlet, impeller and stator vane was analyzed using commercial Computational Fluid Dynamics (CFD) code. The first improvement measures have been conducted by adding the bluff body in the flow channel to alleviate jet-wake structure and delay flow separation. After the implementation of the optimized bluff body around the impeller exit, CFD results indicated around 3-8% improvement compared with the CFD results of the available pump for the entire range of operating conditions.

6. ACKNOWLEDGEMENT

This work was supported by Thailand National Metal and Materials Technology Center (MTEC) project code P1851268

7. REFERENCES

[1] "Development of performance test rig and efficiency improvement of impeller in Thai irrigation pump full report (P1851268)," National Science and Technology Development Agency, 2019, Chapter 3, pp. 37- 66.

[2] L. Ji, W. Li, W. Shi, H. Chang and Z. Yang. “Energy characteristics of mixed flow pump under different tip clearances based on entropy production analysis,” Energy, vol.199, 2020, pp. 117447.

[3] A. Patil, S. Sundar, A. Delgado and J. Gamboa, “CFD based evaluation of conventional electrical submersible pump for high-speed application,” Journal of Petroleum Science and Engineering, vol.182, 2019, pp. 106287.

[4] S. Kim, K. Y. Lee, J. H. Kim and Y. S. Choi, “A Numerical Study on the Improvement of Suction Performance and Hydraulic Efficiency for a Mixed-Flow Pump Impeller”, Mathematical Problems in Engineering, vol.2014, Article ID 269483

[5] J. Charoensuk, “Computational Fluid Dynamics and its Application in Engineering Problems”, Ladkrabang, 2018, Chapter 2, pp 25-87.

[6] ANSYS, ANSYS Academic Research, Release 19 R3, Help System, CFX-Documentation 2019. ANSYS, Inc.

Adaptive Cutting Force Control for CNC Milling Machine

Noppadol Maneerat[1], Adisak Khaengsarigid[2] and Bundit Pasaya[3]

[1]*Faculty of Engineering King Mongkut's Institute of Technology Ladkrabang, Bangkok, THAILAND, noppadol.ma@kmitl.ac.th*

[2]*Faculty of Engineering King Mongkut's Institute of Technology Ladkrabang, Bangkok, THAILAND, 58601314@kmitl.ac.th*

[3]*Faculty of Engineering King Mongkut's Institute of Technology Ladkrabang, Bangkok, THAILAND, bundit.pa@kmitl.ac.th*

Abstract.

This paper presents the adaptive cutting force control for CNC milling machines. The research scheme divided the mathematical models, consisted of two parts: model of the feed drive system. Then it's designed to the adaptive cutting force controller using Lyapunov's method. The dynamometer is used to sense the cutting force and feedback to the cutting force controller. The output signal of the controller is a feed rate volume of CNC controller to control the feed drive system during a milling process. For experimental, it's defined 3 different depths of cut(DOCs). The experimental results compared to that between the actual cutting force response and the target cutting force. As experiment result, it can control the cutting force smoothly, the tool life increased and acceptable practice.

Keywords. Adaptive control, Cutting force, CNC milling machine; Feed drive system, Mathematical Models.

1. INTRODUCTION

The utilization of CNC milling machine has expanded rapidly in THAILAND, such as a metal forming industry and metal machining needs to increase efficiency and reduce production costs. The advantage of CNC milling machine is optimization of the production process, and a not very skilled CNC operator features. However, the disadvantages of conventional milling operation are the calculation of parameters of CNC milling machines, such as the spindle speed and feed rate in order to identify the cutting force appropriated for the DOC and the hardness of work piece. The most parameters are defined by CAD/CAM programmer which calculated from a manual of end mill tools. Thus, the utilization of many CNC milling machine is ineffective. The condition of operating the CNC milling machines require that parameters must be configured very carefully in order to avoid any damages and/or failure. Consequently, many CNC milling machines cannot work effectively and work under the milling process conditions that are not the optimal

criteria. Cutting force [1-5] is one of the important parameters of CNC milling machines. It is very useful the quality inspection of End mill tool and work piece. Moreover, the suitable cutting force prevents tool breakages, improves the surface quality of work piece, and enables further development of cutting-force CNC controllers. Therefore, the use of CNC milling machines will rely on the expertise of the CNC milling machine. To address the issues, [6-9] proposed the adaptive cutting force control system. The authors however ignored the parameter of the feed drive system used in the analysis, giving rise to design the cutting force control.

According such the problems, this research presents the cutting force control for CNC milling machines, which online adjusted the CNC parameters while CNC milling machine runs on. The control system is designed to adaptive cutting force sliding mode control to optimize the milling process, reduce the tool wear, reduce the tool breakage [1-3], and increase the tool life [1]. The controller performs to control the cutting speed [1,2] by adjusting the feed rate volume in real time [6]. For control system design, it's divided the mathematical models consisted of two parts: Model of the feed drive system, in which the friction force was integrated into the model and Model of the milling process. Then, the controller is designed to be the adaptive sliding mode cutting force control. The target cutting force considers based on the hardness of steel, feed rate, cutting speed, and spindle speed, which is determined by CNC operator. The cutting force errors were then computed and were inputs of a Lyapunov's algorithm-based adaptive mechanism [10,11] for the output tracking error convergence and the cutting force [5,6]. The experimental results indicated that the proposed integrated technique could reasonably control the cutting force and subsequently the cutting force, thus a good candidate for use in CNC milling machines.

2. MATHEMATICAL MODELS OF THE CUTTING PROCESS

The CNC milling machine consists of the feed drive system for 3 set (X-Y-Z Axes) and spindle system, as shown in Figure 1

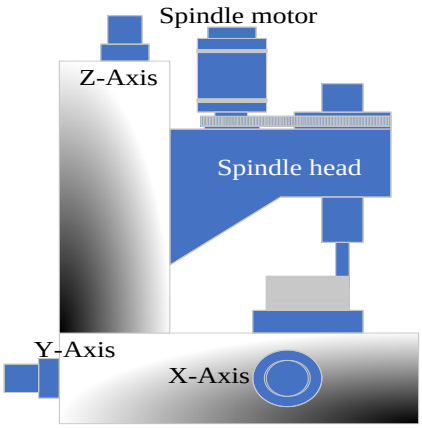

Figure 1 CNC Milling Machine

The principle of the CNC milling machine is that the work piece must be installed on atop the machine tool table. The machine operator will enter the part program to the CNC Controller, press the cycle start button for the CNC milling machine activated. After that, each axis of the feed drive system moves according to the part program.

2.1. Feed Drive System

Generally, the feed drive system of CNC milling machines have the basic components as follows: servo motor driver, servo motor, ball screw, ball nut, coupling, slide way, thrust bearings, saddle, machine tool table, end mill tool, and lubrication system as shown in Figure 2. The work piece will move horizontally along X-axis and Y-axis while end mill tool moves vertically along Z-axis. For the milling process, the dynamometer must be installed on machine tool table to sense the cutting force to the cutting force controller

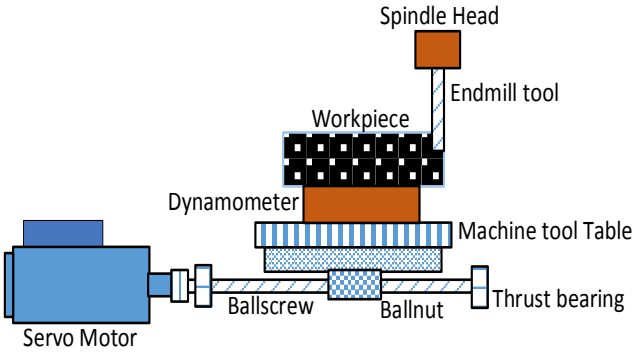

Figure 2 the feed drive system

The basic of CNC milling machine is that the work piece is mounted on a machine tool table, and moving toward the end mill tool, called milling process. The block diagram of the milling process is written, as shown in Figure 3. It can be defined by using the mathematical model of the milling process into second order equation [7]. From the analysis, the mathematical model of the process consisted of 2 parts: the model of feed drive system and model of milling process as shown in Figure 3

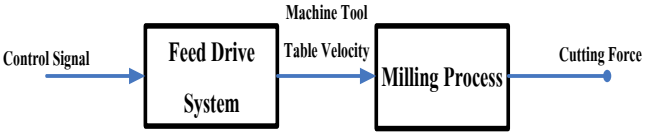

Figure 3 Block diagram of the milling process

2.2. Model of feed drive system

A mathematical model of feed drive system, it consists of servo motor driver, servo motor, ball screw, ball nut, coupling, slide way, thrust bearings, saddle, and machine tool table as shown in Figure 4. It can be modeled mathematically by the first order equation of 1.

$$f_r = ms\dot{x} + d\dot{x} \tag{2.1}$$

where

m : the moment of inertia.

d : the damping coefficient.

x : the machine tool table position

$\dot{x}$: the machine tool table velocity

$\ddot{x}$: the machine tool table accelerate

f_r : the control signals.

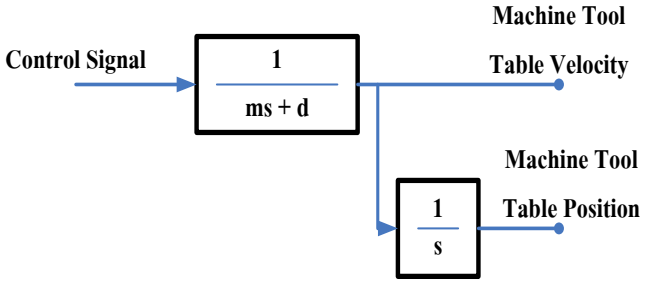

Figure 4 Block diagrams of the feed drive system

2.3. Model of the milling process

A model of the milling process is the work piece which mounted on a machine tool table, and moving toward the end mill tool as shown block diagram in Figure 5. Consequently, the milling process can be defined by mathematical modeling the first order equation in 2.

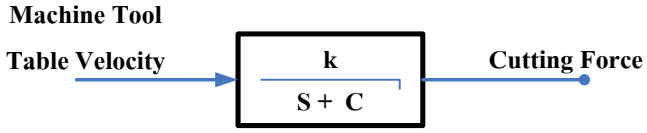

Figure 5 Block diagrams of the milling process.

$$k.v = \dot{F}_c + cF_c \tag{2.2}$$

where

F_c : cutting force.

v : the machine tool table velocity

k : the milling process gain

c : the coefficient of cutting force, based on cutting depth and spindle speed.

Equation (1) and (2) can be written as the transfer function of the milling process, shown in equation (3).

$$kf_r = m\ddot{F}_c + (mc + d)\dot{F}_c + dcF_c \tag{2.3}$$

Then, the equation (3) enter into the design process of cutting force controller.

3. CONTROLLER DESIGN

In the design of the adaptive cutting force control, the model of feed drive system and model of milling process were combined into the cutting force process transfer function. The output of the cutting force controller is defined to be the feed rate by adjusting the feed rate volume to the CNC controller, as shown in the figure. 6, which it's designed as adaptive cutting force control, using Lyapunov's function.

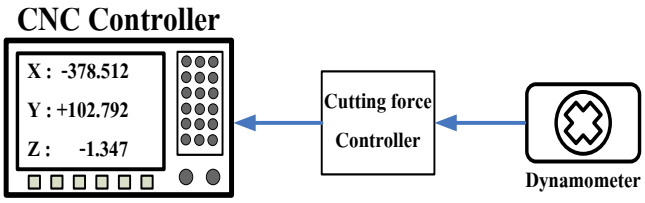

Figure 6 Block diagram of Cutting force controller

From equation (3), the state space equation can be rewritten as equation (4).

$$m\ddot{F}_c + (mc + d)\dot{F}_c + dcF_c = kf_r \tag{4}$$

Defined the signal control as

$$f_r = \hat{m}\ddot{F}_d + \hat{\alpha}\dot{F}_d + \hat{\beta}F_d - KdE \quad (5)$$

Where

F_d is the target cutting force.

Kd is PD control gain.

α is equal to . $(mc + d)$ and $\tilde{\alpha} = \alpha - \hat{\alpha}$

β is equal to . dc and $\tilde{\beta} = \beta - \hat{\beta}$

defined

$$\tilde{F} = F_c - F_d \,,\; E = \dddot{\tilde{F}} + \lambda\tilde{F}$$

where

$\tilde{F}$ is the error of cutting force.

λ is the sliding mode gain.

Substitute equation (5) into equation (4)

$$m(\dddot{F}_c + \ddot{F}_d) + \alpha(\ddot{F}_c + \dot{F}_d) + \beta(\dot{F}_c + F_d) = k(\hat{m}F_d + \hat{\alpha}F_d + \hat{\beta}F_d - KdE) \quad (6)$$

Substitute in equation (6), and derived at equation (7).

$$m\dddot{\tilde{F}}_c + \alpha\ddot{\tilde{F}}_c + \beta\dot{\tilde{F}}_c = \tilde{m}\ddot{F}_d + \tilde{\alpha}\dot{F}_d + \tilde{\beta}F_d - KdE \quad (7)$$

Equation (7) is written a state error, and derived at equation (8)

$$\dot{e} = Ae + Bw\tilde{\phi} \quad (8)$$

From equation (8) defines the Lyapunov's as

$$V = e^T Pe + \tilde{\varphi}^T \Gamma^{-1}\tilde{\varphi} \quad (9)$$

The Matrix and are symmetry matrix and positive definite.

Differential equation (9) is as follows

$$\dot{V} = e^T P\dot{e} + \dot{e}^T + 2\tilde{\varphi}^T \Gamma^{-1}\dot{\tilde{\varphi}} \quad (10)$$

From equation (10), it specified that and resulted in the adaptation law as follows.

$$\dot{\tilde{m}} = -\gamma_1 \dot{F}_d E$$

$$\dot{\tilde{d}} = -\gamma_2 \dot{F}_d E$$

$$\dot{\tilde{c}} = -\gamma_3 \dot{F}_d E$$

4. EXPERIMENT RESULTS

The experiments of the proposed the cutting force controller were carried out using Makino CNC machine with a 10 millimeter diameter Flat End Mill tool, spindle speed of 3000 rpm, IBM personal computer Pentium 450 MHz, which installed the 6 channel digital to analog converter card, the 3 channel analog to digital converter card and the up-down counter. Moreover, a 200x200mm KISTLER dynamometer is mounted on the machine tool table for measurement of the actual cutting force to feedback to the cutting force controller. The work piece was SKD41 steel

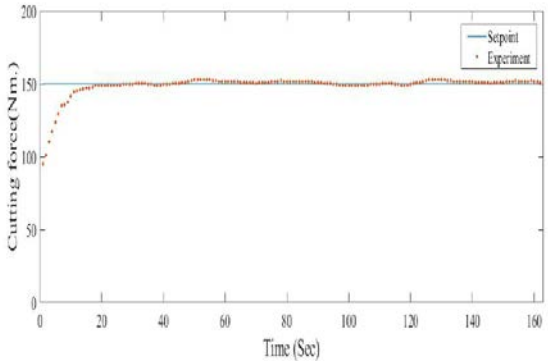

(a)

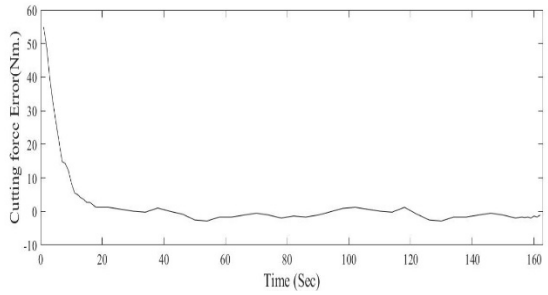

(b)

Figure. 7 Experimental result of milling process at the set point 150 Nm and DOC 1 millimeter. (a) comparison between the actual and the set point. (b) the cutting force error

The experiment results compared to that between the cutting force response and the target cutting force, at 3 different DOCs were 1, 2, and 4 millimeters. The target cutting forces are 150, 200 and 320 Nm, respectively.

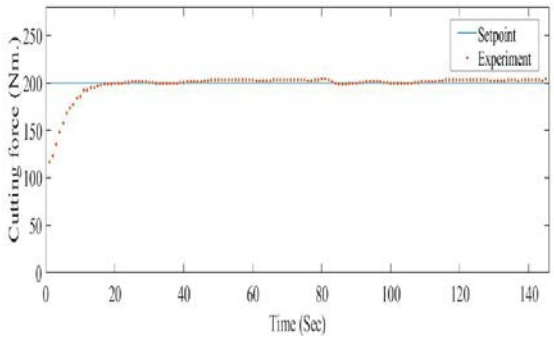

(a)

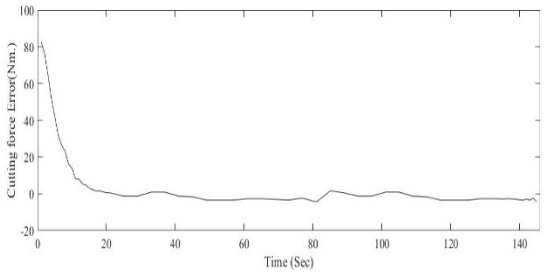

(b)

Figure. 8 Experimental result of milling process at the set point 200 Nm and DOC 2 millimeters. (a) comparison between the actual and the set point. (b) the cutting force error

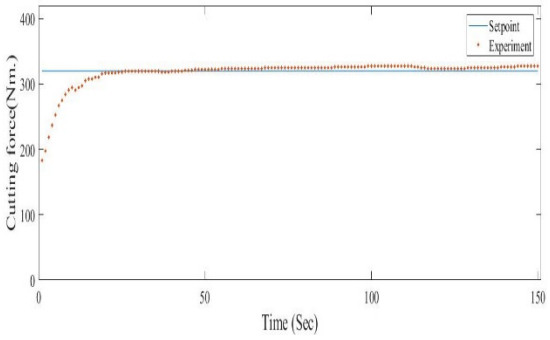

(a)

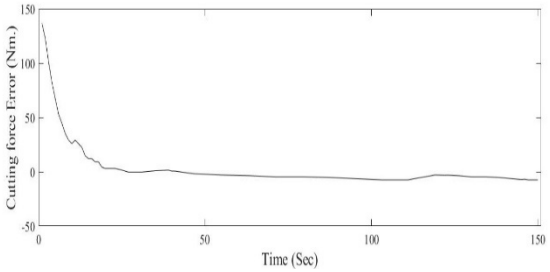

(b)

Figure. 9 Experimental result of milling process at the set point 320 Nm and DOC 4 millimeters. (a) comparison between the actual and the set point. (b) the cutting force error

Figure 7 shows the comparison between the actual cutting force and the target cutting force 150 Nm. (DOC 1 millimeter); Figure 8 shows the comparison between the Figure 7 shows the comparison between the actual cutting force and the target cutting force 150 Nm. (DOC 1 millimeter); Figure 8 shows the comparison between the actual cutting force and the target cutting force 200 Nm. (DOC 2 millimeters); and Figure 9 shows the comparison between the actual cutting force and the target cutting force 320 Nm. (DOC 4 millimeters). The results of the controlling show that the cutting force response of 3 levels was converged to the target value and smooth. The cutting force changed based on the feed rate of the feed drive system. As experiment results, it can control the cutting force smoothly and compensate the up milling and down milling of the end mill tool, the tool life increased and acceptable practice.

5. CONCLUSION

This paper presents the adaptive cutting force control for CNC Milling machines. The design of the controller determines the mathematical model of feed drive system to adjust the feed rate while CNC milling machine runs on. As a result of the milling process at 3 different DOCs, actual cutting force response will convergence with the target cutting

force, which controls the cutting force smoothly, the tool life increased and acceptable practice.

6. REFERENCES

[1] Y. Altintas, "Manufacturing Automation: metal cutting mechanics, machine tool Vibrations, and CNC Design,": Cambridge University Press, 2000.

[2] N. K Mehta, "Machine Tool Design and Numerical Control," McGraw-Hill, 1996.

[3] L. N. Lacalle and A. Lamikiz, "Machine Tools for High performance Machining," Springer-Verlag London Ltd.

[4] T. Childs, K. Maekawa, T. Obikawa and Y. Yamane, "Metal Machining Theory and Applications," John Wiley & Sons Inc.[5] Hassan El-Hofy, "Fundamentals of Machining process," Taylor & Francis Group, 2007.

[6] F. Cus, U. Zuperl*, E. Kiker and M. Milfelner, "Adaptive self-learning controller design for feed rate maximization of machining process," Journal of Achievement in Materials and Manufacturing Engineering, Vol 31, 2008.

[7] L. K. Lauderbaugh, and A.G. Ulsoy, "Model reference adaptive force control in milling," ASME J Eng Ind, pp 13–21, 1989.

[8] T. Matsumura, T. Shirakashi, and E. Usui, "Adaptive Cutting Force Prediction in Milling Processes," International. Journal. of Automation Technology, Vol.4, 2010.

[9] N. Wang, X. Ze, C. Ai and Y. Ji, "The Adaptive Numerical Control System Based on Cutting Force Restriction," Proceedings of the Sixth International Conference on Intelligent Systems Design and Applications (ISDA'06).

[10] A. Bacciotti and L. Rosier, "Lyapunov functions and stability in control theory," Springer-Verlag,London, 2001.

[11] K. J. Astrom and B. Wittenmark, "Computer Controlled Systems," Prentice Hall, 1984.